ÉCOLE DE TECHNOLOGIE SUPÉRIEURE
UNIVERSITÉ DU QUÉBEC

ARTICLE BASED THESIS
PRESENTED TO
ÉCOLE DE TECHNOLOGIE SUPÉRIEURE

IN PARTIAL FULFILLEMENT OF THE REQUIREMENTS FOR
THE DEGREE OF DOCTOR OF PHILOSOPHY
Ph. D.

BY
Niloofar KAMKAR ZAHMATKESH

WATER DROPLET EROSION MECHANISMS OF TI-6AL-4V

MONTREAL, OCTOBER 28th, 2014

BOARD OF EXAMINERS (THESIS PH.D.)

THIS THESIS HAS BEEN EVALUATED

BY THE FOLLOWING BOARD OF EXAMINERS

Mr. Philippe Bocher, Thesis Supervisor
Mechanical Engineering Department at École de Technologie supérieure

Mr. Florent Bridier, Thesis Co-supervisor
Research Engineer at DCNS Research

Ms. Ruxandra Botez, President of the Board of Examiners
Automated Production Engineering Department at École de technologie supérieure

Mr. Mohammad Jahazi, Member of the jury
Mechanical Engineering Department at École de technologie supérieure

Mr. Pawel Jedrzejowski, External Evaluator
Energy Sector, Rolls-Royce Canada, Ltd.

Mr. Swami Swaminathan, Independent Evaluator
President & Principal Metallurgical Consultant, TurboMet International

THIS THESIS WAS PRENSENTED AND DEFENDED

IN THE PRESENCE OF A BOARD OF EXAMINERS AND PUBLIC

ON OCTOBER 16th, 2014

AT ÉCOLE DE TECHNOLOGIE SUPÉRIEURE

IV

To my loving parents, Raz Amini and Ghasem Kamkar

and my supportive brother, Bahram

without whom I would have never finished this work.

VI

ACKNOWLEDGMENT

This research effort would not have been possible without the guidance and support of my advisor, Professor Philippe Bocher and my co-advisor, Dr. Florent Bridier. Thank you, Philippe, for giving me the opportunity to work with you over the course of this Ph.D. Your continuous support, patience and immense knowledge helped me in all the time of this research and writing this thesis. Thank you, Florent, for all that you have taught me. You are a dedicated professional who have never denied me help when asked even though you were quite busy. I respect and admire you both, for being awesome mentors.

I would also like to thank Dr. Pawel Jedrzejowski for your help and insightful comments during this project. Professor Mohammad Jahazi Professor Ruxandra Botez, and Dr. Swami Swaminathan, thank you for serving on my committee and providing guidance toward the completion of this degree.

I would like to thank Professor Mamoun Medraj, for the experiments done at Concordia University. I would like to appreciate the help and support provided by Dr. Andreas Uihlein, Alstom, Switzerland for running the rig test at Alstom. I also thank Mr. Marin Lagace, Hydro-Quebec, for your help on doing the confocal microscopy at IREQ.

I would like to acknowledge the help of entire materials laboratory at ETS, particularly Radu Romanica, Jean-Guy Gagnon, and Olivier Bouthot. I am indebted to my colleagues helping me at materials lab, especially Dr. Majid Hosseini for helping me through the experiments at the beginning of my work, Dr. Vincent Savaria for helping me learn ANSYS and Polyworks software, Dr. Nicolas Vanderesse for doing the image processing job on my SEM images and EBSD maps, and Dr. Hossein Monajati for all the residual stress measurements and ANSYS works. I would also like to thank Mr. Mohammad Sadegh Mahdipoor, for all the great helps you provided me during the experiments at Concordia University. I wish you all success in your endeavors. My sincere thanks extend to all my colleagues at LOPFA. Thank you for

your discussions, supports, kind words, and well wishing. I would like to express my sincerest thanks to Dr. Jean-Charles Stinville. Thank you, Jean-Charles, for always being there for me, your discussions, and all the fundamentals you taught me.

Finally, though no amount of "Thank yous" will suffice, I would like to wholeheartedly thank my parents and my only brother, the foundation of my life, for their support and encouragement throughout my entire life. Dad, thank you for your love of life. For allowing me paint on your canvas when I was a little girl. You are my first art teacher. Thank you for telling me what I am cable of and for never saying "no" when I asked for any helps. You will always be my hero. Mom, thank you for spending countless hours after you got home from work to patiently teach me math. Not that you only taught me math, I have learned what true compassion, unconditional love, and being a selfless person really mean. Bahram, you are the highlight of my childhood. You never wanted to see me get hurt and I felt all safe when you were around. Thank you for all the times you listened to me and gave me a shoulder to cry as if nothing else mattered. Without each of you, I would be nowhere near the person I am. I love you all.

MÉCANISMES D'ÉROSION PAR IMPACTS DE GOUTTELETTES D'EAU SUR L'ALLIAGE TI-6AL-4V

Niloofar KAMKAR ZAHMATKESH

RESUMÉ

L'érosion par impact de gouttelettes est un phénomène pouvant mener à la ruine de matériaux métalliques dans de nombreux environnements. A titre d'exemple, l'érosion par gouttelette d'eau de pluie ou de vapeur sur les composants aéronautiques tels que les aubes de turbomachines et certaines parties du fuselage peut induire la détérioration progressive de ces dernières. Dans le cas spécifique des turbines à gaz couplées avec un système de brumisation (*Inlet Fogging System*), ce phénomène d'érosion est un point clé dans le dimensionnement de pièces.

Le système de refroidissement par brumisation est la méthode la plus couramment utilisée dans les turbines à gaz pour compenser les variations de température entre les saisons. Une augmentation trop importante de la température provoquant une chute des performances de la turbine à gaz. L'introduction de gouttes d'eau dans le flux d'air en entrée permet alors la régulation de la température des systèmes d'admission et du compresseur et ainsi une puissance de sortie optimale des turbines à gaz. Cependant, l'endommagement par érosion induit par l'introduction de ces gouttelettes d'eau sur les premiers étages du compresseur est problématique.

L'objectif principal de ce travail (projet CRIAQ MANU419) est de comprendre les phénomènes induits par érosion par impact de gouttelette sur un alliage de titane, afin d'optimiser la résistance à l'érosion des aubes de compresseur généralement produites à base de titane. La caractérisation des phénomènes d'endommagement par érosion par impact de gouttelettes sur un Ti-6Al-4V a été de première importance. Les effets de la microstructure du matériau ainsi que des paramètres d'impact des gouttelettes ont été mis en évidence.

Ce travail sur la caractérisation de l'endommagement de l'érosion sur l'alliage Ti-6Al-4V s'articule en deux parties :
-   L'endommagement par érosion par impacts de gouttelettes à travers une approche expérimentale originale. Les données collectées ont été traitées à la fois qualitativement et quantitativement pour effectuer une étude multi-échelle de l'endommagement.
Les effets de l'influence de la vitesse d'impact sur les phénomènes d'érosion afin de représenter les sollicitations induites en service.

Mots-clés : Impact de gouttelette d'eau, Érosion, Ti-6Al-4V, Turbine à gaz, Texture cristallographique

WATER DROPLET EROSION MECHANISMS OF TI-6AL-4V

Niloofar KAMKAR ZAHMATKESH

ABSTRACT

Water impingement erosion of materials can be a life-limiting phenomenon for the components in many erosive environments. For example, aircraft body exposed to rain, steam turbine blade, and recently in gas turbine coupled with inlet fogging system. The last is the focus of this study.

Inlet fogging system is the most common method used to augment gas turbine output during hot days; high ambient temperature causes strong deterioration of the engine performance. Micro-scaled droplets introduced into the inlet airflow allow the cooling of entering air as well as intercooling the compressor (overspray) and thus optimizes the output power. However, erosion damage of the compressor blades in overspray stage is one of the major concerns associated with the inlet fogging system.

The main objective of this research work (CRIAQ MANU419 project) is to understand the erosion induced by water droplets on Titanium alloy to eventually optimize the erosion resistance of the Ti-based compressor blade. Therefore, characterization of the water droplet erosion damage on Ti-6Al-4V receives the major importance. The influence of base material microstructure and impact parameters were considered in erosion evaluation in present study.

This work covers the characterization of the erosion damage on Ti-6Al-4V alloy in two parts:

- The water droplet erosion damage through a novel experimental approach. The collected data were processed both qualitatively and quantitatively for multi-aspects damage study.

- The influence of impact velocity on erosion in an attempt to represent the in-service conditions.

Keywords: Water impingement, Erosion, Ti-6Al-4V, Gas turbine, Crystallographic texture, Impact velocity

TABLE OF CONTENTS

LIST OF TABLES

LIST OF FIGURES

Page

XXII

LIST OF ABREVIATIONS

AFM	Atomic Force Microscopy
ASTM	American Society for Testing and Materials
EBSD	Electron Back-Scattered Diffraction
HLP	High Load Parameters
ID	Impingement Direction
LCF	Low Cycle Fatigue
LD	Longitude Direction
LLP	Low Load Parameters
LPB	Low Plasticity Burnishing
LSP	Laser Shock Peening
MDE	Mean Depth of Erosion
MUD	Multiple of Uniform Distribution
ND	Normal Direction
PDA	Phase Doppler Anemometry
PMMA	PolyMethyl-MethAcrylate
RD	Rolling Direction
RPM	Revolution Per Minute
SEM	Scanning Electron Microscopy
SiC	Silicon Carbide
TD	Transverse Direction
TiN	Titanium Nitride

LIST OF SYMBOLS

C Speed of the sound in a liquid

E Young's modulus

E_d Erosion damage depth

E_k Impact energy

E_R Erosion rate

hcp Hexagonal closed pack

I_p Incubation period

L Crack size

n Erosion velocity exponent

n' Cyclic strain hardening

P Induced pressure by a single droplet on a surface

R_d Erosion damage depth rate

t Testing time

V Impact velocity

$\dot{\varepsilon}$ Erosion rate

$\varTheta$ Angle/inclination

ρ Density of liquid droplet

σ'_f Measure of cyclic stress resistance

INTRODUCTION

Liquid impingement erosion is the result of high speed liquid droplets impacting a solid surface. It has become a significant issue in several conditions such as rain erosion in aircrafts, missiles, and helicopter rotors (Heymann 1992) or more recently, in gas turbine engine applications where inlet fogging and overspray are used to increase the performance and power efficiency during hot days (Khan 2008, Bhargava et al. 2007). Inlet fogging is the most common method used to increase power during hot days due to its low cost. Water droplets are sprayed into the gas turbine inlet to cool the entering air to the engine and increase the air density. Remaining water droplets will enter the compressor, resulting in inter-cooling and increasing the output power (Giampaolo 2006). However, the most challengeable concern is the potential erosion of compressor blades resulted from entering the remaining water droplets to the compressor (over spray stage) which will reduce engine efficiency on a long run.

This research project is part of the CRIAQ MANU 419 project in collaboration with Rolls-Royce Canada. It pursues the main objective of improving the compressor components with a higher water erosion resistance. There are three research groups working on this project: Concordia University group who is working on developing the coatings and modeling of the water erosion phenomenon as well as manufacturing the water erosion rig, École Polytechnique de Montréal group who is also developing hard and super hard coatings, and École de Technologie Supérieure (ÉTS) whose objective is to understand the erosion mechanisms of Ti-6Al-4V alloy used for the in-service compressor blade. As a consequence, the present work mainly focuses on investigating the erosion mechanisms on initial as well as advanced stages of erosion. The influence of impact velocity is investigated regarding to the in-service conditions of the compressor blades.

Over the past decades solid particle erosion has been mostly studied rather than liquid impact erosion. A large number of investigators worked on material removal behavior and especially the influence of impact parameters on erosion damage induced by solid particle on the solid

surface. Fewer studies recently investigated liquid impingement erosion. The concept of erosion rate dependence on mechanical properties or impact parameters received the major dedication through the previous works on liquid impact erosion. Erosion was investigated on various materials with great attempts on correlating the erosion phenomenon with material or mechanical properties like hardness, modulus of elasticity, ultimate tensile strength, etc. (Mann and Arya 2002, Heymann 1969). There are, however, only few studies focused on erosion mechanisms and in particular on the characterization of the damage through the different stages of erosion. In addition, there is little complete experimental data in the literature explaining the erosion mechanisms relative to other impact properties such as velocity. Understanding the influence of all impact parameters is beyond the scope of this work.

Following the water erosion resistance improvement of compressor components, the main objective of the present study is the characterization of water droplet erosion mechanisms on Ti-6Al-4V alloy and the influence of base-material and impact properties relative to the in-service conditions. To reach the main objective, the sub-objectives are defined as follow;

- To understand the erosion mechanisms of Ti-6Al-4V alloy during the material removal process
    - To analyze the erosion behavior during the incubation stage
    - To analyze the advanced stages of material removal
- To describe the influence of microstructural properties of base-material
    - To investigate both rolled and forged microstructure of Ti-6Al-4V
- To understand the influence of water droplets impact velocity on erosion kinetic of Ti-6Al-4V

To tackle these objectives, the document begins with a comprehensive overview of the erosion mechanisms and material removal behavior under water droplet impacts given in Chapter 1. The different viewpoints of previous investigators are discussed. Their attempts to obtain some correlations between the erosion mechanisms and mechanical or material properties are presented. This chapter also includes the review of the important parameters

which influence the erosion resistance and behavior of the materials; typically, impact velocity and droplet size.

The first scientific article published from this work is presented in Chapter 2. It discusses the mechanisms of erosion at the advanced/steady state stages for a rolled Ti-6Al-4V. An original methodology is introduced to investigate different aspects of the erosion behavior. In particular, the crack propagation modes are quantified for the first time in impact erosion phenomenon. The relation of the crack propagation including nucleation is discussed relative to the rolled microstructural properties. A new mechanism for material removal is proposed for the erosion due to water droplet impingements. This chapter responds to the second part of the first objective which is to better understand and discuss the water droplet erosion mechanisms of Ti-6Al-4V alloy concentrating on crack nucleation and material removal.

The initial stages of erosion damage on forged Ti-6Al-4V have been addressed in a second article which is presented in Chapter 3. The mechanisms involved at the earlier stages of material removal are investigated through different techniques such as Scanning Electron Microscopy (SEM) and Atomic Force Microscopy (AFM). The evidence of micro-plasticity, grain tilting and intergranular damage due to droplet impacts is discussed and a novel mechanism of damage initiation is proposed. Transgranular sub-surface cracks formation and surface protrusions were observed as the first indication of damage initiation. This chapter responds to the first part of the first objective, meaning understanding the nucleation of cracks at early stages of erosion. Chapter 2 and 3 together discuss the influence of microstructure on erosion mechanism and respond to the second objective of the work.

The third article of this work investigates the influence of water droplet impact velocity on erosion behavior of Ti-6Al-4V in Chapter 4. Impact velocity is the parameter which influences the most the kinetics of erosion phenomenon (Hattori 2010). The influence of the impact velocity is investigated both qualitatively and quantitatively. The base material and velocities range are selected based on the in-service conditions of gas turbines to simulate various regions of compressor blades. This work responds to the third objective of the

4

project, which is to understand the influence of representative impact velocities on erosion behavior. Other parameters should be investigated in future works for fully representation of the in-service conditions.

Finally a substantial summary and discussion of the research work presented in Chapters 2 to 4, is given in Chapter 5. It allows the outcomes of this work to be linked to obtain the objective of the work and discusses the understanding of the erosion phenomenon in certain aspects. Conclusions of the work are presented afterwards in this chapter following by general remarks and recommendations.

CHAPTER 1

LITERATURE REVIEW

The progressive material loss induced by repeated solid or liquid impacts is called impact erosion. There are many kinds of erosion such as solid particle erosion, slurry erosion and abrasion, cavitation erosion, and liquid impingement erosion. Comparing with other kinds of erosion such as solid particle erosion, the liquid impingement erosion has been less studied. Especially there is a relatively limited experimental work on high velocity liquid impact erosion (Zhou et al. 2008) which is the main concern of gas turbines using inlet fogging systems. Understanding the erosion problem may be divided into two major parts. The first part of the problem is relevant to erosion resistance and material removal mechanisms and the second part is the particular influence of the water impingement conditions, such as angle, velocity, size, and etc. The first part of the problem which is understanding the mechanisms of the erosion has generally received less attention than the second part for which more studies may be found in the literature and are discussed afterward in Chapter 4. Erosion can be generally divided in two main stages, i.e., the initial stages of erosion damage and the advanced material removal. The later received the major attention among previous studies while there is limited work on initial stages of erosion. For the purpose of this thesis, the review of the literature is limited here to two sections: discussing the previous work on erosion mechanisms and reviewing the influence of main water impingement parameters on erosion behavior.

1.1   Erosion mechanisms

The simplest mechanism of water impact erosion is referred to as the "water hammer", and ''water hammer pressure'' known as the pressure induced by the droplet impact on the surface which is confirmed by Heymann (1969). At a certain moment during the impingement, shock waves develop in the droplet and breaks away. The lateral out flow forms after and the energy transforms to kinetic energy and impact pressure is released into the base material. Shock wave formation is well known in a droplet impacting a solid. The

shock wave characteristics and stress field generation are presented in Fig. 1-1 (Zhou et al. 2009).
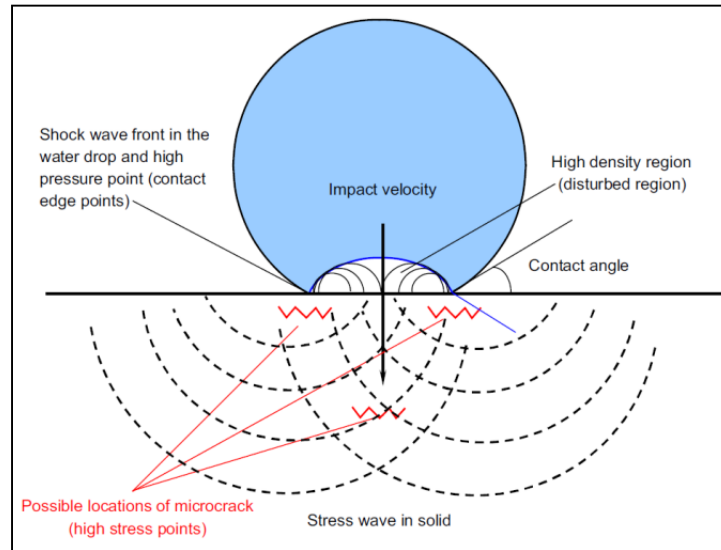
Figure 1-1 The schematic of liquid-solid impact stress and shock wave formation and possible microcrack caused by the impact (taken from Zhou et al. 2009)

Various explanations are reported for material removal mode and great attempts were made in the past also on correlating the erosion with static mechanical properties such as energy absorption, hardness, elastic modulus, or ultimate tensile strength and some correlations have found so far (Garcia and Hammitt 1967, Rao et al. 1970, Frees et al. 1983, Feller and Kharrazi 1984). The common outcome for liquid impact erosion was that, in most cases, improving base material strength properties such as hardness and yield strength increases the erosion resistance.

Another explanation for erosion resistance is its correlation with fatigue resistance of materials (Schmitt 1979). Indeed, due to the repetitive nature of water droplet impingement at high frequency, the erosion process may be associated with cyclic loading and fatigue-like mechanism. Fatigue-like mechanisms were reported for liquid impingement erosion by Hancox and Brunton in 1966; however, fatigue-based theory was initially developed by Richman and McNaughton in 1990 for cavitation erosion damage. They collected data on

various metals and alloys to correlate the cavitation erosion resistance with the introduced fatigue strength coefficient, σ'_f which is a measure of cyclic stress resistance and n´ which is the cyclic strain hardening coefficient. The coefficients, σ'_f and n´, are firstly introduced by Manson and Hirschberg in 1963, through an equation to obtain the relation between total strain and number of cycles. The values can be obtained from cyclic strain-stress curve, strain-life curve, and in some cases from stress based tests reported in the literature (see Manson and Hirschberg 1963). Richman and McNaughton (1990), showed that product of σ'_f and n´ (σ'_f n´) presents a strong correlation between the erosion damage and cyclic deformation properties as is presented in Figs. 1-2 and 1-3. In the same way, features such as striations which accompanying fatigue, were previously reported by Marriott and Rowden (1966) investigating the cobalt-chromium alloy. Afterwards, Beckwith and Marriott (1967) investigated the rain erosion damage on chromium steel and their attempt to correlate the incubation time to the number of cycles for crack nucleation in bending fatigue showed good agreement. Similarly, Thomas and Brunton (1970) observed striation marks investigating the liquid impingement erosion of 50/50 brass. They suggested that fatigue is one probable mechanism of failure in erosion because the liquid impact erosion may be similar to the fatigue phenomenon as the loading is repetitive. A fatigue-based mechanism for water droplet erosion has been however recently questioned by Mann and Arya (2002) since they did not detect any fatigue features neither for cavitation, nor for water jet impingement of Ti-6Al-4V.
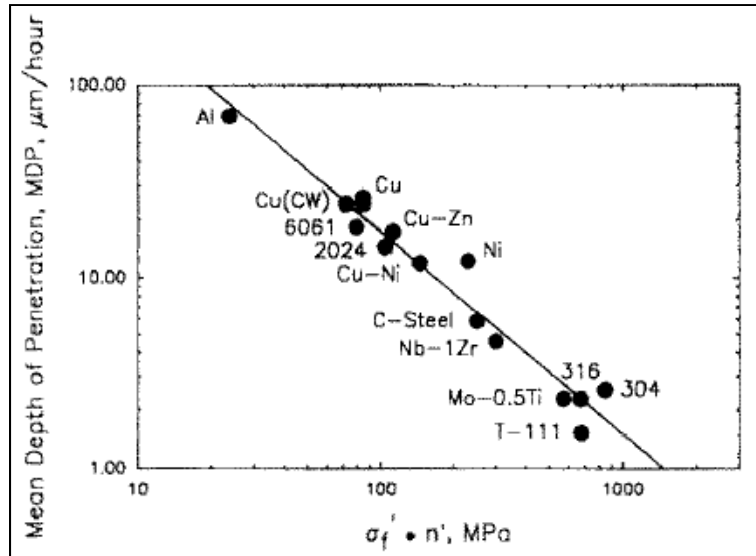
Figure 1-2 Correlation of $\sigma'_f n'$ and mean depth of penetration (taken from Richman and McNaughton 1990)
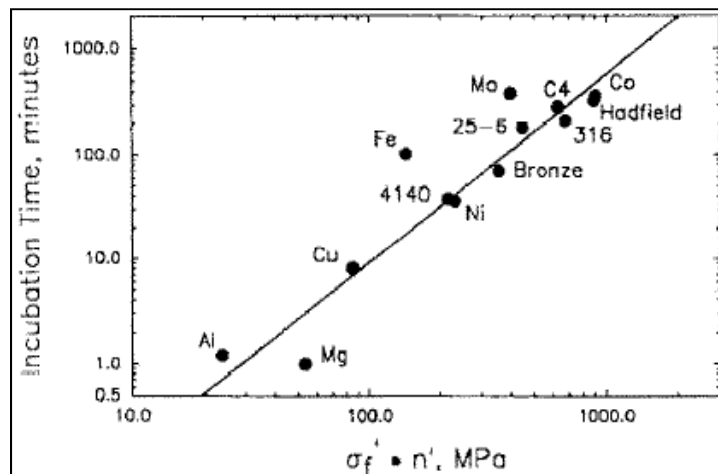
Figure 1-3 Correlation of $\sigma'_f n'$ and incubation time (taken from Richman and McNaughton 1990)

1.2 Erosion behavior in Titanium alloys

Among the influencing parameters on erosion behavior, material properties such as microstructure should not be neglected. The impact of local microstructure on solid and liquid particle erosion was shown by some researchers (Yerramareddy and Bahadur 1991,

Huang et al. 2012). Schmitt (1979) reported that, erosion mechanisms even in a certain material can be varied relative to its microstructure.

Microstructural effect might have a considerable influence on erosion behavior of Titanium alloy due to its anisotropic behavior. The material under investigation in this study is a duplex Ti-6Al-4V, i.e. composed of globular primary hcp α-grains and secondary hcp α-plates, embedded in a bcc β matrix. Duplex Titanium alloys with mainly hcp α-phase and some area of α secondary embedded in bcc β-matrix are known to display elastic/plastic anisotropy. Anisotropy exists in this alloy mainly due to the strong crystallographic texture induced due to the processes like rolling and texture effects play a significant role in the technological characteristics of Titanium alloys.

To explain the elastic anisotropy of duplex Titanium alloys, the angular variation of the Young's Modulus (E) is presented graphically in Fig. 1-4 where Ө is the angle between the c-axis and the loading direction. As is shown when Ө=0˚ meaning when the loading direction is parallel to c-axis, the maximum Young modulus (≈145 GPa) is achieved, while when Ө=90˚ and the loading direction is perpendicular to the c-axis the minimum Young modulus (≈100 GPa) is reported. The inverse pole figure projection of elastic anisotropy is presented in Fig. 1-5.
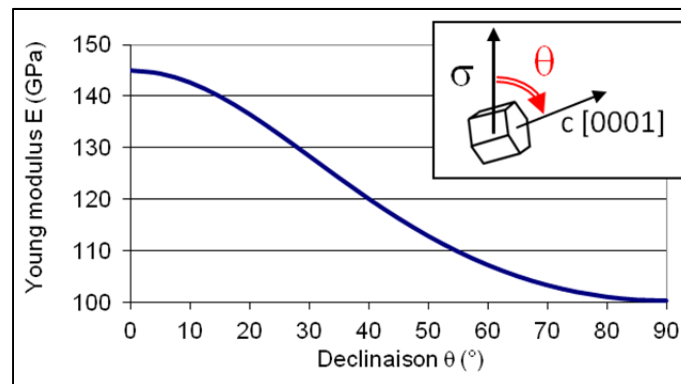
Figure 1-4 Angular variation of E in uniaxial loading
(taken from Bridier et al. 2008)
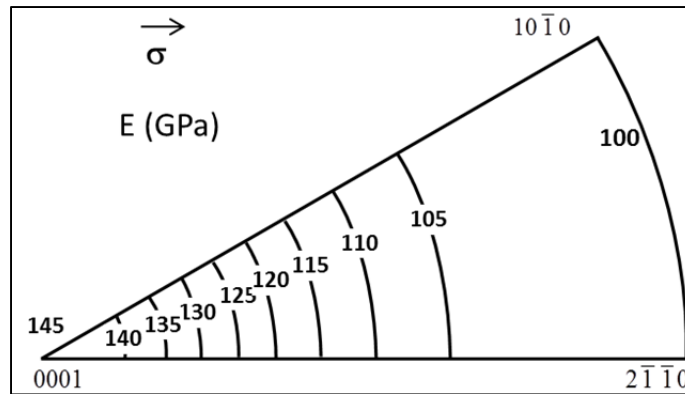
Figure 1-5 Inverse pole figure projection of elastic anisotropy (E) (taken from Bridier et al. 2008)

Plastic anisotropic is also reported for Titanium alloys and is generally related to the different slip systems activated within a particular crystallographic texture. The plastic slip systems for duplex Titanium alloy are presented in Fig. 1-6.
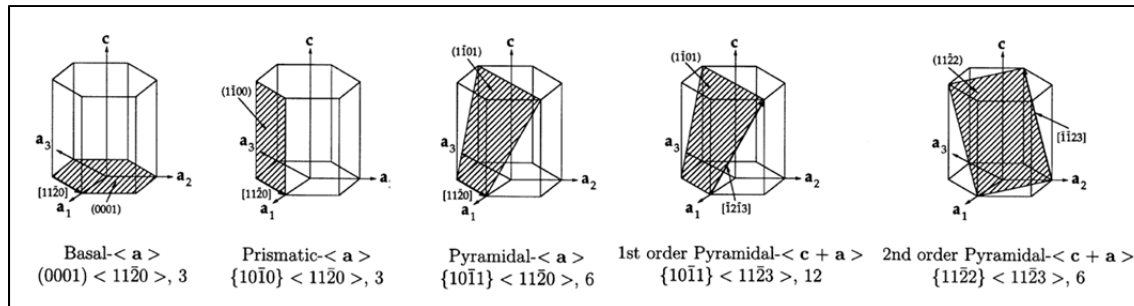
Figure 1-6 Basal : ‹a›, prismatic ‹a›, pyramidal ‹a› slip systems, and first and second-order pyramidal ‹c+a› slip systems in hcp materials (taken from Balasubramanian and Anand 2002)

For instance, Bache and Evans (2001) illustrated the significant differences in monotonic and cyclic loading properties of a rolled Ti-6Al-4V relative to the loading axis; rolling and transverse directions. They showed that loading in transverse direction promotes the yield stress and ultimate tensile strength. For the cyclic loading, loading along the rolling direction offers the optimum cyclic response as well as the increase in stress relation. Therefore, due to

the pronounced elasto/plastic anisotropic behavior of Ti-6Al-4V, an influence of the microstructural conditions on water impact erosion mechanisms may be expected.

Few studies tackled the influence of microstructural features on water erosion resistance. The major contribution on initial damage investigation for a range of materials under water droplet impacts suggest that surface plastic deformation followed by pit formation and surface cracks formation as the damage initiation mechanisms (Thomas and Brunton 1970, Futakawa et al. 2003, Date and Futakawa 2005, Kong et al. 2010). Water droplet erosion mechanisms were investigated by some researchers on pure Titanium and a range of Titanium alloys and their erosion resistance was correlated to their hardness level (Yasugahira et al. 1990). A recent work reported sub-surface plasticity through hardness variations for Ti-6Al-4V submitted to plain water jet impingements without giving clear evidence (Chillman et al. 2007). Intergranular damage is also stated as the dominating mechanism for damage initiation in Ti-6Al-4V alloy under similar test (Huang et al. 2012) however there is no work stating transgranular damage at the initiation stages. The initial damage induced by water droplet is not comprehensively documented and there is still a need of initial local erosion damage investigation. Adler et al. (1974, 1976) reported also crack observations in Ti-6Al-4V subjected to supersonic rain erosion and reported the similarities between fatigue and erosion mechanisms. Similar observations were also stated by Robinson et al. (1995) for untreated and laser treated Ti-6Al-4V under water droplet erosion tests. However, they did not provide distinct evidence of fatigue features and, therefore, the cyclic nature of material removal is still indeterminate.

The detailed review of the literature on the advanced and initial erosion mechanisms is presented in chapter 2 and 3 followed by discussing the work to fully characterize the erosion damage induced by water droplet impacts on Ti-6Al-4V alloy. Damage initiation and advanced material removal behavior are discussed on two separate articles with regards to the microstructural aspects.

1.3 Water impingement parameters and their influence on the erosion kinetic

A good contribution of previous studies is on understanding the influence of operational parameters on erosion behavior of materials. The main influencing factors in impact erosion are reported to be impact velocity, impact angle, and drop shape and size.

1.3.1 Impact velocity

The impact velocity plays the most important role in distinction of erosion and corrosion phenomena as well as influencing the erosion behavior (Adler et al. 1972). Coulon (1985) defined the range of velocities for turbines in PWR power station where the corrosion and erosion phenomena can be formed. The velocity ranges achieved by him are presented in Table 1.1.

Table 1.1 Phenomenon defined in velocity range (taken from Coulon 1985)

Phenomenon	Velocity m/s
Corrosion	0-10
Corrosion-erosion	10-50
Erosion-corrosion	50-200
Erosion	200+

Significant amount of work was carried out on the influence of impact velocity on erosion rate. It is reported that the relation between erosion rate ($\dot{\varepsilon}$), usually defined as the cumulative volume or weight loss per erosion time, and impact velocity (V) is in the form of:

$$\dot{\varepsilon} \, \alpha \, V^n \tag{1.1}$$

where n values varies for different materials (Yerramareddy and Bahadur 1991, Ahmad et al. 2009). Lee et al. (2003), in their investigation on steam turbine blade erosion tested different

alloys for the calibration of erosion parameters. They have converged for a common n value about 5 for all the investigated alloys. Fig. 1-7 shows the influence of increasing the impact velocity on erosion rate for some alloys including Ti-6Al-4V. Therefore, increasing the impact velocity is logarithmically proportional to increasing the erosion rate, though it is desired for gaining the required efficiency (Schmitt 1979). Moreover, the variation of the speed along the leading edge for the compressor blades makes it interesting to investigate in the present study how erosion features changes with the variation of speed. This point will be specifically addressed in Chapter 4.
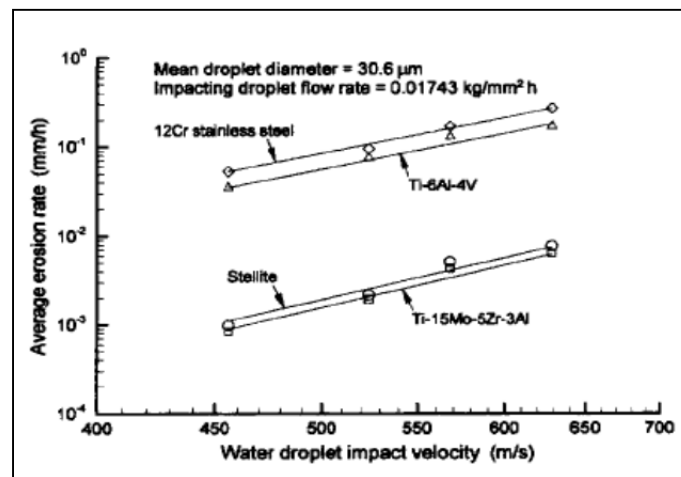
Figure 1-7 Average erosion rate vs. impact velocity
(taken from Lee et al. 2003)

1.3.2   Impact angle

The effect of impact angle is mainly discussed in solid particle erosion. Generally in solid impact erosion, maximum material removal occurs at 90° for brittle materials such as TiN and Titanium whereas the corresponding angle for ductile materials such as Copper, Aluminum, etc. is 22.5°. Fig. 1-8 shows the influence of impact angle on erosion behavior of ductile and brittle material in solid impact erosion (Haugen et al. 1995).
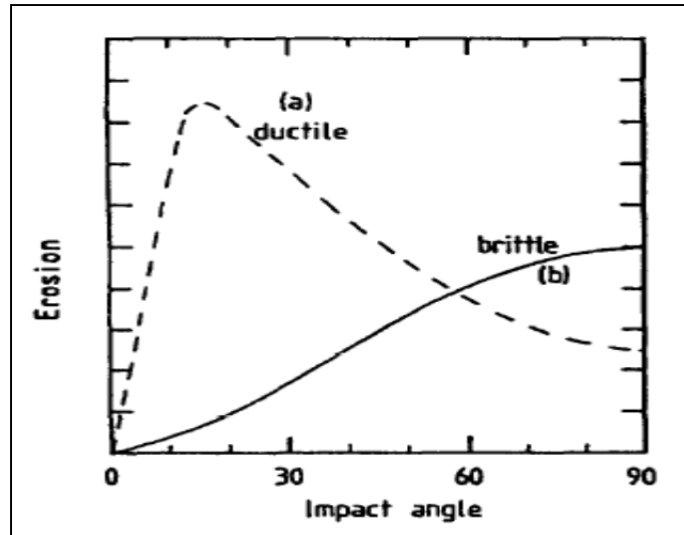
Figure 1-8 Typical solid particle erosion behavior of
ductile and brittle materials as a function of impact
angle (Taken from Haungen et al. 1995)

In case of liquid droplet erosion, since the roughness of the surface changes continuously during the process, the impact angle is not stable. Therefore due to this complexity there is no certain conclusion on the angle of maximum erosion rate (Heymann 1992, Stanisa and Ivusic 1995). This gets more complex for the in-service conditions as the droplets impact the leading edge of compressor blades with the varied angles that induce different types of material removal modes and damage extents.

1.3.3   Droplet size

Adler (1995) found that the damage induced by water droplet erosion is strongly influenced by the droplet radius at the point of impact and not the droplet mass. Indeed shapes of droplets are not perfectly spherical due to different condition of injection force, gravity, etc. In this matter, the equivalent diameter which is the diameter of the flattened droplet that causes more damages is considered as the influencing diameter (Field 1999).

Increasing the droplet size, results in increasing the material removal if the number of impingements is constant (Lee et al. 2003). In water droplet erosion of the blade since there is wide range of droplet sizes, the mean diameter is used in the investigation of erosion (Lee et al. 2003).

On the subject of droplet size, it is noteworthy that one of the issues concerning the use of inlet fogging system in gas turbine engine is the droplet sizing. This is mainly important because of the wide range of statistically distributed droplet size created by the fog nozzles, droplet coalescence, etc. (Chaker et al. 2004).

The influence of droplet size has been studied in the present work and is presented in Appendix I.

1.4 Conclusions of literature review and refining the problematic

The review of the previous work was made in this chapter on general erosion mechanisms and the influencing parameters.

The considerable amount of works on advanced stages of erosion with attempts to correlate the erosion resistance with the mechanical properties did not introduce a clear pattern, even if the general outcome shows that erosion resistance increases with increasing the strength properties. A number of mechanisms were indicated in the literature for material removal phenomenon including fatigue-like mechanism for a range of materials, though the erosion behavior of Titanium alloys, specifically Ti-6Al-4V, has not been well-defined. Also the previous studies concentrated mainly on the mechanical nature of water droplet erosion for advanced stages of erosion, while the number of research on material properties such as microstructural influence is very limited typically on water droplet impingement of Titanium alloys. Thus it is worth to fully characterize both initial and advanced damage induced by water droplet impact erosion considering the local microstructure. The mechanisms of

erosion are comprehensively described and discussed in Chapter 2 and 3 presenting the erosion behavior at advanced and initial stages of erosion, respectively.

Among the influencing parameters, impact velocity is deemed to have the major influence on the erosion behavior. Increasing the velocity increases the initial kinetic energy resulting in more material loss. Experiments were conducted on the influence of the particle velocity on material loss rate and the relation is given by a power law. The power exponent for Titanium alloy was found to be 5.1 under a certain conditions (Lee et al. 2003). Specifically, the influence of impact velocity on erosion rate of Ti-6Al-4V alloy for the in-service speeds has not been studied as for the knowledge of the author, neither the mechanism of material removal is discussed for this alloy. Chapter 4 discusses the previous works in detail and presents the erosion behavior examination of the representative impact velocities to the in-service conditions.

Certain coupons were already available at the beginning of this PhD project, provided by Rolls-Royce. Several batches of tests were performed on different materials with specific test equipment due to sample and equipment availabilities. In particular some coupons were already tested at Alstom whose raw materials were hardly available. Thus, complementary tests were performed to build a scientific approach to the problem, but all possible combination could be studied. Moreover, the type of microstructure or texture of the coupons under investigation was not necessarily the one that would represent the industrial conditions. Some of the complementary tests were then run on new microstructure and using a new rig available at Concordia University to obtain the most possible coherent results. Therefore in light of the experimental procedures and materials under investigation in this work a summary of the test methods used to obtain the erosion mechanism and meet the objectives are presented hereafter. Following is the chart briefly explains the materials and tests in order to make it clearer for the reader.

1.5   Materials and the experimental plans accordingly

1.5.1   Base materials under investigation

Characterization of the base material is conducted at macro and micro scales as well as texture analyses using SEM and Electron Backscattered Diffraction (EBSD) maps at ETS using Schottky-SEM Hitachi SU70. EBSD is a quantitative method of microstructure characterization for the crystalline materials. Material characteristic such as grain size, grain boundary character, grain orientation, texture, and phase identification as well as meso/macro crystallographic texture of the material can be obtained through EBSD analyses.

The erosion mechanism is studied for two base materials divided into two parts: initial and advanced stages of erosion. Characterizations of the two base materials are made at macro- and micro-scales. The brief presentation of the base materials' microstructure and texture is presented in Figs. 1-9 and 1-10. The microstructures are very different both morphologically and crystallographically. The erosion evaluation is done relative to the two presented microstructure and the comparison is made in terms of the damage features and kinetic of the process.
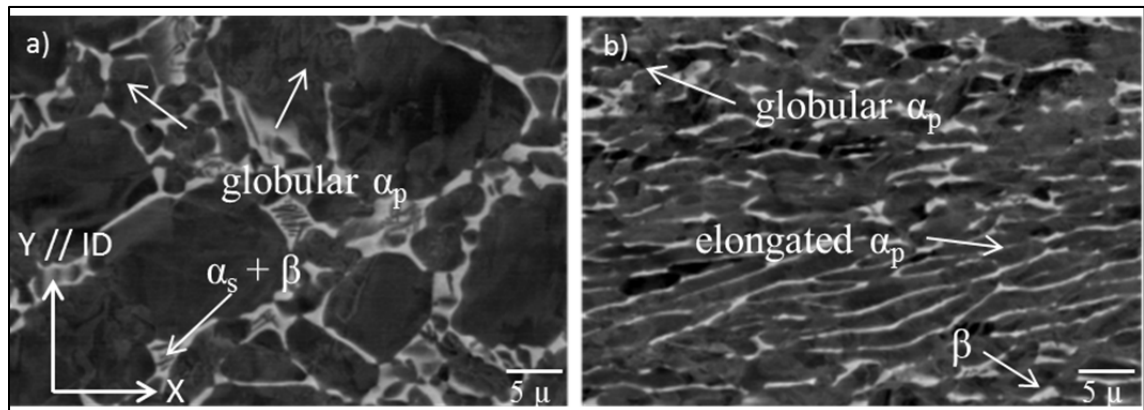
Figure 1-9 SEM micrograph showing the grain morphology: a) forged and b) rolled
base materials
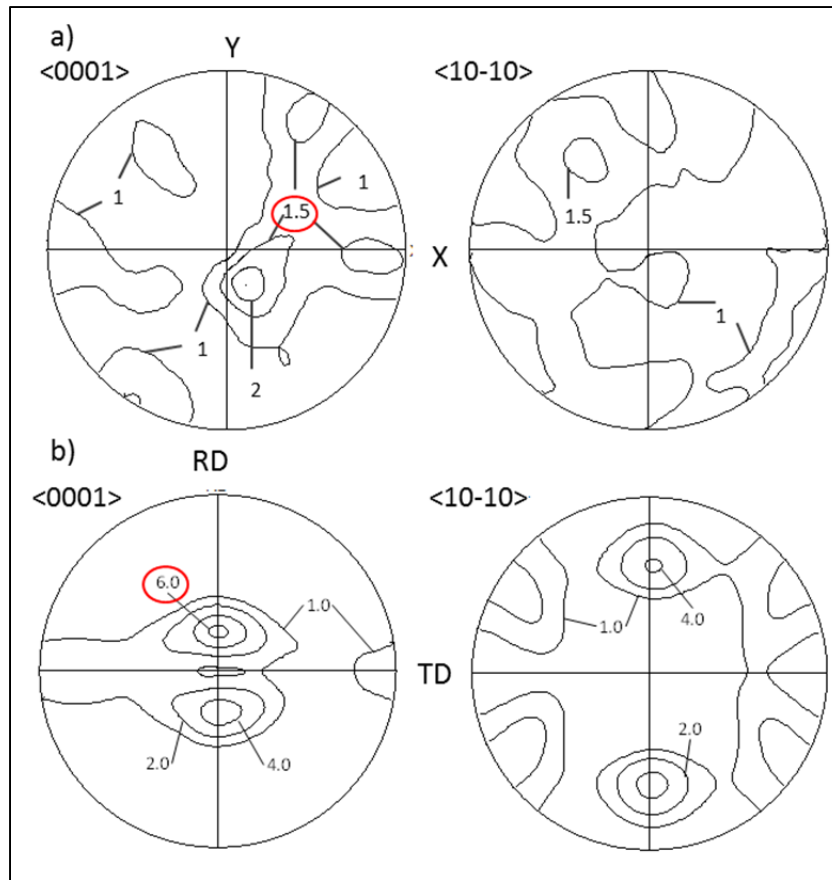
Figure 1-10 Pole figures showing the crystallographic texture of
the grains: a) forged and b) rolled base material

On the other hand there is another rolled material used for the analyses of the impact velocity effect (Chapter 4). This cold-rolled plate is selected based on the in-service blade microstructure and texture so that it represents the similar characteristics to the blade material. The microstructure and texture of the material is presented in Figs. 1-11 and 1-12.
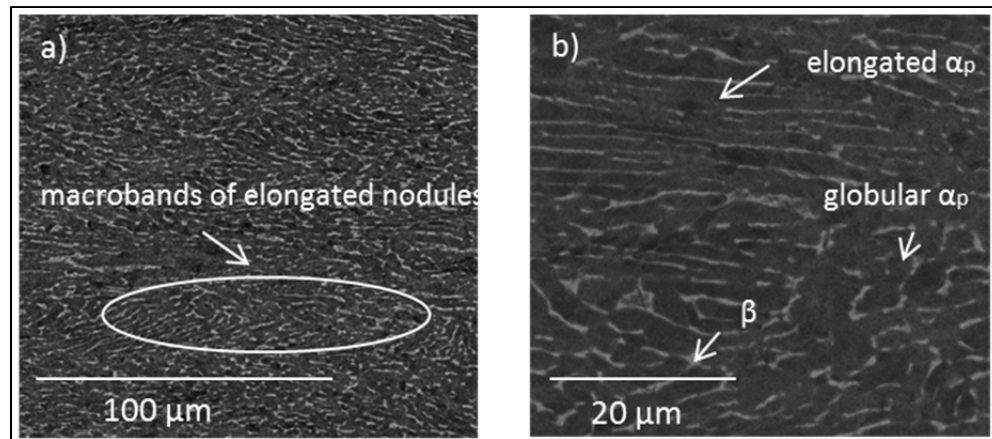
Figure 1-11 SEM micrograph showing the microstructure of cold-rolled plate: a) low and b) high magnification
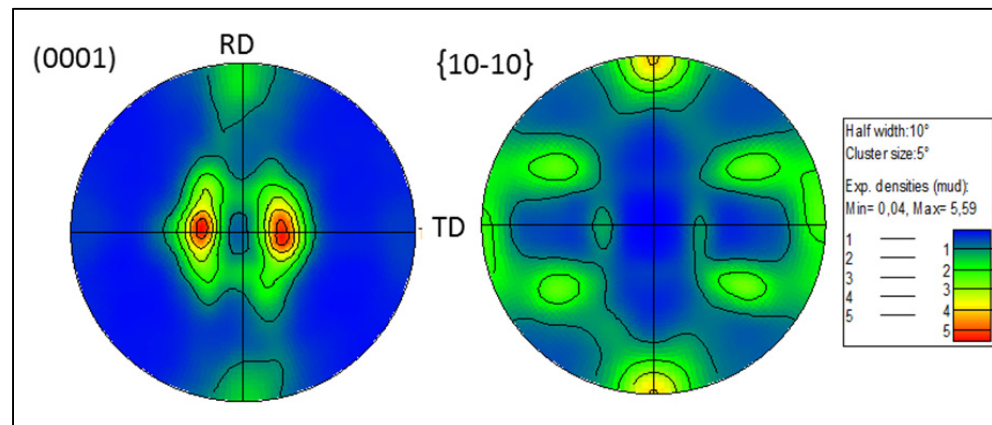
Figure 1-12 Pole figures of the cold-rolled plate

1.5.2   Coupons and erosion rig set up

Coupons are extracted from the presented base materials and the erosion tests are performed on different basis explained later in following chapters to reach a specific objective. The coupons from the forged base material are in a bolt shape and from the two rolled base materials are flat (Fig. 1-13).
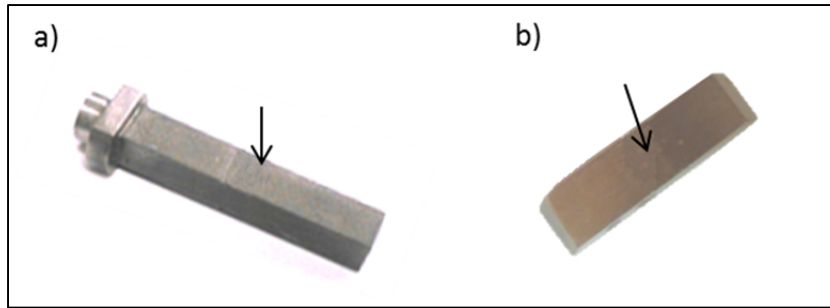
Figure 1-13 Coupons extracted from a) forged and b) rolled base
materials. The impingement surface is showed with the arrows

Water erosion test are performed on the coupons either at Alstom, Switzerland (for the first two objectives: understanding the erosion mechanism as well as influence of the microstructure), or at Concordia university, Canada (for the study of impact velocity influence). While there are some differences between the two water erosion rigs, the principals are the same. It means a static rig in which droplet streams are fixed and the coupons rotate. Through each revolution coupons hit the droplet stream. Therefore the impact velocity in the present study refers to the coupons rotational or linear speed. In the same regard, the number of impingements denotes the number of times the coupon intersects the droplet stream (once per revolution). The differences between the two rigs are mostly related to the number of nozzles (three vs. one for Alstom and Concordia rigs respectively), vertical (Alstom) and horizontal (Concordia) rotations, type of nozzles, speed limits (higher speed limits for rig at Concordia compare to Alstom) and accuracy. The schematic of the water droplet erosion rig is illustrated in Fig. 1-14.
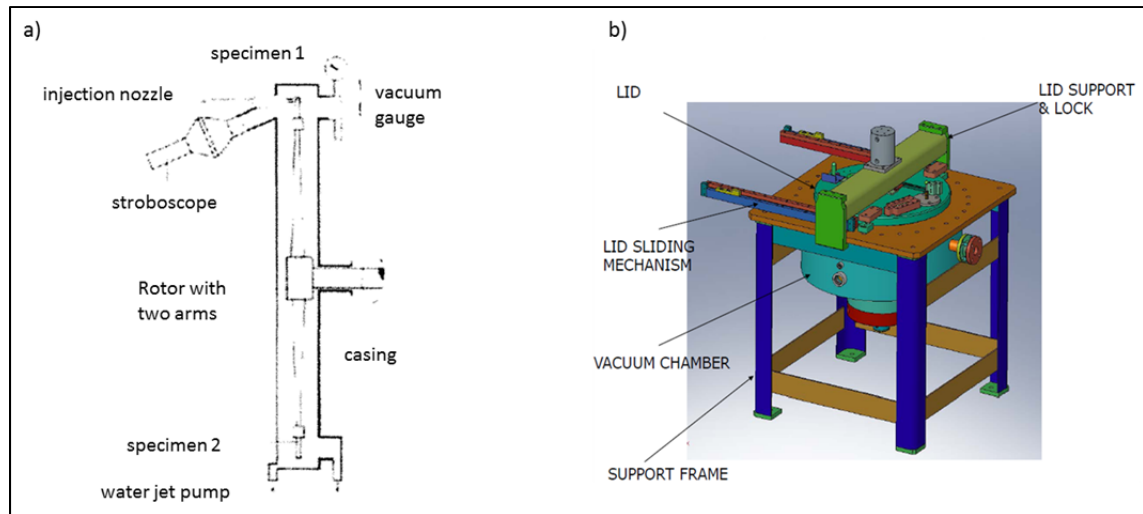
Figure 1-14 Schematic drawing of the water droplet erosion test bench of a) Alstom (taken from www.materials-laboratory.power.alstom.com) and b) Concordia

The eroded coupons then present three lines of erosion if eroded at Alstom (Chapter 2 and 3) and one erosion line if at Concordia (Chapter 4) as presented in the following chapters.

1.5.3   Erosion curves

To obtain the erosion curves for all the investigated conditions, the interrupted tests were run until the coupons reach to the advanced stages of erosion. At each interruption based on the number of impingements or exposure time, the coupons are weighed and in the end, erosion curves are obtained through measurements of cumulative mass loss versus impingement numbers. Obtaining an erosion curve is a time consuming process as it requires a good time around 5-10 minutes between the each interval weighing the sample, turning off and on the machine, waiting for vacuum chamber to reach a certain value, etc. This time plus the run time of the machine is the required time to get one erosion curve. For the investigation of the coupons at different stages of erosion, once the erosion curves are obtained, the erosion stages can be identified. Then, other bare coupons were tested until the exact desired point on the curve (erosion stage). These points were obtained either based on the number of impingements or the exposure time of erosion. Certain set ups and conditions used for each test are discussed through the following chapters.

1.5.4   Erosion characterization

Erosion characterizations are done on the coupons at different erosion stages using SEM at macro and microscopic scales as well as quantitative measurements. This provides the information on the erosion behavior at different scales and reveals the macro and micro-scopic aspects of the erosion i.e. the features which are only visible through e.g. macro or microscopic observations. Quantitative measurements are performed in order to quantify the observations for example the sizes of cracks, inclination, etc.

Macroscopic analyses of the erosion are carried out through width and depth of the erosion lines as a parameter to identify the erosion mechanism. These analyses are made observing the erosion damage from above the coupons or through cross sectional polishing and measurement of the damage depth.

On the other hand, microscopic evaluation mainly addresses the crack studies in terms of nucleation and propagation modes. Observations are done on both eroded surfaces and cross sections which lead to obtain information about the possible sub-surface damages.

Quantitative evaluation is mainly important to give a quantified insight on the dependence of the damage generated by water droplet erosion relative to base material microstructure. It is done through measurement of hundreds of cracks' size and inclination. Crack inclination is referred to the angle of crack propagation relative to the erosion plane. The rules used in the measurement of size and inclination are presented in Appendix II.

1.5.5   Summary of the experimental plans

The following chart (Fig. 1-15) describes all the materials under investigation and corresponded tests as whole.
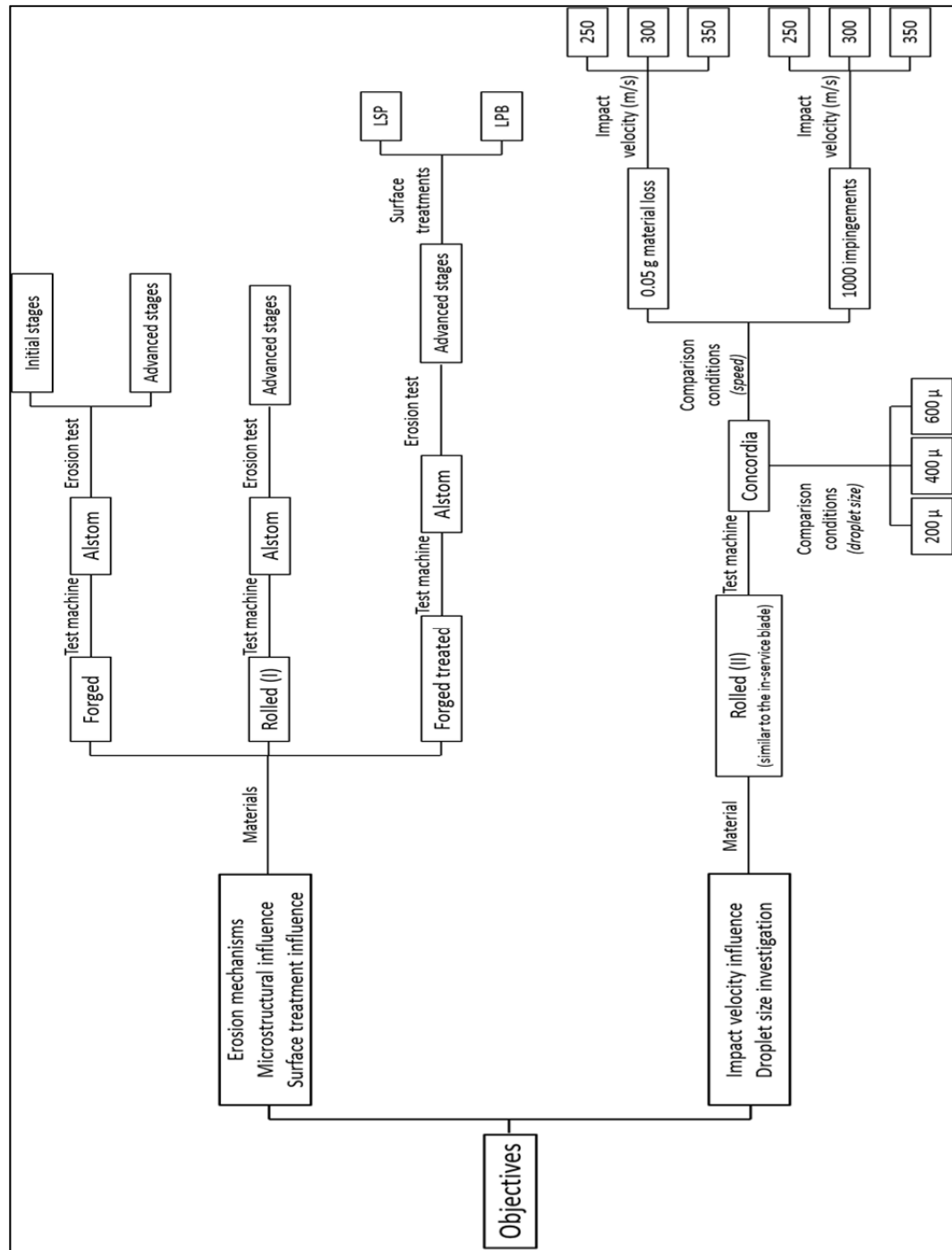
Figure 1-15 Materials and experimental plans

CHAPTER 2

ARTICLE 1: WATER DROPLET EROSION MECHANISMS IN ROLLED TI-6AL-4V

N. Kamkar [1], F. Bridier[1], P. Bocher[1], P. Jedrzejowski[2]
[1]Mechanical Engineering Department, École de Technologie Supérieure (ÉTS), 1100 Notre-Dame Ouest, Montreal, QC, Canada H3C 1K3
[2]Rolls-Royce Canada Ltd-Energy, 9545 Cote-de-Liesse, QC, Canada H9P 1A5

Abstract

Water impingement erosion of Ti-based parts is an issue encountered in many situations: aircraft body exposed to rain during flight, steam turbine blade, and inlet fogging used in gas turbines. The present work focuses on identifying the mechanisms of water droplet erosion of Ti-6Al-4V. Coupons of rolled Ti-6Al-4V have been exposed to high-speed water impingement erosion tests up to the advanced stage. Progressive cross-sectional polishing revealed both surface and sub-surface damage features at different scales. Qualitative observations and quantitative measurements were done on the eroded surface craters. Many micro-cracks along the erosion craters have been observed. The damage appeared to be dependent on the local microstructure morphology and the crystallographic texture of base material. A progressive mechanism for water droplet erosion during maximum erosion rate stage is proposed. It involves the nucleation of crack networks under the droplets impingements, cracks' propagation and/or merging, tunneling or removal of large fragments of material due to linkage of cracks, water smoothing and, cyclically, nucleation of new sets of cracks.

2.1   Introduction

Liquid impingement erosion is the result of high-speed liquid droplets impacting a solid surface. It has become a significant issue in several applications such as low-pressure steam turbine blade as well as rain erosion in aircraft, missile and helicopter rotors [1]. Water droplet erosion could also be a challenge in gas turbines equipped with inlet fogging [2, 3]. Water droplets are sprayed into the gas turbine inlet and cool the air entering to the engine. Remaining water droplets enter the compressor (over spray), resulting in the inter-cooling of the compressor and increasing of the output power [4].

Erosion under impingement of water has been studied by several authors over the years. The mechanical nature of erosion under water droplets or jet impingement is recognized by most of the researchers. Obara et al. [5] highlighted the strong influence of tensile stress waves on the occurrence of cracks during the impact of a liquid jet on polymethyl-methacrylate (PMMA). The resistance of base-materials to water impingement erosion is then generally linked to various mechanical properties of the investigated alloy: absorption energy, hardness, toughness, elastic modulus, or ultimate tensile strength. Regarding Titanium alloys, Yasugahira et al. [6] correlated the water droplet erosion resistance of pure Titanium and a range of Titanium alloys with their respective Vickers hardness. Adler et al. [7, 8] also reported in the 1970s the observation of cracking within a Ti-6Al-4V alloy submitted to supersonic rain erosion and underlined the similarities between fatigue and erosion mechanisms. Particularly, localized cracks and lateral sub-tunneling phenomena were reported at that time for the investigated Titanium alloy. Similar observations were made twenty years later by Robinson and Reed [9] who studied the water droplet erosion of untreated and laser surface treated Ti-6Al-4V. They revealed micro-cracking and suggested a link between erosion resistance and fatigue resistance, without however giving clear evidence of fatigue-related damage along the analyzed erosion craters. For cavitation erosion, Richman and McNaughton [10, 11] compiled a lot of data obtained on various metallic materials and also suspected the cyclic nature of erosion under repeated loading. They qualified the cavitation erosion process as a cyclic deformation mechanism and introduced

the fatigue strength coefficient as a driving parameter for cavitation resistance. Mann and Arya [12], however, questioned in 2002 the theory of Richman and McNaughton as they did not observed fatigue cracks neither for cavitation nor for water jet impingement of Ti-6Al-4V and other alloys. The cyclic nature of erosion damage and the intrinsic mechanism of material removal are nowadays still unclear. Moreover, the particular influence of the microstructure has not been specifically investigated, particularly in the case of water impingement at advanced stages of erosion of Titanium alloys which present very fine-grained and complex microstructures. The impact of local microstructure was shown for sand-blast erosion as Yerramareddy and Bahadur [13] related solid particle erosion with microstructural precipitation due to thermal ageing of Ti-6Al-4V. The microstructural dependence of material removal at earlier stages of erosion under plain water jet impingement for Ti-6Al-4V were studied by Huang et al. [14], reporting the grain boundary damage as the most dominant mechanisms during the initial stages of erosion. If water impingement erosion induces high compressive and tensile stress/strain fields, localized plasticity is assumed to occur under the repetitive loading of water droplet impacts. It appears then very interesting to fully characterize the local erosion damage, particularly relative to surrounding microstructure.

The present work focuses specifically on liquid droplet erosion of Ti-6Al-4V, an alloy which is frequently used in low-pressure blades of steam turbines and compressor blades in gas-turbines, as well as many critical parts of aircrafts [1]. The advanced stages of water droplet erosion were investigated on rolled Ti-6Al-4V, with the objective of obtaining the erosion mechanism as well as influence of microstructure. A rolled microstructure was chosen for this study because it is characterized by a high anisotropy appropriate to investigate the effects of the microstructure on erosion mechanism.

2.2 Materials and methods

2.2.1 Materials

The base-material used for the study is a rolled Ti-6Al-4V. Analyses were conducted in terms of morphology and crystallographic texture of the microstructure using a scanning electron microscope (SEM) Schottky Hitachi SU70. The rolled Ti-6Al-4V microstructure is composed of elongated primary α-grains with locally some area of equiaxial α-grains (Fig. 2-1(a)). At a macroscopic scale, the elongated primary α-grains are organized into macro-bands of a few hundreds of micrometers. The presence of very fine secondary α-phase platelets embedded in a β-phase matrix can also be found as depicted in Fig. 2-1(b).

The crystallographic texture measurements were obtained by electron back-scattered diffraction (EBSD) with an Oxford- Channel 5 system. Large EBSD maps of 4.5x1.5 mm^2 with a 2 mm step size were realized and are depicted in Fig. 2-2. The local crystalline orientation is given in the EBSD map relative to the droplets impingement direction (ID//ND). The corresponding pole figures for both (0001) and {10–10} planes were calculated from the EBSD data and are shown in Fig. 2-3. It can be noted that the present material presents a strong crystallographic texture. The maximal multiple of uniform distribution (MUD) factor is 6.38 for the {0001} pole figure. The preferential orientation indicates that most α phase presents a <0001> direction inclined by 15 degrees with the normal direction (ND) of the rolled plate. Due to the elasto-plastic anisotropy of the hcp α-phase in Titanium alloys, such a strong crystallographic texture is known to primarily influence the mechanical resistance of the alloy relative to the loading direction. As an example, Bache and Evans [15] showed an increase of yield strength from 970 MPa up to 1100 MPa between longitudinal and transverse direction of a highly textured rolled plate of Ti-6Al-4V. Similar anisotropy in fatigue resistance was observed and such differences in mechanical behavior were related to the ability to induce slip in the various plate orientations [16]. Therefore, the present rolled Ti-6Al-4V alloy is of particular interest in investigating the influence of the microstructure on the erosion resistance.
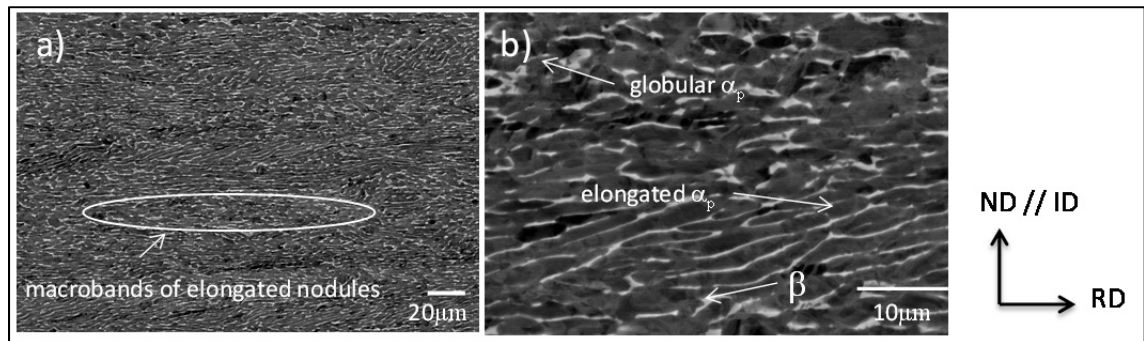
Figure 2-1 SEM micrograph of rolled microstructure a) lower and b) higher magnification
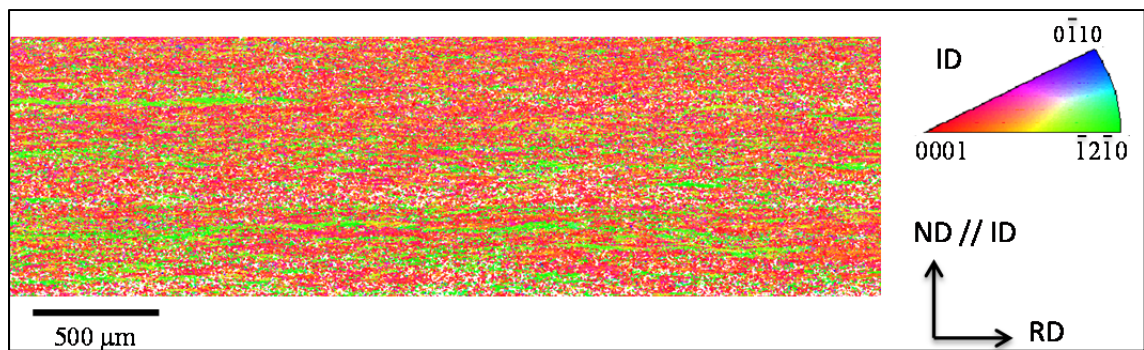
Figure 2-2 Large EBSD map of rolled microstructure
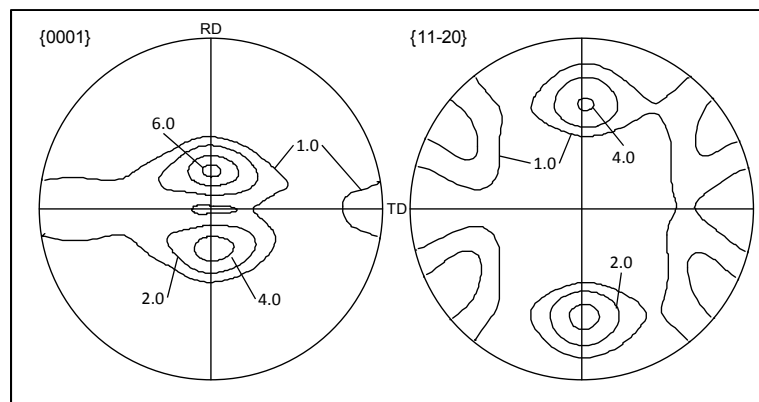
Figure 2-3 Pole figures of rolled microstructure

2.2.2 Hardness of investigated alloy relative to measurement direction

According to the literature, the hardness of the substrate is one of the important mechanical properties controlling the erosion resistance of a material [17, 18]. Even though they are results indicating the importance of other properties, it is generally accepted that increasing the hardness of the material results in increasing the erosion resistance. Hardness measurements of the investigated rolled microstructure were conducted on both the eroded surface, i.e., with a loading direction along ND//ID, and on the perpendicular plane ID-RD, i.e., with a loading direction along TD. The hardness measurements were realized using a Clemex CMT microhardness indenter with two loads (100g and 500g). Each hardness value is the average of minimum five indentations accurately measured under SEM. The hardness values are given in Fig. 2-4 for both directions ID and TD. The scatter of each measurement is given as an error bar reflecting maximal and minimal values. Note that the scatter of the results is reduced with 500g load relative to 100g since larger indents cover more grains and give more representative estimation of the hardness value in a single direction. Hardness values in the ID direction are much higher than in the perpendicular direction TD, i.e., 350 HV vs. 300 HV, approximately. It is interesting to note that this variation of hardness is in the same order of magnitude as the increase of hardness reported for some surface treatment of similar Titanium alloys. As an example, Kim et al. [19] reported an increase from 300 for base metal to 360 HV within the hardened layer of a Ti-6Al-4V submitted to various levels of Laser Shock Peening. As no residual stresses are present in the investigated material (in an annealed state), the increase of hardness for the rolled plate relative to indent direction can be directly linked to the strong crystallographic texture and the associated elasto-plastic anisotropy of the material.
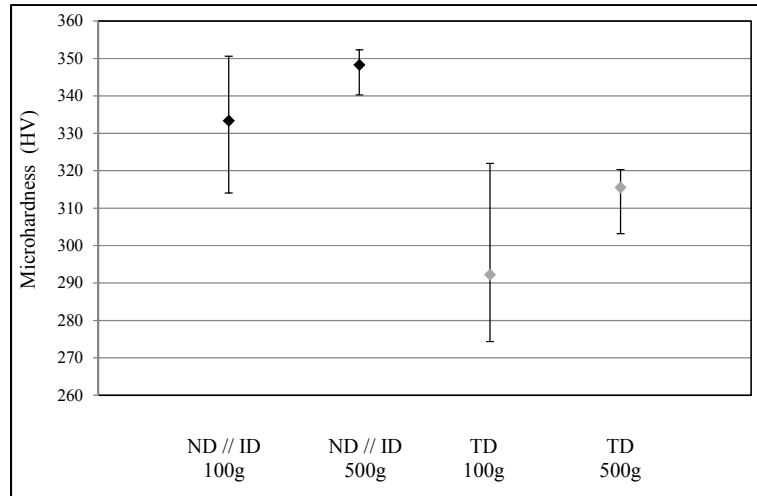
Figure 2-4 Microhardness values for rolled Ti-6Al-4V on different surface

2.2.3   Water erosion testing

A flat sample of 25 mm length, 8 mm width and 3 mm thickness was used for the water droplet erosion tests. Fig. 2-5 shows a schematic of the sample with ID direction being the water droplet impingement direction. This direction is parallel to the normal direction (ND) of the rolled plate. The water droplet erosion tests were performed according to the ASTM international G73 standard [20] with three parallel nozzles leading to three lines of erosion craters depicted in Fig. 2-5. Rotational speed of the disk was 5500RPM with the arm length around 60cm which gives the linear impact speed of 350m/s. The linear speed was controlled by controlling the rotational speed of the rotor and the droplet speed was neglected with respect to linear speed which is set to 350m/s. The samples were subjected to repetitive impact under three parallel jets. The samples were impacted once per revolution. The term ''number of impingement'' will refer to the number of times the sample intersects the droplet stream.

This impact velocity is well within the regime where erosion is the main driving mechanism for wear of impacted surface [21]. An average droplet size of 0.6 mm was used. Droplet size was controlled by calibrated nozzles. Nozzle diameter was 0.3mm. Droplet size

measurements were done according to Phase Doppler Anemometry (PDA) and it is validated for the 0.3mm diameter nozzle the mean droplet diameter is 0.6mm.

The impact angle was 90 degrees relative to impacted surface and tests were done at ambient temperature and the vacuum pressure was 25 mbar. After a certain number of impingements, the weight of the sample was precisely measured. The total number of impingements was estimated to 300,000 for the investigated sample.
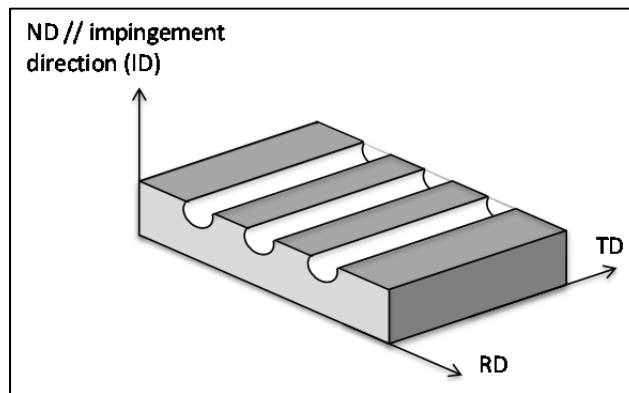
Figure 2-5 Schematic of the eroded sample with three lines of water droplet impingement on top surface

2.2.4 Methodology for erosion craters characterization

The characterization of the erosion damage was performed at advanced stages of erosion. Characterization methods were conducted through qualitative observation and quantitative measurements using SEM. The systematic investigation of the three erosion lines provided sufficient repeatability of the results. The erosion craters were characterized through observations of the eroded surface as well as by progressive cross sectional polishing of the ID-RD plane; i.e. to increase the statistics samples were polished and observed at different cross sections. In order to observe the cross sections, samples were finely cut with diamond blade, grinded and then polished using Buehler vibratory polisher on the cross surfaces. In order not to alter the erosion features, backscattered electron microscopy was used to reveal

the local microstructure along the erosion craters and no chemical etching was used. The damage caused by water erosion was imaged at various magnifications; typically at x50 for larger scale evaluation of craters and tunnels geometry, as well as at x2500 for cracks observations and measurements.

2.3 Results

2.3.1 Cumulative mass loss during erosion testing

Fig. 2-6 gives the cumulative mass loss of the sample as a function of number of water droplet impingements. An initial incubation time may be observed up to 30,000 impingements, followed by an acceleration stage between 30,000 and 150,000 impingements and following by deceleration and steady state stage which are the advanced stages of erosion. This erosion kinetic under water droplet impingement has been largely described by Heymann [1], who for most materials identifies 5 successive stages: the incubation stage, the acceleration stage, the maximum rate stage, deceleration stage, and the final steady-state stage. Robinson et al. [9] reported the lack of any incubation time for a non-treated Ti-6Al-4V when exposed to droplets with an impact speed of 500 m s^{-1}. Although the incubation period is not the focus of the present work, it is interesting to note that the cumulative mass loss versus impingement numbers did present an incubation time for the investigated rolled Ti-6Al-4V. As the impact velocity in the present study is 350 m s^{-1}, i.e., lower than the velocity used by Robinson et al., it is possible that the initial mechanisms behind early stages of erosion might change for different microstructures and future work should concentrate on this issue. In the present work, the erosion features were only characterized on the very last interruption of the test, i.e., after 300,000 impingements. This stage is circled in Fig. 2-6 and is considered as advanced stages of erosion. As at this stage, the erosion craters are relatively deep, the erosion features at both macroscopic and microscopic scales were analyzed all along the craters edges. The mechanisms which will be identified from these observations are then valid to describe only the advanced stages erosion mechanisms. Future work are planned to consider the early stages of erosion by running water impingement erosion tests on a self-

designed rig with the possibility to fully characterize the samples after each interruption of the test.
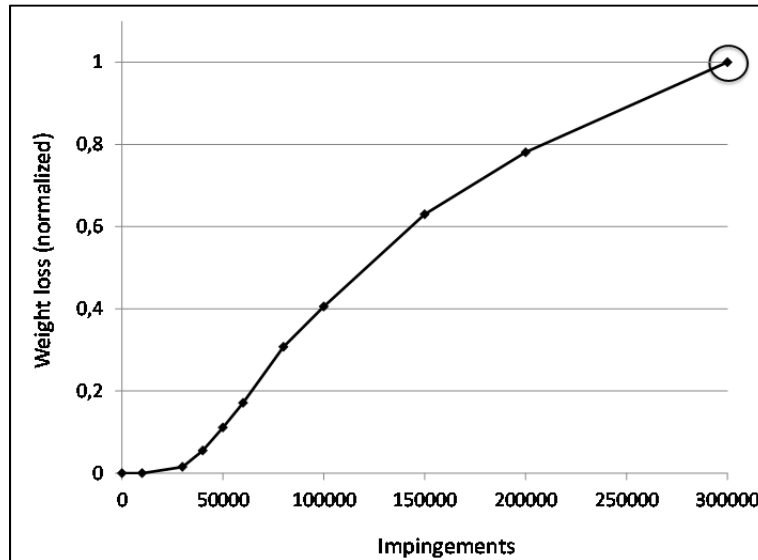
Figure 2-6 Cumulative mass loss vs. number of water droplet impingements

2.3.2 Macroscopic characterization of erosion craters

Macroscopic analyses of the samples were conducted on the eroded surface RD-TD and on the perpendicular cross-sectional plane ID-RD. Eroded surface examination reveals a localized damage along the three erosion lines as illustrated in Fig. 2-7. The erosion is largely advanced along the three impingement lines and some circular craters may be recognized. The diameter of all these erosion craters at the surface was roughly measured and an approximate diameter average was estimated to 1.27±0.2mm. The dimension of craters at the investigated steady stage is then roughly double the size of the droplet diameter of 0.6 mm. Lateral sub-tunnel formation could be observed through the cross section (Fig. 2-8). This phenomenon was also reported by Robinson et al. [9] for un-treated and laser surface treated Ti-6Al-4V submitted to water droplet erosion. Note that the observation of the erosion surface only, is not sufficient since sub-surface damage features such as sub-tunnel might be hidden and the eroded volume of material can be underestimated.
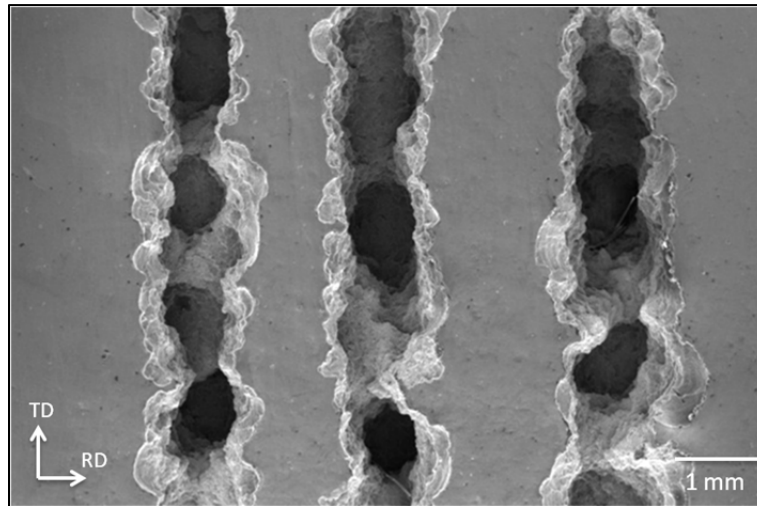
Figure 2-7 Localized damage craters induced by water droplets
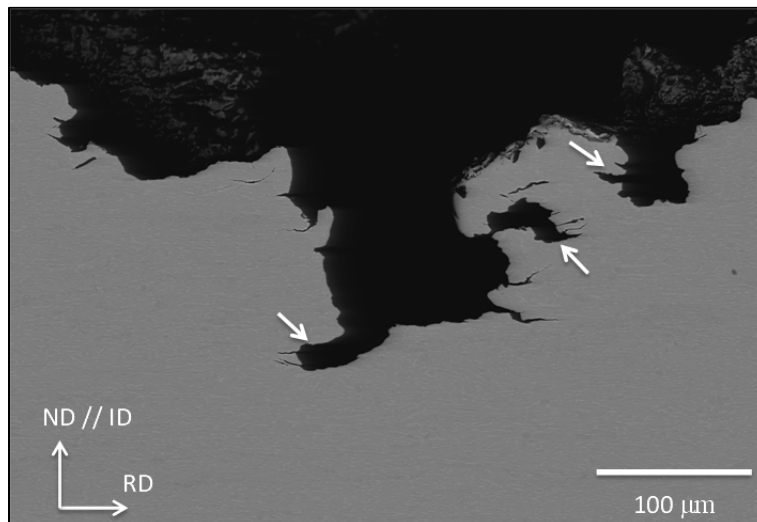
Figure 2-8 Cross-sectional view illustrating craters depth and lateral sub-tunnel formation (white arrows)

2.3.3 Microscopic analyses of eroded sample

From each cross section performed on the eroded sample, three craters corresponding the three lines of erosion could be observed and characterized. Thereby, several hundreds of SEM pictures were taken at high magnifications along the edge of the eroded craters and erosion features were systematically imaged using back-scattered electron imaging to reveal

local microstructure. Surface and sub-surface cracks were observed at various depths. Fig. 2-9 shows an example of both surface (white arrows) and sub-surface (black arrows) cracks. Note that this cross sectional view only gives a two dimensional appreciation of a three dimensional erosion craters, as it can be observed on Fig. 2-8. However, due to the very small size of the cracks, particularly relative to the surrounding microstructure, the authors consider that the cross section view of such small cracks allows to consider these cracks as simply nucleated and not as the result of a crack propagation in the out-of-plane direction. Surface and sub-surface cracks were then identified to nucleate within the primary α-grains. Transgranular nucleation of cracks is consistent with various experimental observations of Low Cycle Fatigue in α and α/β Titanium alloys [22] and indicates high level of plastic strains along the craters, most probably due to intense pressures from impact of water droplets.

Crack propagation cases are depicted in Fig. 2-10. Transgranular crack propagation mode was observed as illustrated in Fig. 2-10(a). Several cases of crack propagation through the merging of many isolated nucleated cracks were also noted as illustrated in Fig. 2-10(b). Such propagation mode implies the nucleation of many cracks at close locations and nucleated in a similar orientation. Such mechanism may be easily predictable within the investigated rolled microstructure since primary α-grains exhibit a strongly elongated shape and the alloy itself shows a strong crystallographic texture, i.e., most of the α-phase grains present a close crystal orientation relative to impingement direction. Numerous observations of striation marks were made for the sample as it is shown in Fig. 2-10(c). Striations confirm the transgranular nature of crack propagation mechanism and indicate the intrinsic cyclic damaging mechanism associated with water droplet impingement erosion. An example of two cracks about to merge together and to lead to the detachment of a larger fragment of material is given in Fig. 2-10(d). Figs. 2-10(e) and (f) illustrate surface cracks which propagated over many grains and which are about to result into the formation (Fig. 2-10(e)) or the continuation (Fig. 2-10(f)) of lateral sub-tunnels, respectively. The mechanism of lateral sub-tunnels is thought to produce even more intense pressures within them leading to damage propagation on a larger scale than the cracks imaged in Figs. 2-10(a) to (c). As sub-

tunnels are running parallel to the eroded surface, their propagation leads to the removal of sizeable fragments of material.

At a few locations of which an example is given in Fig. 2-11, the craters' edge presented also a relatively smooth aspect as opposed to the rough aspect left from transgranular crack propagation depicted in Fig. 2-10. Such smooth edges are thought to be related to the polishing effect under repetitive impacts of water droplets. Some polishing may be an additional partial mechanism of erosion in the present case, following crack propagation and detachment of material fragments, and preceding the occurrence of new cracks nucleation. Note that the term polishing here does not refer to the mechanism detailed by some authors relative to erosion of ductile materials under impingement of fine solid particles, where polishing refers to surface friction heating either above the melting point of the alloy or through high temperature creep [7, 8]. For the present material, the polishing is thought to be due to a fine grain-scale surface smoothing process of rough surfaces left by former transgranular crack propagation.
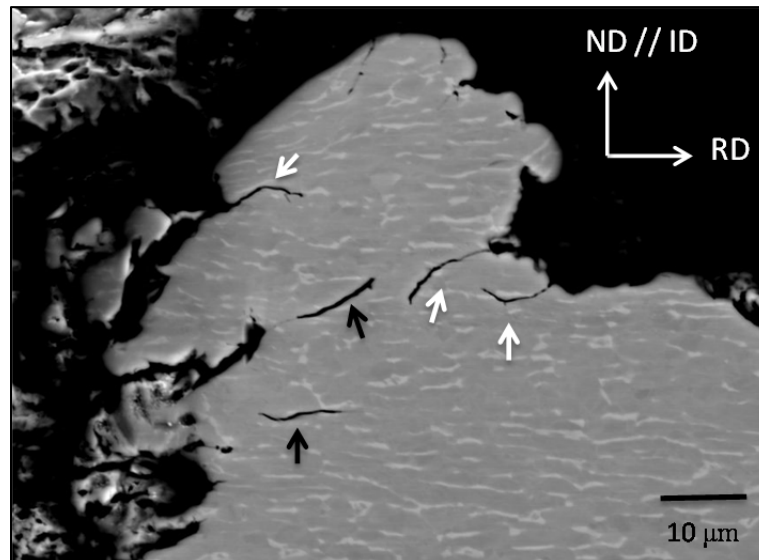
Figure 2-9 Surface (white arrows) and sub-surface (black arrows) cracks
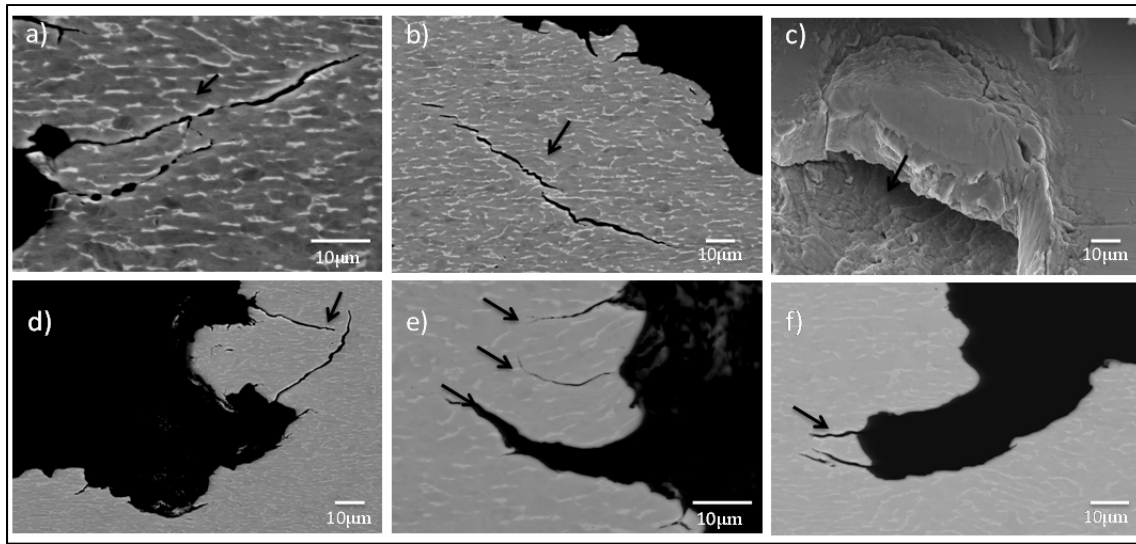
Figure 2-10 Crack propagation cases
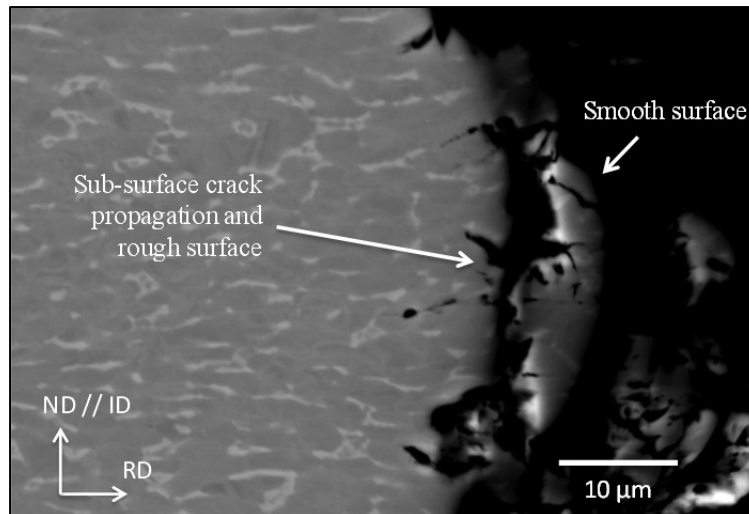
Figure 2-11 Example of rough and smooth surface along erosion crater's edge

2.4   Discussion

In the present work, characterizations were performed after water droplet erosion reached the steady stage leading to millimeter sized craters. Hence, it is important thereby to underline that the conclusions in terms of erosion mechanisms concern primarily the advanced stages of erosion. The erosion craters due to water droplet impingement were imaged and the

damage features directly associated to the microstructure of the investigated Ti-6Al-4V alloy. Surface and sub-surface crack nucleation, transgranular crack propagation or merging of multiple cracks was observed. These numerous observations lead the authors to propose a mechanism for erosion damage induced by water droplet impingement. As illustrated in Fig. 2-12, the water impingement erosion mechanisms identified in the present Ti-6Al-4V during advanced stages of erosion are:

    1) nucleation of surface and sub-surface networks of cracks;

    2) transgranular propagation and/or merging of cracks;

    3) detachment of material fragments and potential formation of lateral sub-tunnels with rough surfaces;

    4) water smoothing of the surfaces.

Cyclically, new networks of cracks will nucleate at or below the smoothed surface. These cracks will propagate outward the surface leading to the formation of sub-tunnels and/or removal of large fragments of material, and so on.
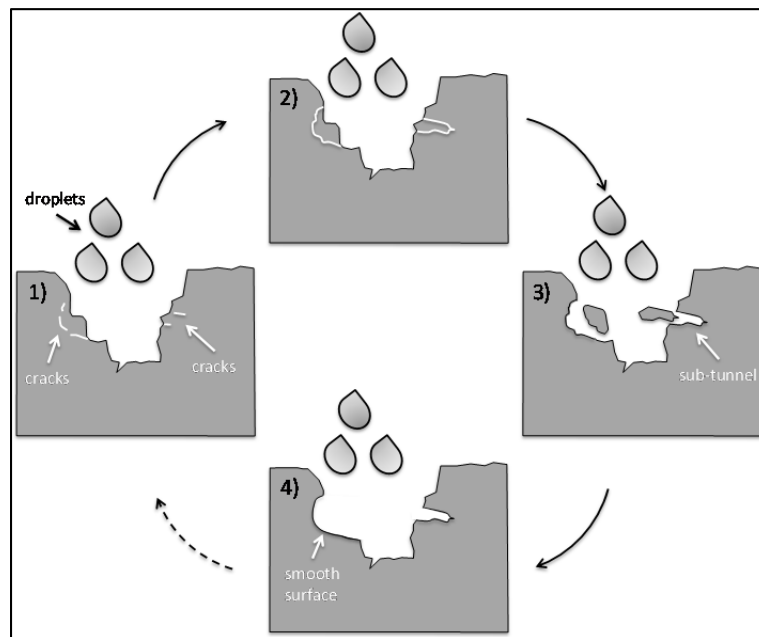
Figure 2-12 Schematic of the water polishing mechanism

Cracking within the local microstructure appears to be a major contributor to the erosion mechanism. In order to give a more quantified insight on the dependency of the damage relative to base-material microstructure and crystallographic texture, the size and the inclination of all observed cracks were systematically measured at high magnification via SEM. A total number of 131 cracks were measured along the craters edges of the three erosion lines of the sample. The term inclination refers here to the angle between impingement direction ID and the main crack propagation direction observed on cross section. An inclination of 0 degree refers to a crack propagating in a perpendicular direction relative to ID, i.e., a parallel direction RD.

Fig. 2-13 shows the quantitative measurements of the crack size. The average crack size of 27 μm is very small relative to the diameter of the droplets and average size and depth of the erosion craters. This small scale of cracks is due to the very fine-grained nature of Titanium alloys, particularly in the case of near-α and α/β alloys used for many applications. The limited size of observed cracks indicates clearly that erosion mechanisms occur largely at the microscopic scale and in a very microstructure dependent manner. Concerning the crack inclination, its distribution is plotted in Fig. 2-14. It clearly centered around 20 degrees with a maximum and minimum value of 86 and 0 degrees, respectively. Such a non-random distribution in crack inclination shows that cracks tend to propagate in a preferential orientation, which in this case is the rolling direction. As illustrated in Fig. 2-10(e), cracks propagate in similar orientations. The authors are aware that the cracks propagate here in a three-dimensional direction and that cross-sectional view only gives partial information. However, the non-random character of the distribution observed for crack inclination gives a strong trend in how the microstructure may influence the crack propagation, and thereby the induced erosion.
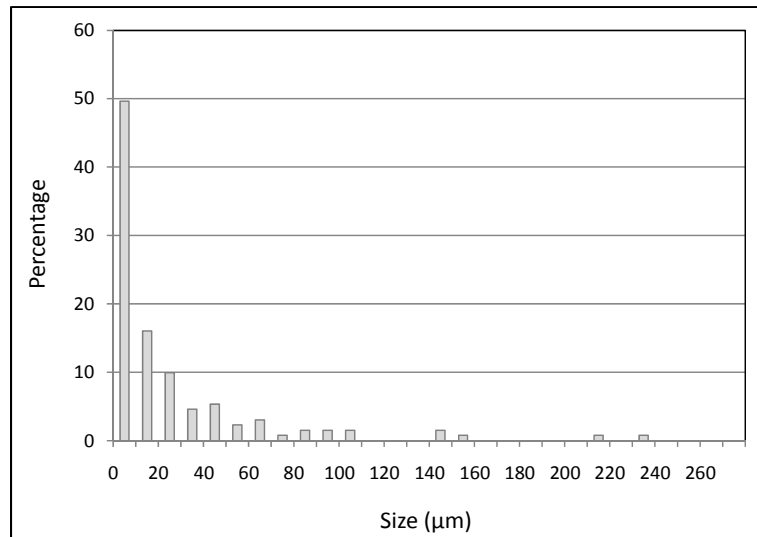
Figure 2-13 Distribution in size of the cracks measured
along the craters edges
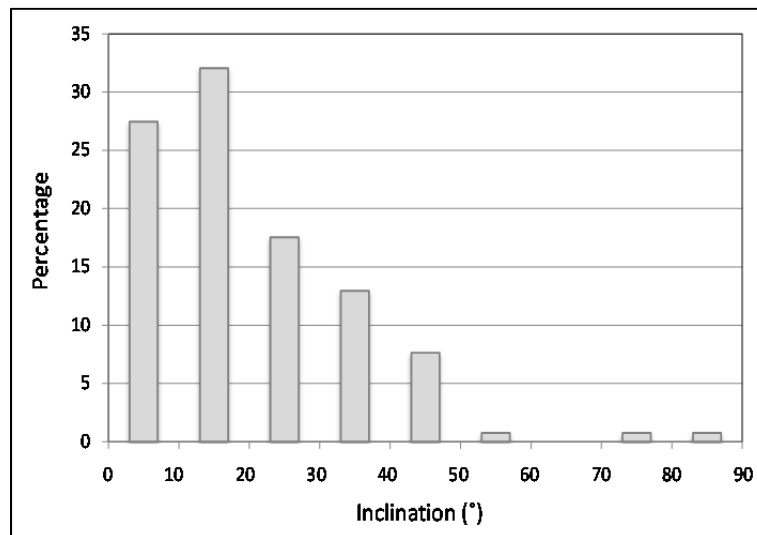
Figure 2-14 Distribution of cracks inclination relative to
water droplets impact direction

It is interesting to recall finally the variation in hardness observed in the investigated rolled plate with an indentation direction along either RD or TD directions. Considering this variation in hardness, as well as the preferential cracking orientation relative to the microstructure, a change in erosion rate may be expected with a very different impingement direction relative to rolled material. However, due to the thinness of the investigated rolled

plate, no water droplet impingement tests could be performed with an impingement direction along the TD or the RD directions for example. The variation in erosion resistance with different microstructures will be part of future work, specifically investigating Titanium alloys presenting different levels of crystallographic textures as well as water impingement tests with drastically different direction of impingement relative to the preferential texture.

To conclude, the above results and discussion concern the advanced erosion stages under specific erosion conditions. It is not intended to suggest that there is, under all conditions of impingement speed, angle and droplet size, a single mechanism of material removal during water impingement erosion for Ti-6Al-4V alloys. The discussion simply stresses, under the classical conditions used in this work in terms of water droplets velocity, angle and size, the dominance of a particular mechanism implying crack initiation and propagation, i.e., fatigue based mechanism highly dependent on local microstructure. Therefore, the influence of Titanium alloys microstructure and its potential morphological and crystallographic anisotropy should be considered to predict more accurately water impingement erosion resistance.

2.5   Conclusions

Water droplet impingement erosion of a rolled Ti-6Al-4V alloy was investigated. The erosion features were analyzed at various scales relative to the local microstructures and an erosion mechanism could be proposed. The latter cyclically involves the nucleation of sub-surface and surface cracks; their propagation and merging outward the surface; the removal of large fragments of material occasionally leading to the formation of lateral sub-tunnels; and eventually the water smoothing of freshly fractured surface under the repetitive impact of water droplets. Quantified analysis was possible with the measurements of hundreds of cracks along the eroded craters edge and the inclination of nucleated or propagated cracks relative to the impingement direction appears to be directly linked with the morphology and crystallographic texture of the alloy.

References

[1] F.J. Heymann, Liquid impingement erosion, in Wear, ASM Handbook, Vol. 18, ASM, 1992, pp. 221-232.

[2] J.R. Khan, T. Wang, Simulation of inlet fogging and wet-compression in a single stage compressor, Proceedings of the ASME Turbo Expo (2008) GT2008-50874.

[3] R.K. Bhargava, C.B. Meher-Homji, M.A. Chaker, B. Bianchi, F. Melino, A. Peretto, S. Ingistov, Gas turbine fogging technology: a state-of-the-art review-Part1: Inlet evaporative fogging-Analytical and experimental aspects, Journal of engineering for gas turbines and power 129 (2007) 443-453.

[4] A. Giampaolo, The Gas Turbine Handbook: Principles and Practice, 3rd Edition, Fairmont Press, Inc, 2006.

[5] T. Obara, N.K. Bourne, J.E. Field, Liquid-jet impact on liquid and solid surfaces, Wear 186-187 (1995) 388-394.

[6] N. Yasugahira, K. Namura, R. Kaneko, T. Satoh, Erosion resistance of Titanium alloys for steam turbines blades as measured by water droplet impingement, in Titanium Steam Turbine Blading, Palo Alto, 2988, Pergamon, New York, pp. 385-401, 1990.

[7] W.F. Adler, Analysis of particulate erosion, Wear 37 (1976) 345-352.

[8] W.F. Adler and R.F. Vyhnal, Rain erosion of Ti-6A1-4V, 4th International Conference on rain erosion and associated phenomena, Meersburg, Germany, May, 1974.

[9] J.M. Robinson, R.C. Reed, Water droplet erosion of laser surface treated Ti-6Al-4V, Wear 186-187 (1995) 360-367.

[10] R.H. Richman, W.P. McNaughton, Correlation of cavitation erosion behaviour with mechanical properties of metals, Wear 140 (1990) 63–82.

[11] R.H. Richman, W.P. McNaughton, A metallurgical approach to improve cavitation-erosion resistance, J. Mater. Eng. Perform. 6 (5) (1977) 633–641.

[12] B.S. Mann, V. Arya, An experimental study to correlate water jet impingement erosion resistance and properties of metallic materials and coatings, Wear 253 (2002) 650-661.

[13] S. Yerramareddy, S. Bahadur, Effect of operational variables, microstructure and mechanical properties on the erosion of Ti-6Al-4V, Wear 142 (1991) 253-263.

[14] L. Huang, J. Folkes, P. Kinnell, P.H. Shipway, Mechanisms of damage initiation in a Titanium alloy subjected to water droplet impact during ultra-high pressure plain waterjet erosion, J. Mater. Process. Technol. 212 (2012) 1906-1915.

[15] M.R. Bache, W.J. Evans, Impact of texture on mechanical properties in an advanced Titanium alloy, Materials Science and Engineering A319-321 (2001) 409-414.

[16] F. Bridier, P. Villechaise, J. Mendez, Analysis of the different slip systems activated by tension in a α/β Titanium alloy in relation with local crystallographic orientation, Acta Materialia 53 (2005) 555-567.

[17] G.L. Sheldon, Effects of surface hardness and other material properties on erosive wear of metals by solid particles, J. Eng. Mater. Technol. Trans. ASME 99 (1977) 133–137.

[18] I. Finnie, Some observations on the erosion of ductile metals, Wear 19 (1972) 81-90.

[19] J. Kim, S.K. Cheong, Effect of laser peening process on the mechanical behavior of Ti-6Al-4V, Report for Seoul National University of Technology, p.1, 2010.

[20] ASTM Standard G73, 2004 (2010), standard test method for liquid impingement erosion using rotating apparatus, ASTM International, West Conshohocken, PA, 2010, DOI: 10. 1520/C0033-03R06, www.astm.org.

[21] P.A. Coulon, Erosion − corrosion in steam turbines II: a problem largely resolved, Lubrication Engineering 42 (1986) 357-362.

[22] F. Bridier, P. Villechaise, J. Mendez, Slip and fatigue crack formation processes in an α/β Titanium alloy in relation to crystallographic texture on different scales, Acta Materialia 56 (2008) 3951–3962.

CHAPTER 3

ARTICLE 2: WATER DROPLET IMPACT EROSION DAMAGE INITIATION IN FORGED TI-6AL-4V

N. Kamkar [1], F. Bridier[1], P. Jedrzejowski [2], P. Bocher [1]

[1]Mechanical Engineering Department, École de Technologie Supérieure (ÉTS), 1100 Notre-Dame Ouest, Montreal, QC, Canada H3C 1K3

[2]Rolls-Royce Canada Ltd-Energy, 9545 Cote-de-Liesse, QC, Canada H9P 1A5

Abstract

Identifying the mechanisms of water droplet erosion of Ti-6Al-4V parts is a critical issue encountered in many situations from aircraft body exposed to rain during flight to steam turbine blade. Understanding the erosion mechanism and particularly initiation mode of the damage is an essential need for the studies concerning improving erosion resistance of the components. The present work focuses on the early damage stages of forged Ti-6Al-4V parts exposed to high-speed water impact erosion. Qualitative observations and quantitative measurements were done both on and below the surfaces that are undergoing deformation due to water droplet impingements. Progressive cross-sectional polishing revealed surface and sub-surface microplasticity and micro-cracking. Microcracks have intergranular features at surface and present transgranular characteristics below the surface. From these observations a damage mechanism was proposed to explain the early stages of water erosion. These observations, together with information gathered from more advanced erosion stages tend to prove that a mechanism typical of low cycle fatigue may control the nucleation and early growth of cracks below the surface of the parts subjected to high-speed water droplet impingement.

3.1 Introduction

Liquid impingement erosion has been of practical concerns for many years, primarily for low-pressure steam turbine blades as well as aircraft, missile, and helicopter components subject to rain erosion. Recently, the issue was also pointed out for gas turbines coupled with the inlet fogging system. Erosion may occur at the leading edge of compressor blade when inlet fogging system is used to improve engine efficiency. The droplets impacts result in erosion of these components and have become a challenge in recent gas turbine history [1-3].

Various studies have been carried out toward documenting material response to water impingement erosion phenomena [4-6]. Great attempts were made to correlate the erosion rate of a large range of materials to various mechanical properties such as absorption energy (absorbed energy through a controlled mechanism, here the energy of an impact on a solid), hardness, toughness (ability of a material to absorb energy and plastically deform without fracturing), elastic modulus, or ultimate tensile strength [4-6]. The general outcome of all the studies has been that enhancing the strength properties such as hardness and yield strength increases the erosion resistance.

Fatigue-like mechanisms were discussed over the years for water impingement erosion due to the cyclic nature of the water impingement erosion. Conn and Rudy [7] reported fatigue as one probable mechanism associated with the rain erosion behavior of some elastomers and composites. Richman and McNaughton [8, 9] introduced fatigue strength as a driving parameter for cavitation erosion resistance. Momber et al. [10] proposed a low cycle fatigue model for a low-carbon steel under and water jetting process. This was questioned by Mann et al. [6] as they did not observe any fatigue related damage for Ti-6Al-4V under cavitation and water jet impingement erosion. Adler et al. [5, 11] observed localized cracks and reported similarities between fatigue and erosion mechanism for the Ti-6Al-4V alloy subjected to supersonic rain erosion. Robinson et al. [12] also suggested the link between erosion resistance and fatigue resistance of untreated and laser surface treated Ti-

6Al-4V under water droplet erosion tests without however, giving any clear evidence of fatigue features. Recently, the cyclic nature of water droplet erosion damage was clearly identified by Kamkar et al. [13] through the observation of trans-granular cracks and striation marks in Ti-6Al-4V and the material removal mechanisms were reported to be a fatigue based mechanism.

Despite the considerable amount of investigations on the advanced stages of erosion, limited studies have been carried out on the early stages of water erosion phenomena, particularly during the incubation and onset of material removal. It should be noted that there are still some arguments about the presence of incubation period in Ti-6Al-4V alloy [10]. Initial stages of water impingement erosion were merely considered by few researchers. Thomas and Brunton [14] have investigated the material removal mechanisms of several alloys and reported micro-scale surface plastic deformations as the first evidence of the erosion damage. They observed that for most of investigated materials, erosion begins with shallow depressions on the surface followed by grain tilting, pit appearance, groove formation, and material removal. Uniform yielded surface and slip bands were reported for cobalt contrary to surface depressions characteristics for other investigated materials. Consequently they argued that the presence of these local yieldings is due to the inhomogeneity of loading or material properties. Similarly, Futakawa et al. [15] and Date and Futakawa [16] have looked at some alloys under impact erosion test with mercury and reported plastic deformation on the surface and pit formation for the damage initiation in SS316. Slip bands around the pits were clearly observed. They showed from their SEM observations evidence of plastic deformations in the form of sharp edge protrusion and depression. Similarly Kong et al. [17] reported that plastic deformation followed by crack nucleation is the damage mechanism under high velocity impacts during plain water jet milling on gamma titanium aluminide.

Regarding Titanium alloys, Chillman et al. [18] reported sub-surface plastic deformation in Ti-6Al-4V alloy through hardness variations after plain water jet exposure and announced compressive stresses on the target regions as the result of droplet impacting the

surface. No clear evidence of surface plastic deformation was reported. More recently in 2012, Huang et al. [19] reported intergranular cracks at the initial stages of erosion on Ti-6Al-4V under plain water jet impingement and proposed intergranular damage as the dominant mechanism for erosion initiation. It is worth noting here that transgranular cracks were also observed on the advanced stages of erosion for Ti-6Al-4V submitted to water droplet impact erosion test suggesting the possibility of different mechanisms controlling crack formation during water impingements [13].

The overall understanding of all these investigations points out that damage in water droplet impingement initiates by localized plastic deformation. However, the material behavior at the initial stage is still not clearly documented and local erosion damage characterization on the surface as well as beneath the surface under few numbers of impacts is essential. To this regard, the objective of the present work is to examine the water erosion impingement mechanisms in a forged duplex titanium alloy (Ti-6Al-4V) focusing on the early stages of material removal, i.e., the initial damage mechanisms during the incubation period and the onset of material removal under water droplet impingement.

3.2 Materials and methods

3.2.1 Experimental set up and water erosion test

Water droplet erosion tests were performed with three parallel water jet nozzles on bolt coupons of 45 mm length, 8 mm width, and 8 mm thickness on a rig according to ASTM international G73 standard [20] at Alstom, Switzerland [21]. Fig. 3.1 presents a schematic of the eroded sample showing the three lines of erosion craters aligned with the Z direction. The Y-axis is parallel to impingement direction (ID). Controlling the linear speed was done through the rotational speed of the rotor and the droplet speed was neglected with respect to the rotor speed. The linear droplet impact speed was set to 350 m/s with the disk rotational speeding at 5500 RPM and an arm length of 600 mm. This

impact velocity is well within the regime where erosion is the main driving mechanism for wear of impacted surface [22]. The samples were subjected to repetitive impacts under an angle of 90 degrees relative to the impacted surface. The coupons were impacted by the three droplet streams once per revolution and the term ''number of impingements'' refers to the number of times the sample intersects the streams.

The test was performed under 25 mbar vacuum pressure, and at ambient temperature. Droplet size was controlled by calibrated nozzles. Nozzle diameter was 0.3 mm giving a mean droplet diameter of 0.6mm according to Phase Doppler Anemometry (PDA) measurements performed by the rig operator.
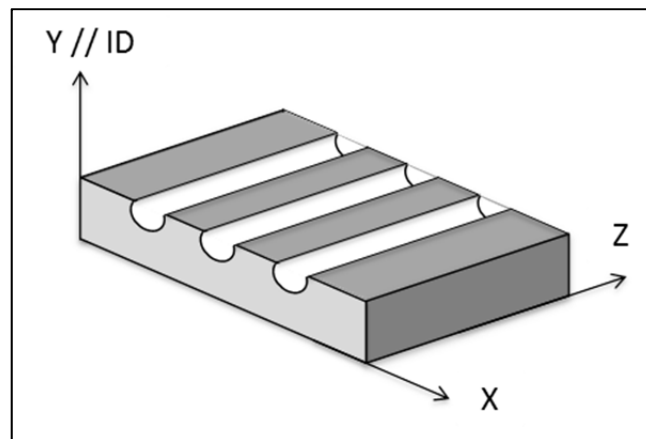
Figure 3-1 Schematic of the eroded sample with three lines of water droplet impingement on top surface

A primary concern in this study was to identify the earlier stages of erosion, which is commonly called incubation period. In this regard, tests were run up to an advanced stage of erosion on one coupon. The erosion curve was obtained thanks to many interruptions and weight measurements and the different erosion stages were identified. In particular, the incubation period was precisely determined and two tests were performed on other coupons up to the number of impingements corresponding to the incubation period and the onset of material removal (1000 and 20000 impingements respectively).

3.2.2   Materials and sample preparation

The material subjected to water droplet impingement erosion test in this study is a forged duplex Ti–6Al–4V presenting a homogeneous globular microstructure with the large proportion (around 70 percent) of equiaxed primary α-grains with the average size of 25μm as depicted in Fig. 3-2(a). The rest of the microstructure is very fine lamellae areas composed of secondary α plates (α_s) embedded in a β-phase matrix as shown in Fig. 3-(b).

The microstructure characterization and crystallographic texture measurement of the samples were obtained using a Scanning Electron Microscope (SEM) Schottky Hitachi SU70 and Electron Back-Scattered Diffraction (EBSD) mapping with an Oxford - Channel 5 system. To perform SEM imaging and EBSD mapping, a specific surface preparation with SiC paper grinding and diamond vibromet polishing were applied to the coupons. A typical EBSD map of 4.5x1.5 mm^2 with 2 microns step size is depicted in Fig. 3-3 bearing the local crystalline orientations presented with inverse pole figure coloring relative to the droplet impingement direction used during erosion tests (Y//ID). It can be noted that the investigated material has almost no macroscopic crystallographic texture but presents some regions, of few hundreds of microns large, with strong crystallographic textures (illustrated in Fig. 3-3). In these regions the α-phase has a major crystallographic orientation as they present the same color indicating the same crystallographic orientation. Since crystals in other parts of the material are randomly textured such features are called macrozones and are typical of forged α/β or near-α Ti-alloys. Macrozones are known to have a strong influence on the local mechanical response of the material, particularly under fatigue loading [23, 24]. Pole figures calculated from EBSD presents a few more pronounced poles located around the rim and in the center for basal plane (Fig. 3-4). But the maximal multiple of uniform distribution (MUD) factor is 2.4 for <0001> pole perpendicular to the impingement direction (Y//ID). The pole figure for the macrozone A (Fig. 3-3) shows much stronger values suggesting possible variations of mechanical properties in the material from one location to the next. The <0001> pole has a MUD

factor around 20 which is very high, meaning that distribution of grains' crystal orientation in this region is almost all pointing in the same direction.
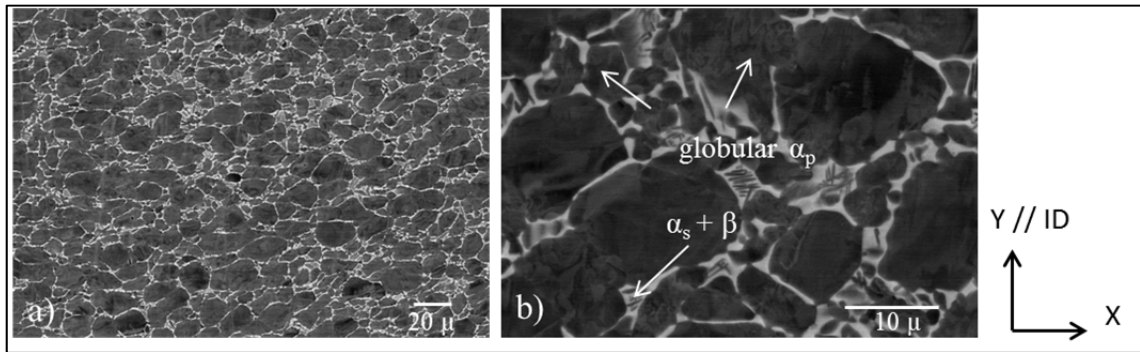
Figure 3-2 Back-scattered electron micrograph of forged microstructure: a) lower and b) higher magnification
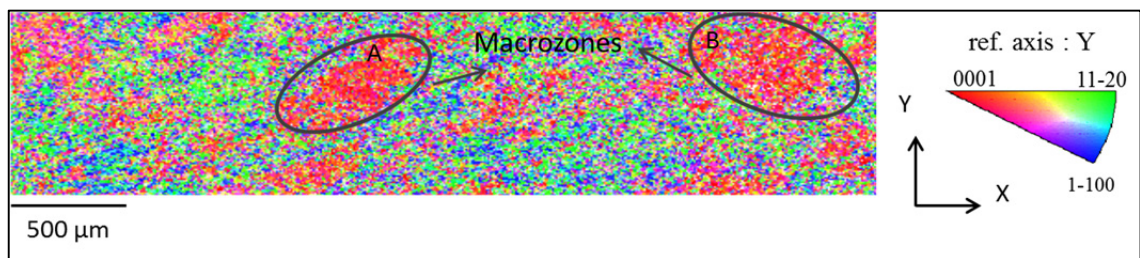
Figure 3-3 Large EBSD map of the typical forged microstructure used for water impingement test (Y is the impingement direction). Zone A and B are macrozones found in the forged microstructure

52
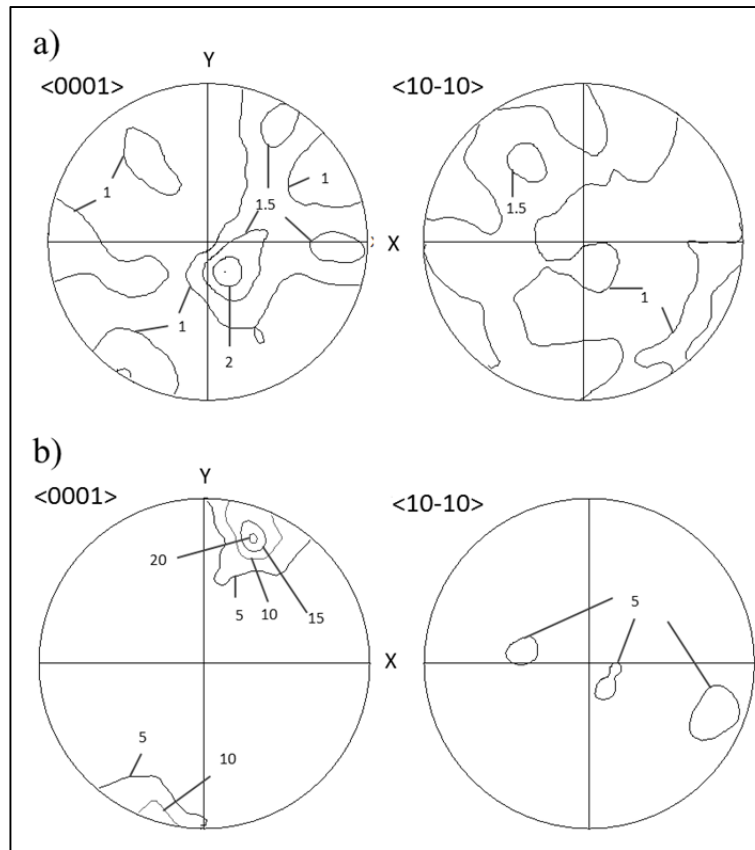
Figure 3-4 a) pole figure of overall forged microstructure
shown in Fig. 3-2 and, b) local macrozone A, (Y is
impingement direction)

Before impingements, the surface of the coupon was grounded with SiC papers, polished
with monocrystalline diamond suspension and polishing cloth and finally
electrochemically-polished with refrigerated A3 solution under 30 Volt for 7 seconds. The
electrochemical polishing process was performed on the surface in order to attain an
unstress surface as well as revealing the microstructure. Fig. 3-5 shows the SEM
micrograph of the electro-polished surface on the XZ plane prior to the erosion test and
damage. This perfectly reveals the microstructure and allowed later on to clearly relate the
induced erosion damage with the local microstructural features of the material.
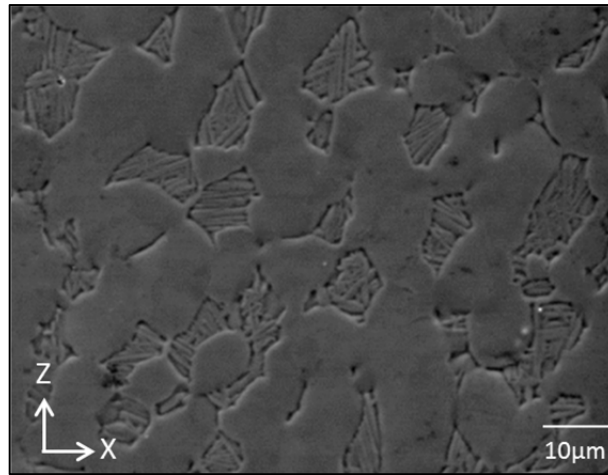
Figure 3-5 Secondary electron micrograph
revealing electro-polished surface prior to
erosion tests

Hardness measurements were realized using the Clemex CMT microhardness indenter with 500g load on XY plane of the sample. An average hardness value of 293±12 HV was obtained from the averaging of 15 individual indentations whose diagonals were accurately measured under SEM.

3.2.3   Characterization procedure and methodology

Initial erosion damage features were examined by SEM and AFM to document the slight damage initiation on the impacted surface. The AFM scanning was realized in tapping mode with a scanning frequency of 0.2 Hz and a scan length of 95 to 97 μm using Si cantilever from Di Enviroscope 5.30 – Veeco. The data was processed via NanoScope Analysis 1.40 software.

To evaluate the initial damage on the surface, SEM observations were made both on the slightly damaged surface as well as through progressive YZ sectional polishing of the plane along the erosion trace (YZ plane) following the similar methodology detailed by the authors in [13]. In order to reach this section, samples were finely cut using low speed diamond blade cutting machine at YZ plane. The cross surface were first ground with SiC

papers and then vibromet polished with monocrystalline diamond suspension. The induced damage was then imaged and evaluated both on the surface and the section.

3.3 Results

3.3.1 Cumulative mass loss curve

The cumulative mass loss during water droplet erosion of forged Ti-6A1-4V versus impingement number is plotted in Fig. 3-6. Mass loss values were normalized through feature scaling to range the data between 0 and 1.The stages of erosion as described by Heymann can be clearly identified for the investigated material up to the advanced stages of erosion [23]. The present work showed an incubation period. 1000 impingements was chosen as intermediate within the initiation stage of erosion in order to be well within the incubation period and the onset of material removal was taken for 20000 impingements as the material loss is just started. Similar observation was also reported in the previous work for rolled Ti-6Al-4V under the same experimental condition [13]. Two new samples were impinged up to the required number of impingements.
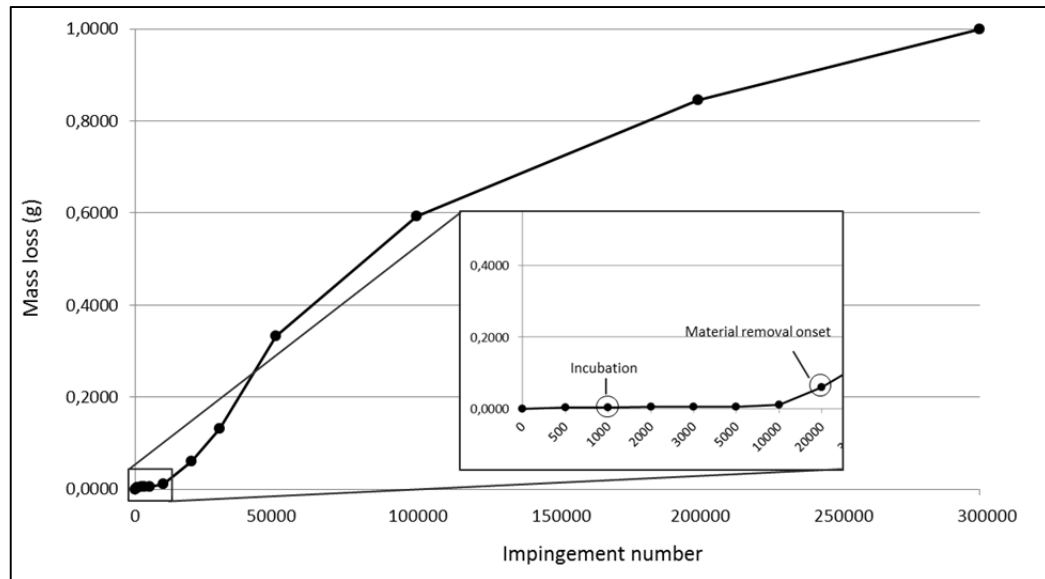
Figure 3-6 Normalized cumulative mass loss vs. number of water droplet impingements

3.3.2 Macroscopic observation of the damage

The erosion features typically found at the incubation period are shown in Fig. 3-7(a) and (b). Around the incubation period no clear erosion lines can be noted. However, the sample presents local damage that can be observed at higher magnifications (Fig. 3-7(b)). The damage sites are found randomly distributed within the three impingement regions. They appear to be micro-scale surface protrusions which are out of the plane, isolated in some areas and can be only found along the droplet impact streams. These features are in contradiction with the general understanding of erosion mechanisms being initiated with mostly surface depressions, micro-voids or pit formation at the surface.

Erosion damage advances as the number of impingement increases and the erosion lines are progressively revealed in Fig. 3-8. The damage is not distributed uniformly along the impact traces, giving the opportunity to see various degradation stages on a given sample. In this respect, different zones where identified showing the damage progression from grain boundary damage to crater formation corresponding to zone A to D respectively. As

in this study the focus was made on the damage progression at the very initial stages, protrusions and the following pits, surface cracks, and material removal features were investigated.
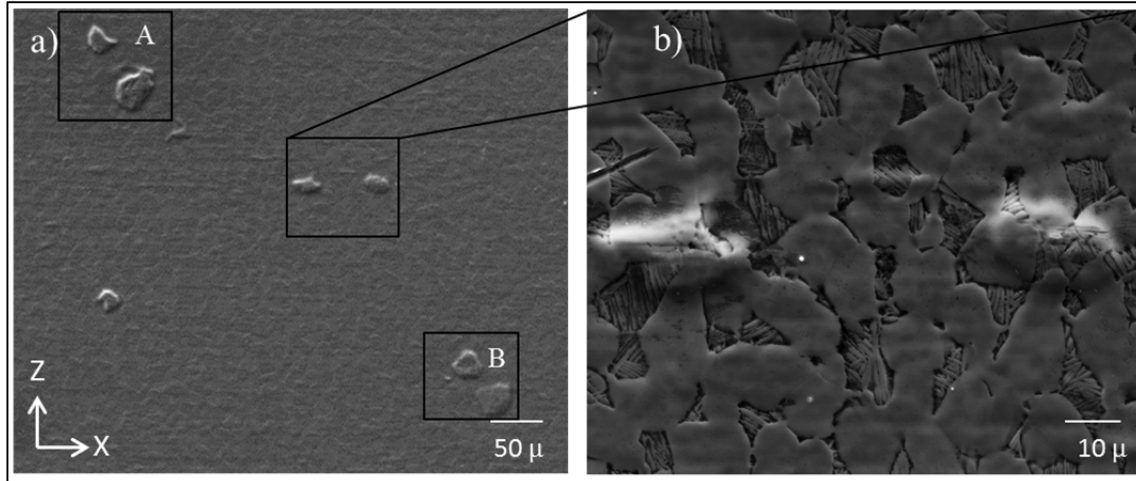
Figure 3-7 SEM micrograph of erosion features typical of the incubation period (1000 impingements) showing: a) large scale and, b) high magnification
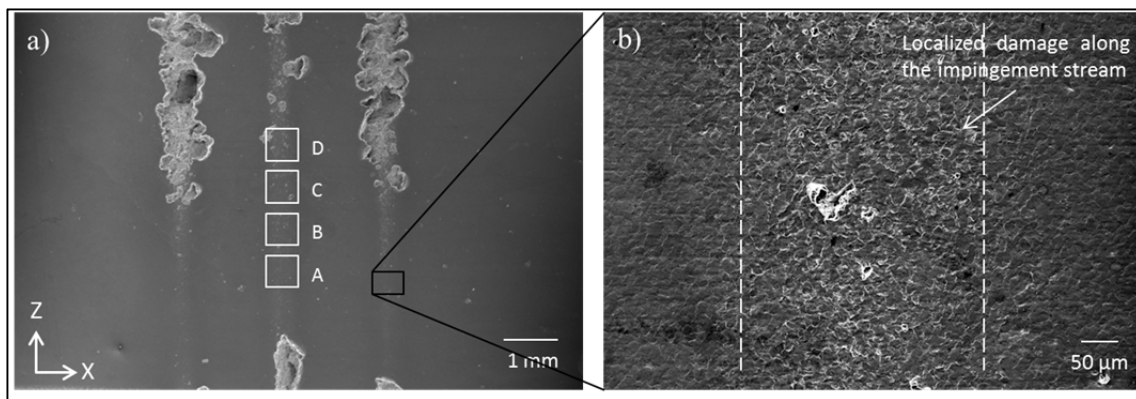
Figure 3-8 SEM micrograph of erosion features at onset of material removal (20000 impingements): a) traces of erosion line and b) high magnification of the erosion line (zone A to D present the erosion progression)

3.3.3 Microscopic observation of the damage

Protrusions from Fig. 3-7(a) are illustrated at higher magnification in Fig. 3-9. The sizes of the protrusions are 10 to 50 μm in width and 2 to 20 μm in height. They were observed on both α_p grains and α_s lamellae. A slight depression sometimes was observed around the edges of the protrusions.

Both the topography of original electro-polished surface and protruded surface were documented by AFM profilometric images. It is clear that the original surface topography is relatively flat as only little contrasts are found revealing grain boundaries; whilst, the protruded surfaces reveal detectable contrast on the impacted surface, indicating out of plane surface. The shallow depressions are clearly observed right off the edges of the protrusions (Fig. 3-10). The height of the protrusions and local depression were statistically analyzed using the profiles documented from the AFM. Fig 3-11, presents the section profiles along the 4 protrusions illustrated in Fig. 3-10 (b) and (c). As indicated, the heights of the protrusion are about 2μm and the shallow depression around the protrusions edges are clearly observed and are about half a micron.
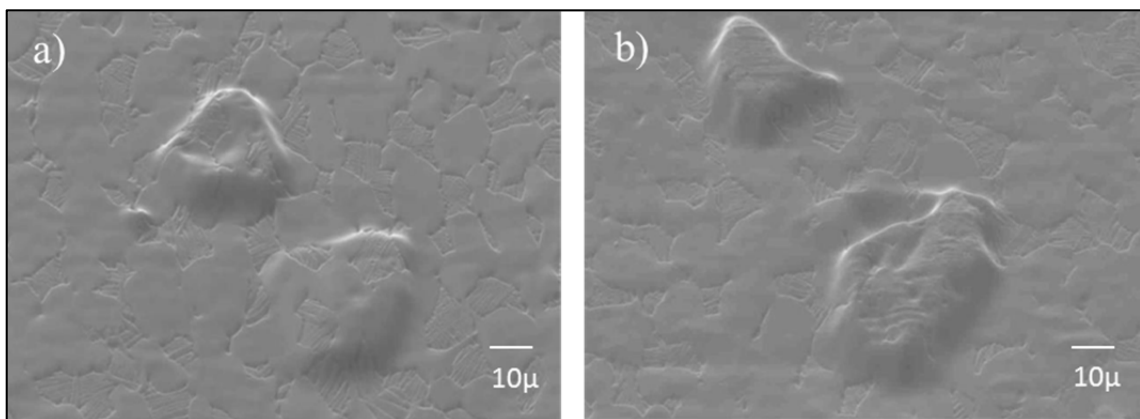
Figure 3-9 SEM surface protrusion at initial stage of erosion from Fig. 3-7 (1000 impingements): a) zone A and b) zone B
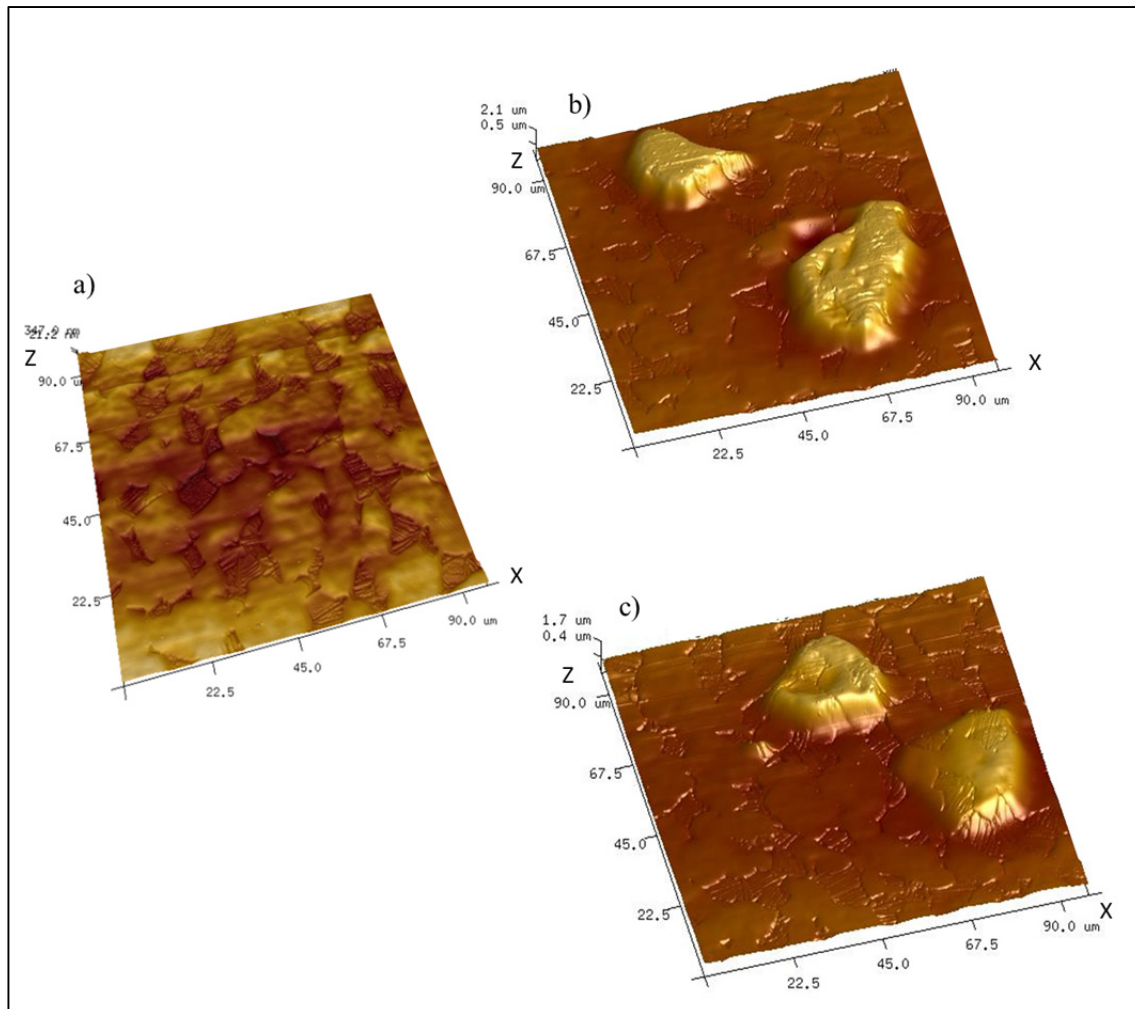
Figure 3-10 AFM topography of a) original surface, and b,c) surface protrusions at (1000 impingements)
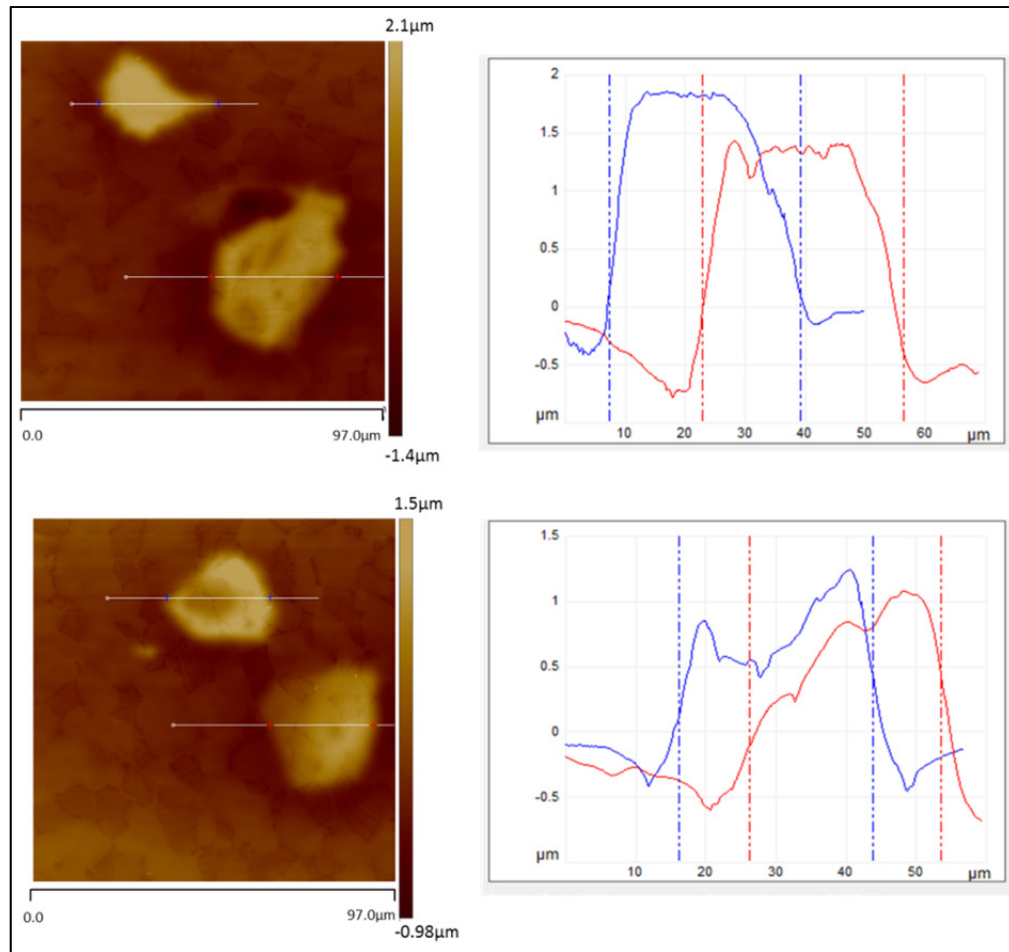
Figure 3-11 Section analyses of the protrusions heights, (1000 impingements)

Advanced erosion features were realized corresponding to zone A, B, C and D in Fig. 3-8 where the erosion damage is progressed through A to D. Zone A illustrated in Fig. 3-12 shows that the first evidence of erosion progression, is grain tilting if compared to the image of the original microstructure (Fig. 3-5). One can see that the contrast on the grain boundaries illustrates the height variation of the grains due to the grain tilting as a result of large number of droplet impacts and their pressure on the surface (Fig. 3-12(a)). Fig. 3-12(b) reveals also the presence of many crystalline slip bands within primary α grains as discussed later.

AFM profilometric images of this zone also clearly shows the changes in surface topography. The undamaged surface (Fig. 3-13(a)) is relatively flat, whilst the damaged surface reveals a very slightly roughened surface with noticeable contrast and direct evidence of grain tilting which has resulted in considerable height variation across grain boundaries (Fig. 3-13(b)). In order to better understand the effect and magnitude of grain tilting, data processing has been conducted on the AFM data using Bruker NanoScope Analysis 1.40. Two average height profiles were displayed in Fig. 3-14. The angles of grain tilting were calculated for 13 selected grains. The average of measurements indicates tilting up to 2.3° with a mean value of 1.2±0.6°. Although the angles of grain tilting were considerably small, the tilting of grains has given rise to steps between the adjacent grains, and therefore the surface has roughened to some extent (Ra=0.103 μm) relative to the original polished surface (Ra=0.062 μm).
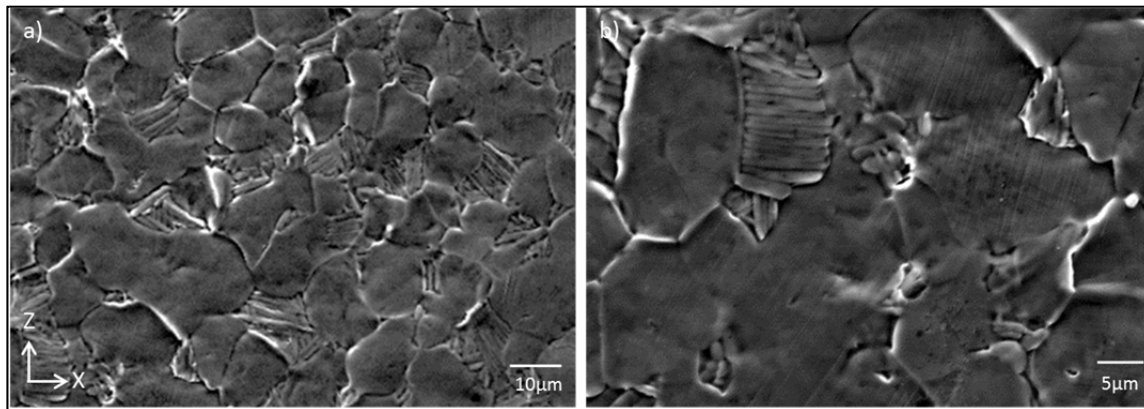
Figure 3-12 Grain tilting observed around zone A after water droplet impacts (20000 impingements): a) large scale b) high magnification
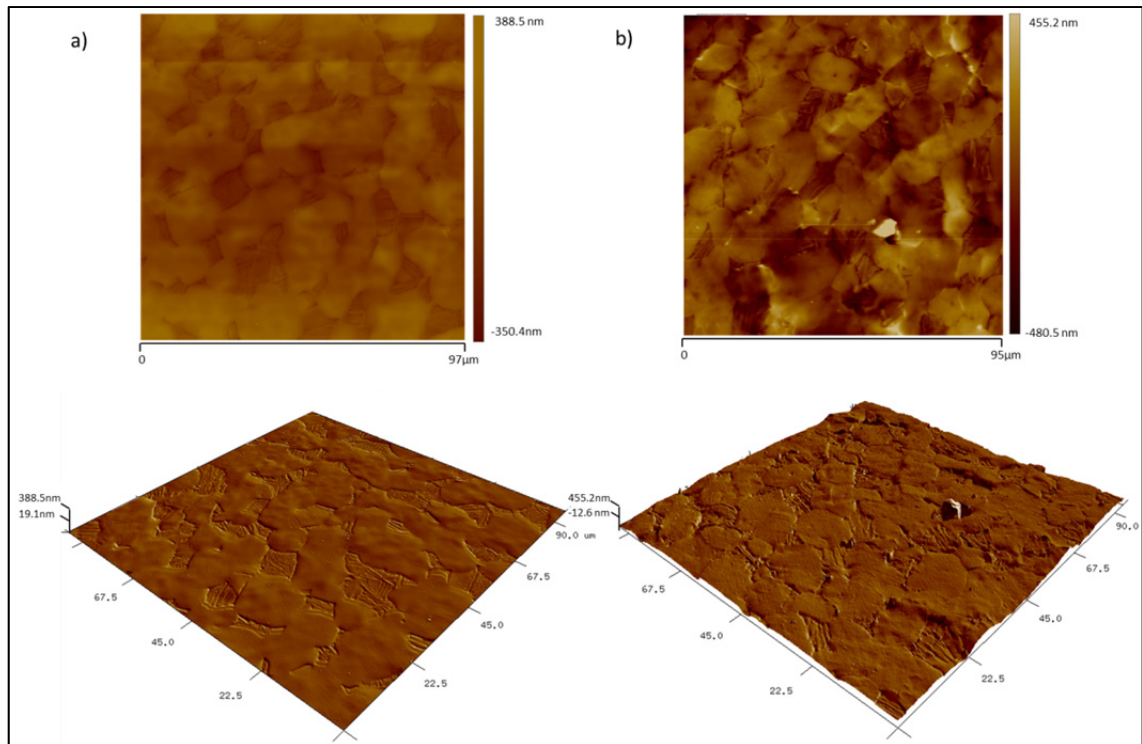
Figure 3-13 AFM height profiles of a) original surface and b)early damage induced by few droplets (20000 impingement stage)
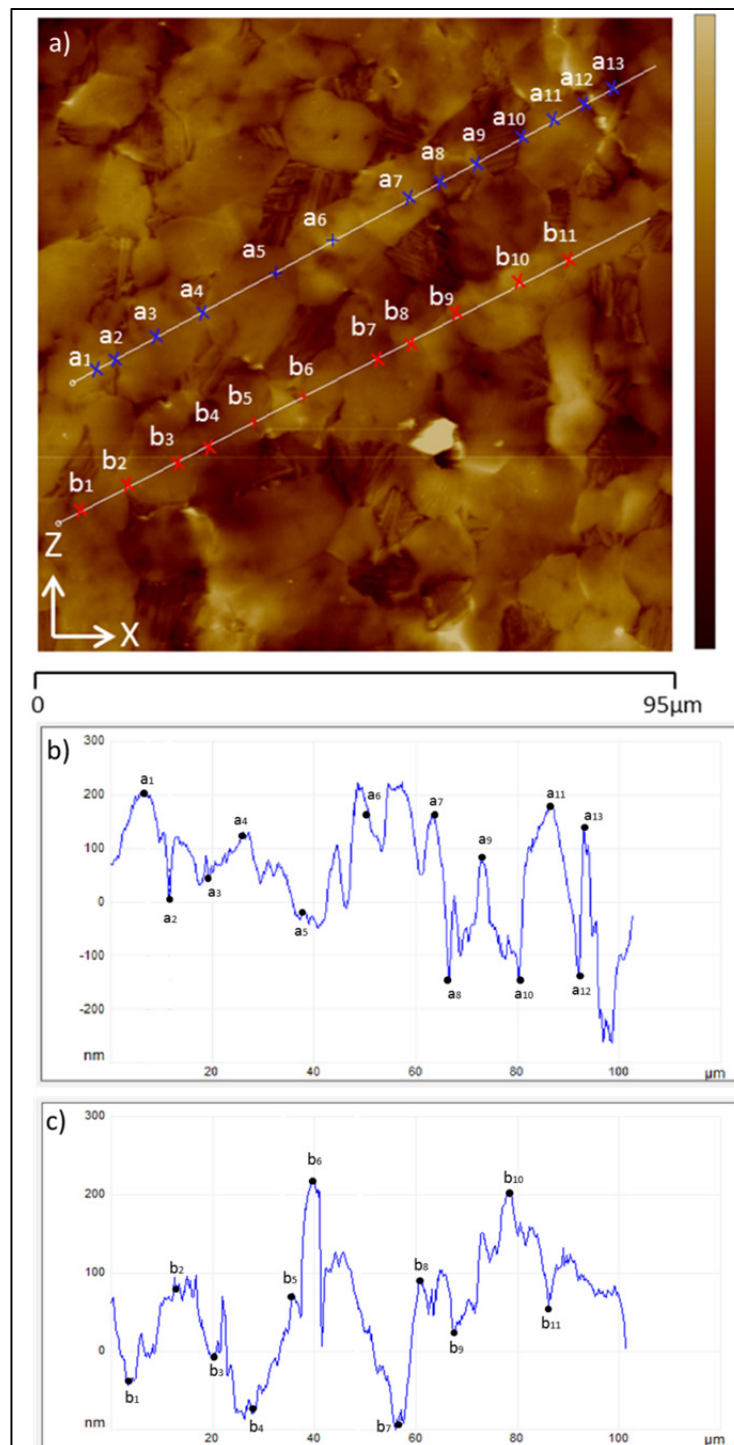
Figure 3-14 Section height profile across the tilted grains
(20000 impingement): a) AFM height image showing the
extracted profiles, b) extracted height profile of line a,
and c) extracted height profile of line b

Increasing the number of droplet impacts results in more grain tilting and severe grain boundary damage, as depicted in Fig. 3-15. Intergranular cracks were observed in the areas around zone B. Examples are illustrated with arrows in Fig. 3-15. These intergranular cracks tend to propagate along the grain boundaries and eventually meet at the triple junctions, leading to material chipping off and micro-voids formation. These features are particularly evident in zone C (Fig. 3-16). Advanced damage and significant material removal consequently occur and as the number of impact increases erosion progresses. Corresponding to zone D, craters are found on more advanced damaged surface seen in Fig. 3-17. Striation marks were also observed inside the craters which suggest a cyclic nature to water droplet impact damage mechanism.
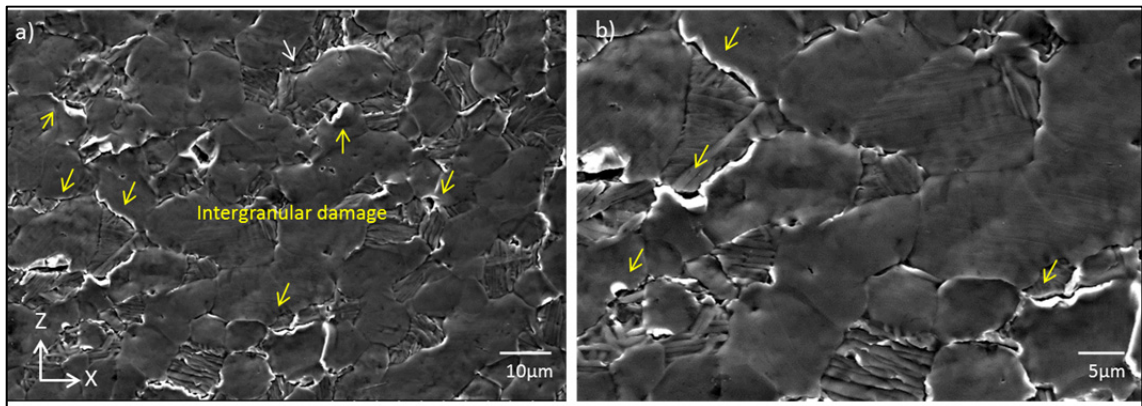
Figure 3-15 Intergranular damage observed at zone B (20000 impingements): a) large scale, b) high magnification
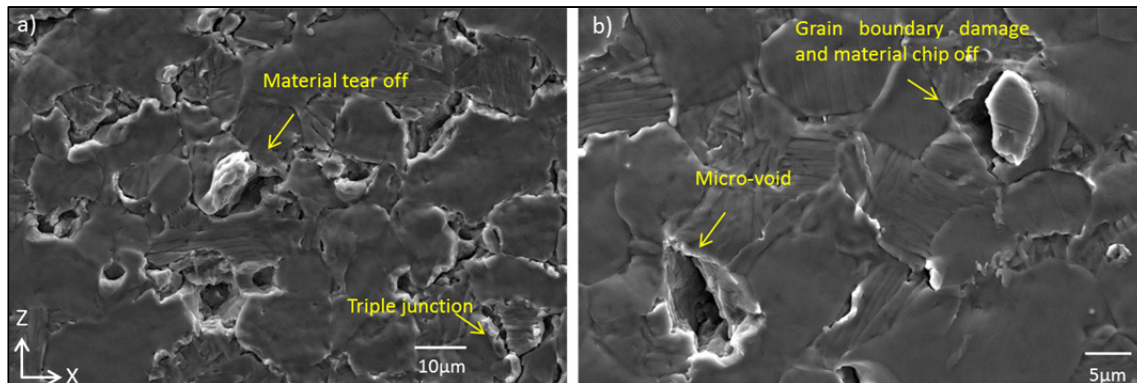
Figure 3-16 SEM micrograph of features observed at zone C (20000 impingements): a) triple junction and material tear off, b) material chip off and micro-voids formation
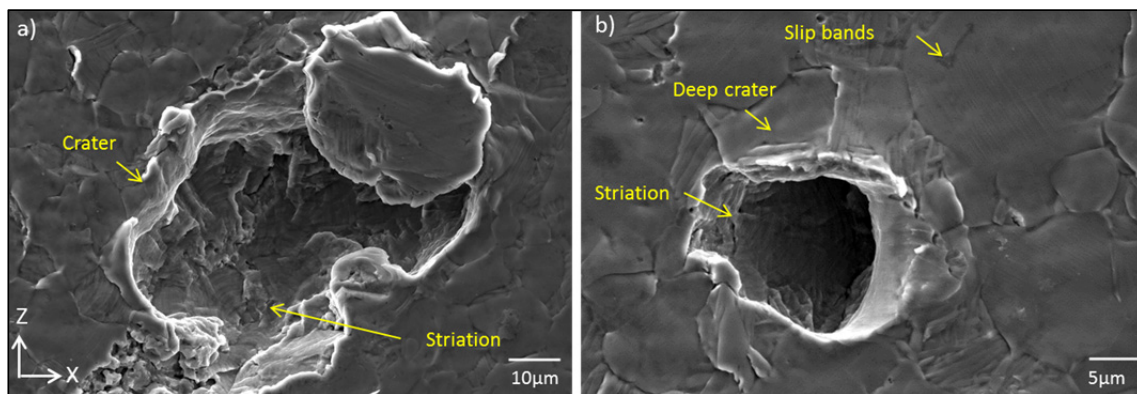
Figure 3-17 SEM micrograph of features at zone D (20000 impingements): a) Crater formation and striation marks, b) deepening the craters and slip lines around the craters

3.3.4   Local microplasticity

Slip bands were observed in primary α-grains on the surface at both incubation stage as well as about onset of material removal as shown in Fig. 3-18. These slip lines were distributed sparsely over the surface at incubation stage; on the other hand they were systematically formed around the rim of craters at the stage of material removal (zone D). The presence of these slip bands suggest that the protrusions or grain boundary tilting and eventually small craters are the result of significant local plastic deformation. Such slip lines were also reported by Futakawa et al. [15] for some alloys under impact erosion test with mercury.
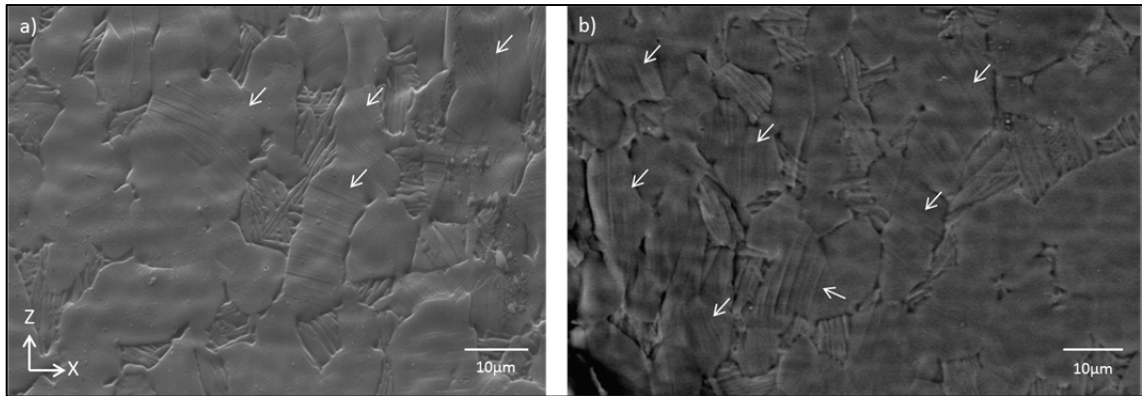
Figure 3-18 Slip bands a) incubation period (1000 impingements) and b) onset of material removal (20000 impingements)

Cross surface polishing was performed on the sample along the erosion line in order to investigate underneath the protrusions observed at initial stages of erosion damage. In order to precisely reach the cross section of the protrusions, progressive polishing using micro caliper was carried out on the sample. Fig. 3-19(a) shows the polished cross section of a protrusion whereas Fig. 3-19(b) is the same area imaged with a 45 degrees tilt. The latter aims to present in one image, both the impinged surface and corresponding sub-surface. The initial surface deformation mechanism of the material is related with the presence of micro-cracks right underneath the protrusion. At this stage, it is actually a network of micro-cracks that were formed at about 100-150 µm below the sample surface. The size of the observed cracks ranged from 10 µm to 30 µm which is around the average α-grain size. Cracks propagate in a transgranular mode, mostly within the α-grains and almost up to the grain boundaries which may act as a microstructure barrier. There are also some secondary cracks propagating within the lamellar matrix.

The orientation of the cracks tend to propagate at 45 degrees with respect to the loading direction, suggesting that the high plasticity zone is in this region and that cracks have nucleated along high shear stress planes. Some cracks also propagate at around 90 degrees but they are likely to be secondary ones. Then their propagation path may depend on either the local stress state or the microstructure, both crystallographically and morphologically.

It should be noted that some protrusions were also observed without the presence of any cracks underneath (Fig. 3-20), showing that the protrusions formation is most probably due to the localized plastic deformation and is not necessarily the consequence of subsurface cracks.
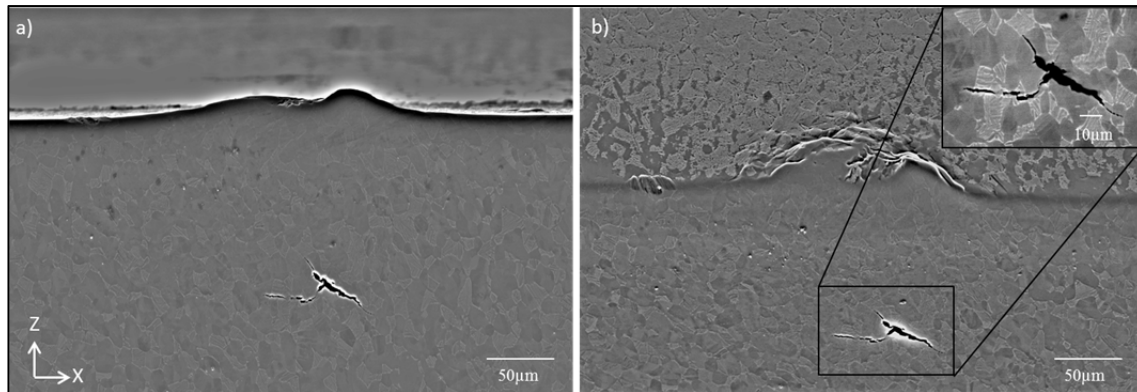
Figure 3-19 Sample cross section revealing underneath of the protrusions, (20000 impingements)
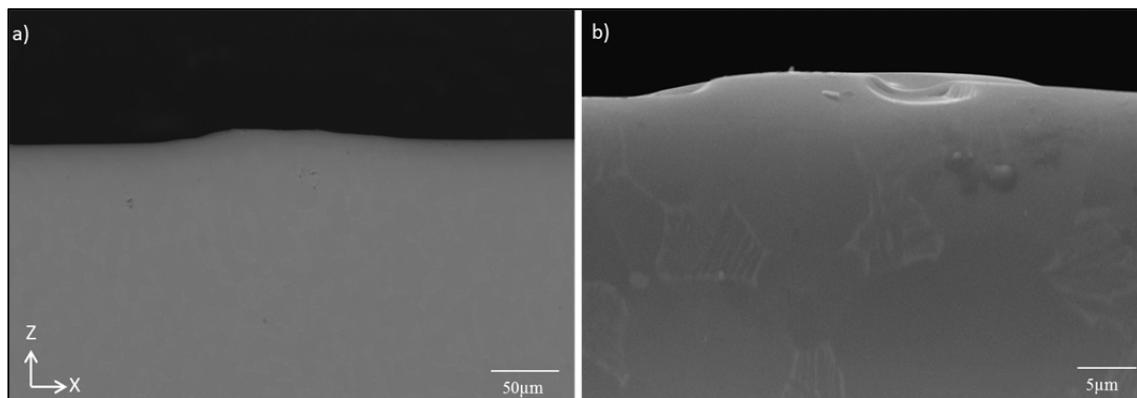
Figure 3-20 Protrusions without cracks underneath (20000 impingements): a) large scale and b) higher magnification

3.4 Discussion

As the work presented here focused on the early erosion damage of forged Ti-6Al-4V exposed to water droplet impacts, the regions under investigation were impacted with only limited numbers of impingements. It reveals the initiation mechanisms of the material

removal process. The investigated surface evolves from a slight local damage to a larger scale material removal in form of craters.

Surface features indicated that severe plasticity is taking place due to the local pressure generated by droplet impacts. However, the Hertz theory of impact predicts that the maximum pressure and plasticity is expected under the surface and larger stress fields are expected at these locations [26]. As shown in Fig. 3-18, sub-surface cracks are formed underneath the protrusions at a distance of between 100 to 150μm, suggesting that the maximum impact pressure occurs around these depths.

The surface protrusion or appearance of the protrusions on the surface then cannot be only related to the presence of sub-surface cracks as some protrusions did not present any cracks beneath the surface (Fig. 3-20). An explanation could lie in the local sub-surface plasticity as observed in several mechanical surface treatments [27-28].

Transgranular cracks were systematically observed on the primary cracks below the protrusions and these cracks were always observed at about 45° from the Y or impact direction. This nucleation mode is typical of low cycle fatigue of near-α and α/β Titanium [24]. The observation of transgranular cracks as the first damage mode of water erosion (at the incubation stages, i.e. the 1000 impingements) suggest that repetitive nature of water droplet impacts may result in low cycle fatigue induced by strong plastic strain of the water droplet impact pressure.

Increasing the number of impingements results in more surface plastic deformation and more slips activations as shown in Fig. 3-18. Thus, intergranular cracks start to form at the initial stage, as depicted in Fig. 3-15(a) possibly due to some plastic incompatibilities between deformed grains. The non-uniform distribution of the grain boundary damage over the surface may be due to the different crystal orientation of the neighboring grains or the random nature of droplet impacts. At this stage the damage is heterogeneously distributed on the surface, both at macro and microscopic scale. Widely distributed

intergranular cracks as well as some central grain damage were also reported by Huang et al. [19] when analyzing a similar stage of damage induced by plain water jet on Ti-6Al-4V. Striation marks were also reported in transgranular crack propagation mode. Striation marks were found in the most severely deformed regions of the sample at the initial stage of erosion. These marks are typical of the advanced erosion stages [13]. In both cases, the striations reveal the cyclic nature of material removal process and transgranular crack formation seems to be the primarily damage mechanism. Therefore it might indicate that the material removal mechanism of the initial stages of erosion is not distinct from the advanced stages of damage. Local severe plasticity issues seem to be the main mechanisms that lead to transgranular cracks that control the erosion damage mechanism, pointing out a fatigue-like mechanism in the previous work [13].

3.5   Conclusions

The present work concentrates on the onset of water erosion damage in forged Ti-6Al-4V for typical industrial operation conditions. The damage initiation was documented at the incubation and the onset of material removal based on the experimental evidence. Sub-surface cracks resulting from severe local plastic deformation appears to be a major contributor to early erosion and transgranular cracks are likely to form at first. The mechanism of damage initiation is proposed as follows: (i) droplet impact pressure causes high local stress field underneath the surface at the impact location, (ii) the region is plastically deformed and a local residual stress field is likely to be generated (significant compressive residual stresses close to the elastic limit), (iii) high local deformation cycles are generated and cracks form as in LCF conditions, (iv) the cracks will grow forming a network of sub-surface cracks, (v) the sub-surface plasticity is thought to be responsible for the surface upheaval. The repeated deformation cycles result in grain tilting and finally intergranular crack nucleation at the surface. Following transgranular crack nucleation were observed and are responsible for the material removal as the erosion advances due to the increased number of impacts.

References

[1] R.K. Bhargava, C.B. Meher-Homji, M.A. Chaker, B. Bianchi, F. Melino, A. Peretto, S. Ingistov, Gas turbine fogging technology: a state-of-the-art review-Part 3: Practical considerations and operational experience, Journal of engineering for gas turbines and power 129 (2007) 461-472.

[2] R.K. Bhargava, C.B. Meher-Homji, M.A. Chaker, B. Bianchi, F. Melino, A. Peretto, S. Ingistov, Gas turbine fogging technology: a state-of-the-art review-Part 1: Inlet evaporative fogging-Analytical and experimental aspects, Journal of engineering for gas turbines and power 129 (2007) 443-453.

[3] C.B. Meher-Homji, T. R. Mee, Gas Turbine Power Augmentation by Fogging of Inlet Air, Proceedings of the 28th Turbomachinery Symposium (1999) Houston, TX, Sept.

[4] N. Yasugahira, K. Namura, R. Kaneko, T. Satoh, Erosion resistance of Titanium alloys for steam turbines blades as measured by water droplet impingement, in Titanium Steam Turbine Blading, Palo Alto, 2988, Pergamon, New York (1990) 385-401.

[5] W.F. Adler, Analysis of particulate erosion, Wear 37 (1976) 345-352.

[6] B.S. Mann, V. Arya, An experimental study to correlate water jet impingement erosion resistance and properties of metallic materials and coatings, Wear 253 (2002) 650-661.

[7] A.F. Conn, S.L. Rudy, Effects of fatigue and dynamic recovery on rain erosion. ASTM STP 567 (1974) 239-269.

[8] R.H. Richman, W.P. McNaughton, Correlation of cavitation erosion behaviour with mechanical properties of metals, Wear 140 (1990) 63-82.

[9] R.H. Richman, W.P. McNaughton, A metallurgical approach to improve cavitation-erosion resistance, J. Mater. Eng. Perform. 6 (5) (1977) 633-641.

[10] A.W. Momber, Y.C. Wong, E. Budidharma, R. Tjo, Hydrodynamic profiling and grit blasting of low-carbon steel. Tribology International 35 (2002) 271-281.

[11] W.F. Adler and R.F. Vyhnal, Rain erosion of Ti-6A1-4V, 4th Int. Conf. on rain erosion and associated phenomena, Meersburg, Germany, May, 1974.

[12] J.M. Robinson, R.C. Reed, Water droplet erosion of laser surface treated Ti-6Al-4V, Wear 186-187 (1995) 360-367.

[13] N. Kamkar, F. Bridier, P. Bocher, P. Jedrzejowski, Water droplet erosion mechanisms in rolled Ti-6Al-4V, Wear 301 (2013) 442-448.

[14] G. P. Thomas, J. H. Brunton, Drop impingement erosion of metals, Proc. R. Soc. Lond. A. 314 (1970) 549-565.

[15] M. Futakawa, H. Kogawa, R. Hino, H. Date, H. Takeishi, Erosion damage on solid boundaries in contact with liquid metals by impulsive pressure injection, Int. J. Impact Eng. 28 (2003) 123-135.

[16] H. Date, M. Futakawa, effect of tensile waves on impact erosion at soli/liquid interface, Int. J. Impact. Eng. 32 (2005) 118-129.

[17] M.C. kong, D. Axinte, W. Voice, Aspects of material removal mechanism in plain waterjet milling on gamma titanium aluminide, J. Mater. Process. Technol. 210 (2010) 573-584.

[18] A. Chillman, M. Ramulu, M. Hashish, Waterjet peening and surface preparation at 600 MPa: A preliminary experimental Study, J. Fluids Eng. 129 (2007) 485-490.

[19] L. Huang, J. Folkes, P. Kinnel, P. H. Shipway, Mechanisms of damage initiation in a titanium alloy subjected to water droplet impact during ultra-high pressure plain waterjet erosion, J. Mater. Process. Technol. 212 (2012) 1906-1915.

[20] ASTM Standard G73, 2004 (2010), standard test method for liquid impingement erosion using rotating apparatus, ASTM International, West Conshohocken, PA, 2010, DOI: 10. 1520/C0033-03R06, www.astm.org.

[21] A. Uihlein, C. M. Maggi, I. Keisker, Water droplet erosion at steam turbines; testing method and validation, Proc. Milan Inter. Conf. on solid particle and liquid droplet erosion: Part 2 (2012) 81-93.

[22] P.A. Coulon, Erosion – corrosion in steam turbines II: a problem largely resolved, Lubr. Eng. 42 (1986) 357-362.

[23] L. Germain, N. Gey, M. Humbert, P. Vo, M. Jahazi, P. Bocher, Texture heterogeneities induced by subtransus processing of near α titanium alloys, Acta Mater. 56 (2008) 4298-4308.

[24] F. Bridier, P. Villechaise, J. Mendez, Slip and fatigue crack formation processes in an α/β titanium alloy in relation to crystallographic texture on different scales, Acta Mater. 56 (2008) 3951–3962.

[25] F. J. Heyman, Liquid impingement erosion, in: Wear, ASM Handbook, Vol. 18, ASM, 1992, pp. 221-232.

[26] W. J. Stronge, Impact mechanics, Cambridge [England], Cambridge University Press, New York, 2004.

[27] D. W. Hammond, S. A. Meguid, Crack propagation in the presence of shot-peening residual stress, Eng. Fract. Mech. 37, No. 2 (1990) 373-387.

[28] A. Gariépy, F. Bridier, M. Hoseini, P. Bocher, C. Perron, M. Lévesque, Experimental and numerical investigation of material heterogeneity in shot peened aluminum alloy AA2024-T35, Surf. Coat. Technol. 219 (2013) 15-30.

CHAPTER 4

ARTICLE 3: INFLUENCE OF WATER DROPLET IMPACT VELOCITY ON EROSION OF TI-6AL-4V

N. Kamkar [1], F. Bridier[1], P. Jedrzejowski [2], P. Bocher [1]

[1]Mechanical Engineering Department, École de Technologie Supérieure (ÉTS), 1100 Notre-Dame Ouest, Montreal, QC, Canada H3C 1K3

[2]Rolls-Royce Canada Ltd-Energy, 9545 Cote-de-Liesse, QC, Canada H9P 1A5

Abstract

Water droplet erosion is a concern in gas turbines application because it may cause operational problems such as performance degradation and reduction of service life. The parameters which mainly influence the liquid impingement erosion are the impact velocity and droplet size. Several studies have been conducted on the effect of droplet size; however, there are limited to the effect of impact velocity on erosion mechanisms, more specifically for the velocities correlated to the in-service conditions of gas turbines. In this study, effect of impact velocity on liquid impingement erosion was studied for Ti-6Al-4V alloy used as compressor blade in gas turbine. Three different velocities, i.e., 250, 300 and 350 m/s, were selected to represent typical linear speeds along the leading edge of gas turbines compressor blades. It is found that erosion mechanism by liquid impingement proceeds due to fatigue. The incubation period was correlated to the droplet velocity that is found to be similar to the fatigue S-N curve. Erosion rate is significantly influenced by impact velocity. The influence of the impact velocity on erosion rate was investigated and for a particular condition, it is realized to follow the power function of impact velocity and the velocity exponent was nine.

4.1 Introduction

Liquid impingement erosion is a serious problem in many critical components such as blades of low-pressure steam turbines, rain erosion in aircraft, missiles and helicopter and recently

in gas turbine engine where inlet fogging is used to increase power efficiency during hot days [1, 2]. Inlet fogging system may results in erosion damage at leading edge of compressor blade due to the droplet impacts and efficiency lost as a result of change in profile [3].

Among the operational variables which influence liquid impingement erosion, the velocity of the impact is an important variable in governing the severity of erosion and has the most remarkable influence on erosion rate [4, 5].

Considerable amount of works was directed at finding the relationship between erosion rate and impact velocity. The erosion rate markedly varied with impact velocity and preferably described by a power law equation as $E_R \propto V^n$ where E_R is the erosion rate (instantaneous), V is the impact velocity and n values which varies for different materials are reported to be 4-5 for ductile materials and 6-9 for brittle materials depending on the erodent size, impact angle, etc. [6-7]. For some materials a threshold velocity was obtained below which erosion was not detected or the erosion rate is negligible [8]. The threshold velocity was estimated for different pipe steels (low carbon steel S15C, stainless steel SUS304, and alloy steel STPA24) subjected to cavitation or liquid impact erosion; however there is not clear conclusion on its value for different alloys [4]. It is noteworthy that Coulon defined in 1985 ranges of velocities, for various materials including Titanium alloys, where corrosion and erosion phenomena can be distinct. It is reported that for the velocities below 10 m/s no erosion damage occurs and the process is only due to corrosion, from 10 to 50 m/s corrosion mechanism dominates with less erosion occurring, from 50 to 200 m/s erosion mechanism is dominant and above 200 m/s only erosion is observed [1, 9].

Regarding the erosion behavior of Ti-6Al-4V, the mechanisms of material removal have been studied previously [10]. However, only a couple of studies were carried out to investigate the effect of different impingement parameters and particularly of impact velocity. Yarramareddy and Bahadur [7] have investigated the variation of erosion rate with the average velocity of impacting droplets (35 m/s to 80 m/s) and found that the exponent n equals to 2.35 for the power law mentioned earlier. Recently Lee et al. [3] showed the

influence of increasing the water droplet particles impact velocity on erosion rate for some blade materials including Ti-6Al-4V for velocities ranging from 450 m/s to 650 m/s. It is reported in their work that exponent n is about 5.

While such studies have empirically demonstrated the strong dependence of erosion rate on impact velocity, the mechanisms of the material removal relative to impact velocity has not been studied comprehensively. Moreover, no work has been done to correlate these results with the actual compressor rotation speeds and the actual microstructure seen for compressor blades. In this study, the effect of impact velocity on liquid impingement erosion is investigated with regards to the cracks behavior and erosion features for the selected Ti-6Al-4V samples bearing similar microstructural features to the blade materials. The erosion mechanisms are discussed for impact velocities typical of compressor blades in gas turbine.

4.2 Materials and methodologies

4.2.1 Materials and sample preparation

As typical water impingement specimen could not be machined directly from gas turbines compressor blades, the primary concern in this study was to find an appropriate sheet or bar material which would correlate most to the blade material in terms of microstructure and crystallographic texture. Crystallographic texture analyses of compressor blades were carried out and it was found that the blade material presents the typical texture of cold rolled Ti-6Al-4V, although the manufacturing process might not be a plain rolling process. Cold rolled Ti-6Al-4V alloy presents basal or near-basal texture with the [0001] poles up to 40∘ toward the transverse direction (TD) of the deformation path [11]. Therefore textures from cold rolled samples were analyzed on different Ti-6Al-4V plates in order to find the most representative of the blade material for both microstructure and texture conditions.

The material subjected to water droplet impingement erosion test in this study is a 3mm thick cold rolled Ti–6Al–4V plate with a similar texture to a compressor blade (Fig. 4-1 (a)) with

RD//leading edge, TD//blade width direction, and ND//impingement direction. The crystallographic texture measurements were obtained thanks to an electron back-scattered diffraction map (EBSD) with a 2 micron step size on an Oxford - Channel 5 system. The corresponding pole figures for both (0001) and {10-10} planes were calculated from the EBSD data and are shown in Fig. 4-1. It can be noted that the present material is crystallographically textured. The maximal multiple of uniform distribution (MUD) factor is 5.6 for the {0001} pole figure for the rolled plate which is slightly higher than that of in-service blade. The preferential orientation indicates that most α phase presents a nearly basal texture with the poles tilted by 25 degrees with the normal direction (ND) of the rolled plate toward TD direction. Crystallographic texture is known to influence the mechanical resistance of the alloy relative to the loading direction due to the elasto-plastic anisotropy of the hcp α-phase in Titanium alloys. As an example, Bache and Evans in 2001 showed an increase of yield strength from 970 MPa up to 1100 MPa between longitudinal and transverse direction of a highly textured rolled plate of Ti-6Al-4V [12]. Similar anisotropy in fatigue resistance was observed and such differences in mechanical behavior were related to the ability to induce slip in the various plate orientations [13]. Therefore, the impact direction is important either in in-service conditions or in correlating experiments with the in-service conditions.

The microstructure of the rolled plate, shown is Fig. 4-2, presents mostly elongated primary alpha grains α_p and some area of equiaxed α-grains. The elongated primary α grains are organized into macro-bands of a few hundreds of microns. However, the microstructure of the blade (not shown here), presents mostly equiaxed α-grains with some area of elongated grains which can be due to the manufacturing process.
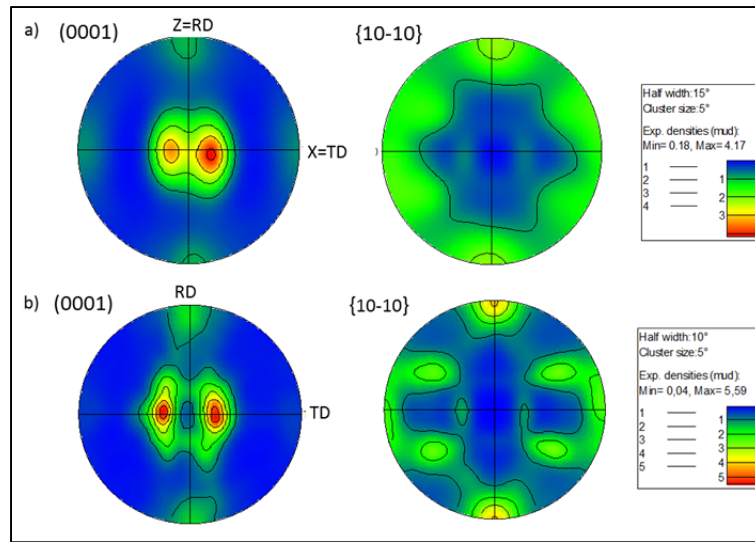
Figure 4-1 a) pole figure of the blade material, b) pole
figure of rolled microstructure
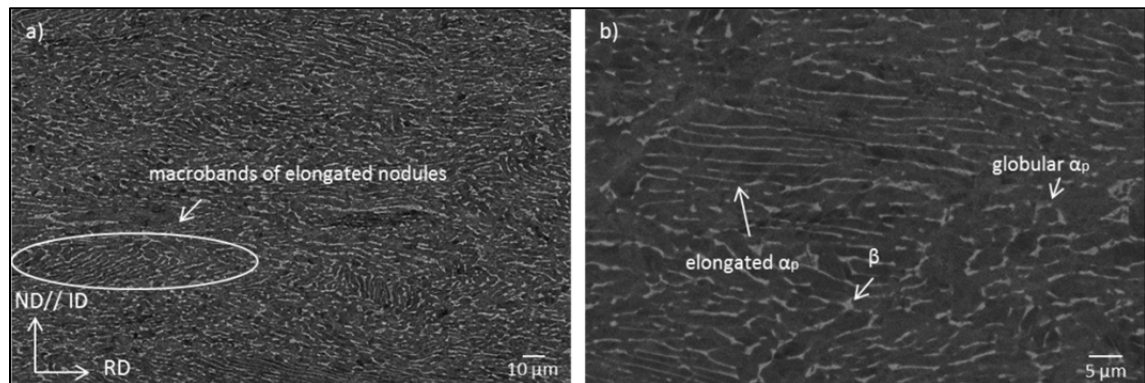
Figure 4-2 SEM micrograph of rolled microstructure: a) lower and b) higher
magnification

4.2.2   Hardness of investigated alloy relative to measurement direction

Hardness is generally assumed to be the property which to a large extent determines the
erosion resistance. Increasing the hardness of base material results in decreasing the erosion
rate of the material [5, 8, 14, 15]. Hardness variations relative to the indentation direction
were reported earlier for a rolled Ti-6Al-4V [10]. Therefore micro-hardness measurements of
the investigated material were conducted with the indentation in two directions: in the

impingement direction, i.e., parallel to ND direction, and in TD direction. The hardness measurements were realized using a Clemex CMT microhardness indenter with 500g to minimize the scatter of the results as larger indents cover more metallurgic grains and give more representative estimation of the hardness value in a single direction. Each hardness value is the average of minimum ten indentations whose diagonals were accurately measured under SEM. The hardness values are obtained to be 313±17 HV and 285±13.2 HV in ND//ID and TD directions respectively. The variation of hardness is due to the strong crystallographic orientation [10].

4.2.3   Experimental set up and water erosion test

Flat samples of 25 mm length, 8 mm width and 3 mm thickness were exposed to water droplet impact erosion tests with a water jet nozzle on a rig according to ASTM international G73 standard [16]. The test was performed under 30mbar vacuum pressure at ambient temperature. Nozzle diameter was 400μm giving a mean droplet diameter of 450μm.

Schematic of the eroded samples is depicted in Fig. 4-3 showing one erosion mark leading to one line of craters with the impingement direction ID parallel to the normal direction (ND) of the plate. The varied linear impact velocities were selected to 250, 300 and 350 m/s. The samples were subjected to repetitive impacts normal to the surface. The coupons were impacted by the droplet stream once per revolution and the term ''number of impingements'' refers to the number of times the sample has intersected the stream.
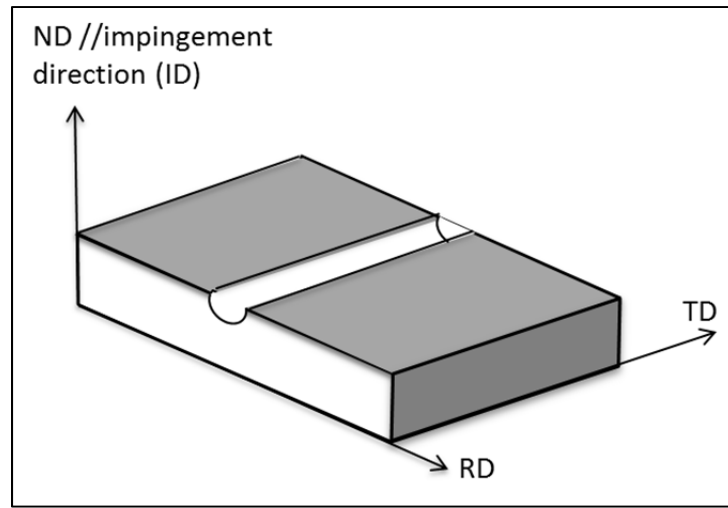
Figure 4-3 Schematic of the sample with an erosion
line due to water droplet impingements on top surface
and the reference directions of the cold rolled plate

Two sets of experiments were designed and performed in order to investigate the influence of the impact velocity on erosion rate and features. The first set compares the samples at the same amount of material loss (0.005 g) to investigate the influence of velocity on early damage features. In the second set of experiment, coupons were eroded with the same number of impingements (100000) to relate erosion features with impact velocity under a certain numbers of impingements. Erosion curve were also obtained thanks to interruptions and weight measurements.

4.2.4   Characterization procedure and methodology

Erosion damage features were characterized at different conditions and the samples were compared through qualitative observation and quantitative measurements using SEM.

To evaluate the erosion damage to greater extent, observation were carried out on both eroded surface and through progressive cross sectional polishing on ID-RD plane. Progressive cross sectional polishing helps to increase the statistics of the evaluations and to better document the damage mechanisms. In order to do that, coupons were carefully grinded

on the cross section with the SiC papers and then polished using Buehler vibratory polisher for 24 hours. The induced damages were then imaged and evaluated both on the surface and the section. This surface preparation does not alter the erosion feature as no chemical etching is used. The damages then were imaged with both secondary and back scattered microscopy at low and high magnifications.

4.3   Results

4.3.1   Cumulative mass loss during erosion testing

The cumulative mass loss during water droplet erosion of rolled Ti-6A1-4V vs. impingement number is plotted in Fig. 4-4. The typical stages of erosion defined by Heymann can be clearly identified for the investigated material up to a steady state with 350 m/s and 300 m/s; however, for 250 m/s, only the onset of material removal could be documented [1]. It is generally found an incubation period in Titanium water droplet erosion; however the length of incubation period varies due to material or erosion parameters (droplet size and distribution, impact velocity, flow rate, etc.) [5, 10]. Taking into account the presence of incubation time for the material under investigation, the length time of the incubation appears to be strongly influenced by the impact velocity. It is relatively shorter when the impact velocity is higher presenting more severe erosion conditions. The incubation period is found to be at 360,000 impingements for 250 m/s, at 72,000 impingements for 300 m/s, and at 14,000 impingements for 350 m/s, giving an approximate exposure time of 36, 6, and 1 minute respectively.
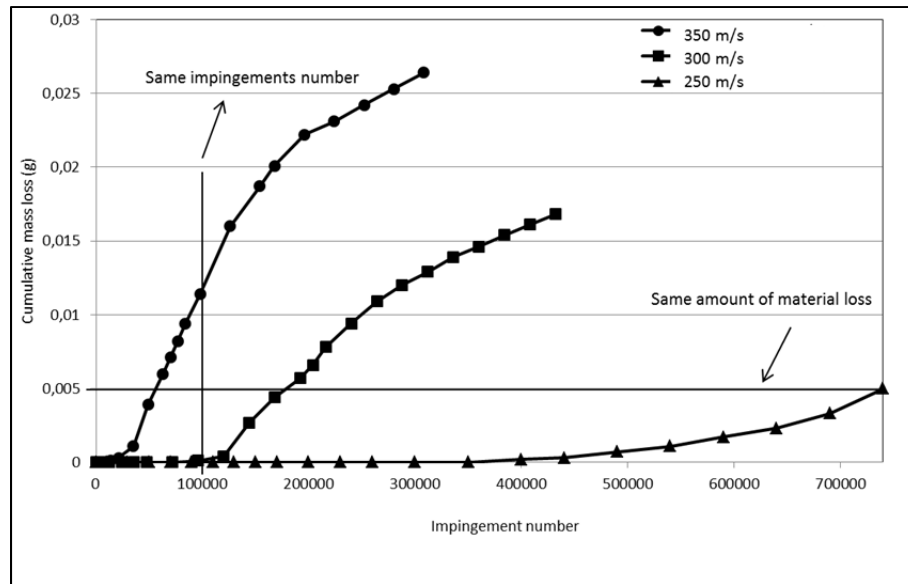
Figure 4-4 Cumulative mass loss vs. impingements number and time
of exposure

4.3.2   Macroscopic observation of the damage

Macroscopic analysis of the samples was conducted on the eroded surface RD-TD and on the perpendicular cross-sectional plane ID-RD. Eroded surface examination reveals a localized damage along the erosion lines as illustrated in Fig. 4-5. These lines are actually the accumulation of multiple circular craters. The damage distribution however varied along the line, i.e. erosion starts from the top of the coupons and progressed along the droplet stream. For the same amount of removed material (Fig. 4-5(a), (b), and (c)), the average width of erosion lines were estimated to be 0.88mm, 0.91mm, and 0.95mm for the coupons impacted with 250 m/s, 300 m/s, and 350 m/s respectively. From the macroscopic observation of the coupons impacted with the same number of impingements (Fig. 4-5(d), (e), and (f)), it is clear that the erosion is more advanced when the impact velocity is higher. The average widths of erosion lines are 1.20mm for 350 m/s, lower to 0.58mm for 300 m/s, and no significant damage were observed for 250 m/s.
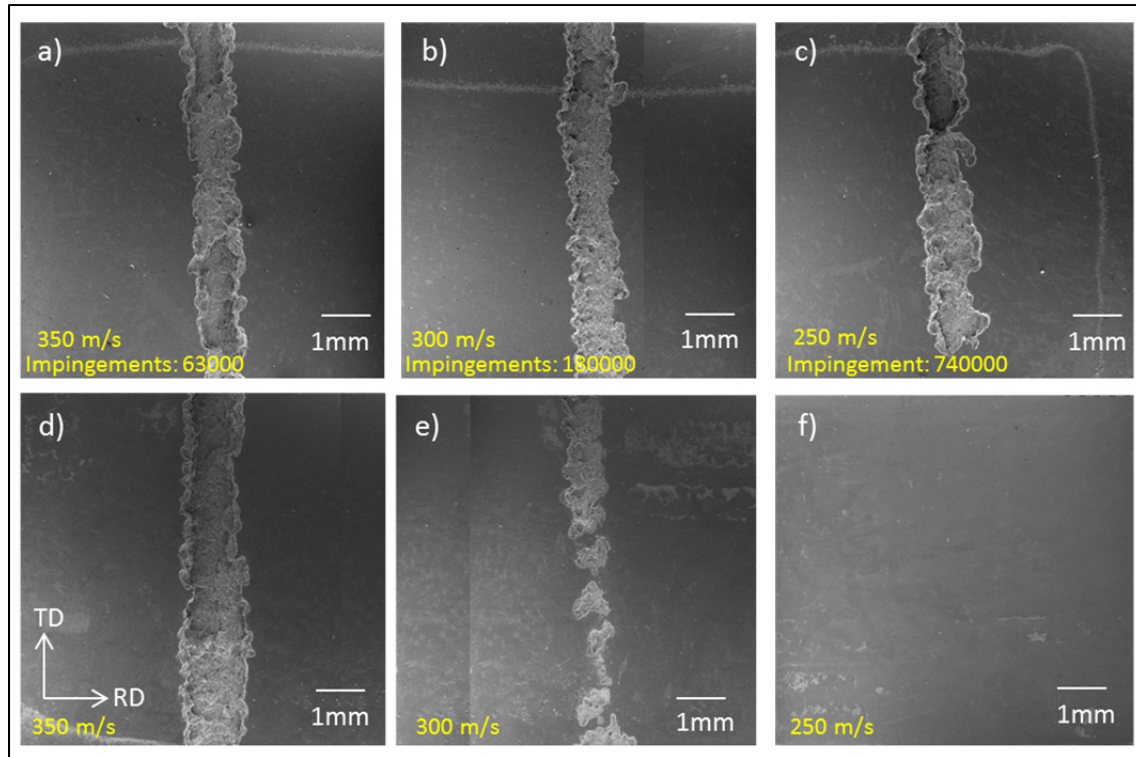
Figure 4-5 Localized damage lines induced by water droplets with varied impact velocity; a, b, and c) same amount of material loss (0.005g) and d, e, and f) same impingements number (100000)

The nearly circular damage induced by only few very first droplets, are referred to a crater in this paper. Note that this damage is not the result of single droplet but few numbers of impingements. The images were taken from the earlier stages of erosion for each velocity and show that the induced damage in Fig. 4-6 at higher velocity impacts results in wider and deeper craters. The craters are smaller when impact velocity slows down to 300 m/s and no visible crater were observed on the coupon impacted with 250 m/s velocity. The only damage in this coupon is some evidence of grain tilting followed by intergranular damage (see Fig. 3-12, Chapter 3).
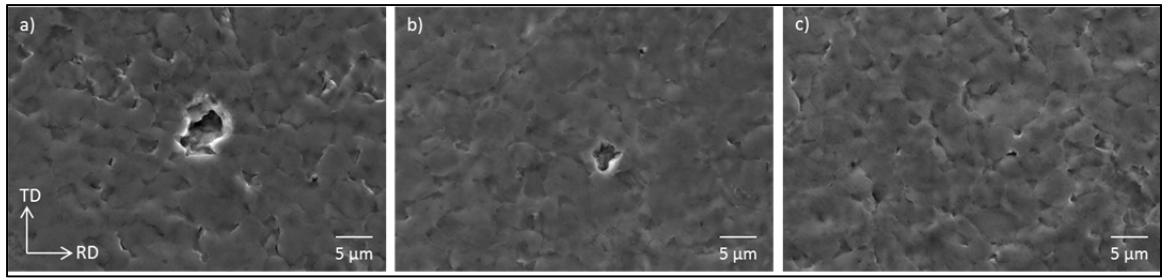
Figure 4-6 Initial damage induced with few impingements; a) 350 m/s, b) 300 m/s, and c) 250 m/s

However, top surface observation is not sufficient to capture the erosion mechanisms [10]. Average depths of penetration were measured via SEM through progressive polishing from top of the coupons where the maximum damage occurs. Some examples are given in Fig. 4-7. For the same amount of material removal, the average depth of penetration was estimated to be 235 μm for 250 m/s, 205 μm for 300 m/s, and 275 μm for 350 m/s. However for the case of same impingement number the estimated average depth of penetration was found to be 240 μm for 300 m/s and 405 μm for 350 m/s. No sign of erosion was observed for 250 m/s impact velocity. The coupons impacted with equal impingement numbers confirm the evidence of severer damage and more material removal as a result of increasing the impact velocity. Other sub-surface damages were also observed on the more damaged coupons such a sub-tunnel formations as indicated with the arrows in Fig. 4-7. Sub-tunnels as reported in [10] appear to form everywhere from close to the surface and further around the bottom of the induced damage.
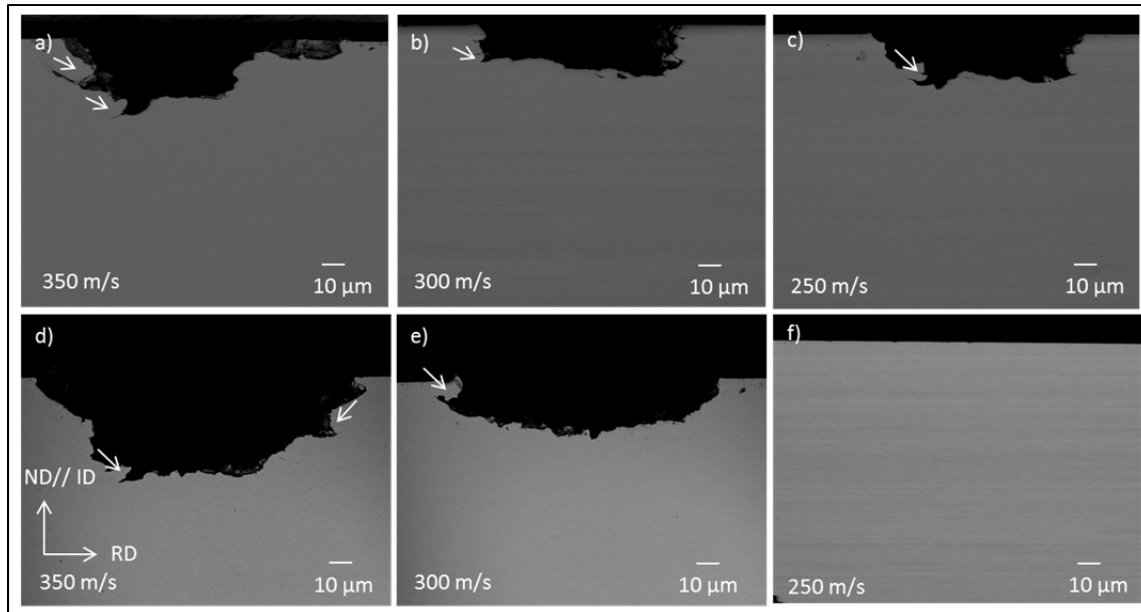
Figure 4-7 Cross-sectional view illustrating craters depths (measure of a distance between deepest visible point of a crater and the sample surface on the cross section), and lateral sub-tunnel formation (white arrows): a, b, and c) same amount of material loss (0.005g) and d, e, and f) same impingements number (100000)

4.3.3   Microscopic analyses of eroded samples

Several hundreds of SEM images were taken at high magnifications along the edge of the eroded craters. Erosion features were systematically imaged using back-scattered electron imaging to reveal the erosion features involved in each coupon. The observed features are in accordance with the previous work for the rolled Ti-6Al-4V microstructure under similar experimental conditions [10]. Surface and sub-surface cracks are formed mostly within primary α-grains, transgranular mode of crack propagation, striation marks indicating the fatigue like mechanisms of material removal, merging of many isolated cracks, and crack propagation in a similar direction were observed more or less on all investigated coupons except for the case with 100000 impingements at 250 m/s where no erosion line and crater were found (Fig. 4-8). Detachment of a larger part of material occurs when two cracks merge together as shown in Fig. 4-8(d) resulting in rapid mass loss. Cracks linkage was observed more frequently on the coupon exposed to 100000 impingements with 350 m/s impact

velocity than 300 m/s. An example of several cracks propagating in a similar direction is given in Fig. 4-8(e), consequently when the cracks meet each other severe material removal will take place due to sub-surface tunnels formation and detachment of large fragment of material. New surface will then be exposed to impingements and the new cycle of crack formation will be started as shown in Fig. 4-8(f). The local morphological feature of the microstructure can eventually promote or restrain such kind of damage mechanisms.
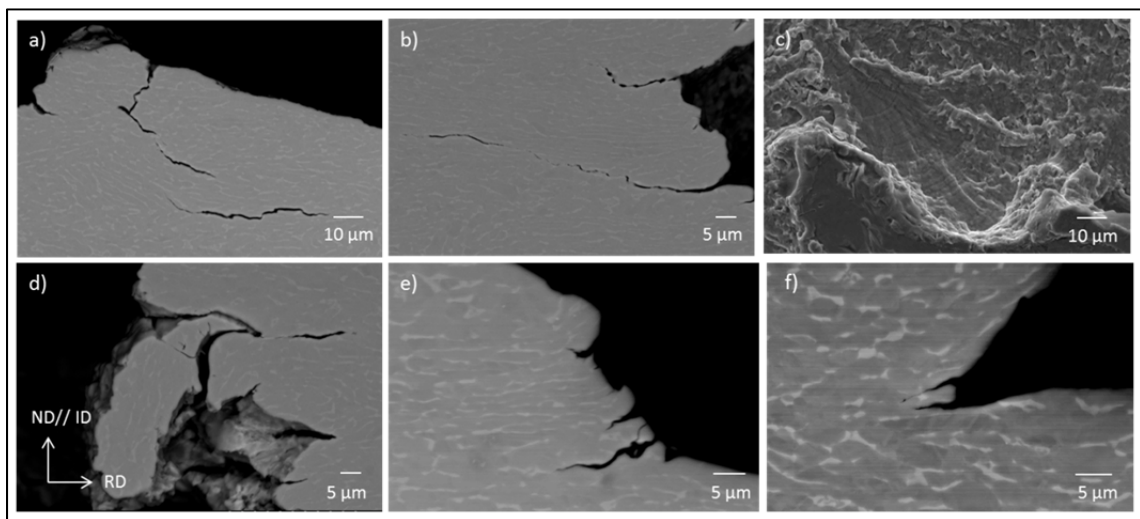
Figure 4-8 Cross sectional view of cracks behavior

4.3.4 Cracks behavior quantification

While the samples follow similar mechanisms of material removal the quantitative measurements of cracks showed there are some differences in terms of number, size and orientation of the cracks.

Quantitative measurements of the crack size reveal that, when the amount of material removal is the same, the number of observed cracks as well as the average crack size do not change significantly with speed variation (crack number ranges from 30 to 35 for the average size of about 9.8 μm). The similarities of the crack size tend to prove that increasing number of impingements for lower velocities can result in the same type of damage as the one

obtained at higher energy but for lower number of impacts. The cracks tend to reach the same length before leading to material removal due to the increased number of impingements than higher impact energy.

In contrary to the cracks size for the equal material removal set up (0.005 g), the cracks showed different statistics when the number of impingements are the same (100000 impingements). For the same impingement numbers, the average crack size for the coupon which is impacted with velocity of 350 m/s was twice the value found for the 300 m/s (13.2 μm versus 5.5 μm respectively). Also the number of observed cracks for 350 m/s is almost twice the number observed for 300 m/s (41 cracks versus 22 cracks respectively) resulting in more material loss and bigger damage (Fig. 4-7). Few very long cracks were also observed in the coupons with the higher impact velocity. This may results from the pronounced impact energy which promotes the crack propagation (Fig. 4-9). No craters and no cracks were observed for coupon with the impact velocity of 250 m/s with however greater time of exposure and volume injected water (see discussion in 4.2). When comparing the two other coupons, it is clear that the average crack size is greater for the higher impact velocity suggesting faster crack propagation during each cycle for higher impact velocities and consequently greater impact energy. The influence of exposure time is quite less pronounced than the impact velocity.
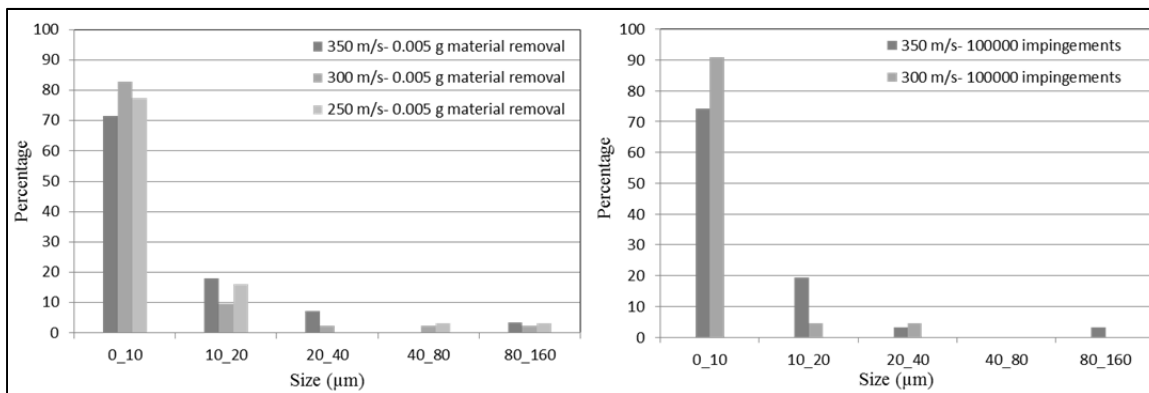
Figure 4-9 Distribution in size of the cracks measured along the craters edges: a) same amount of material loss (0.005g) and b) same impingements number (100000)
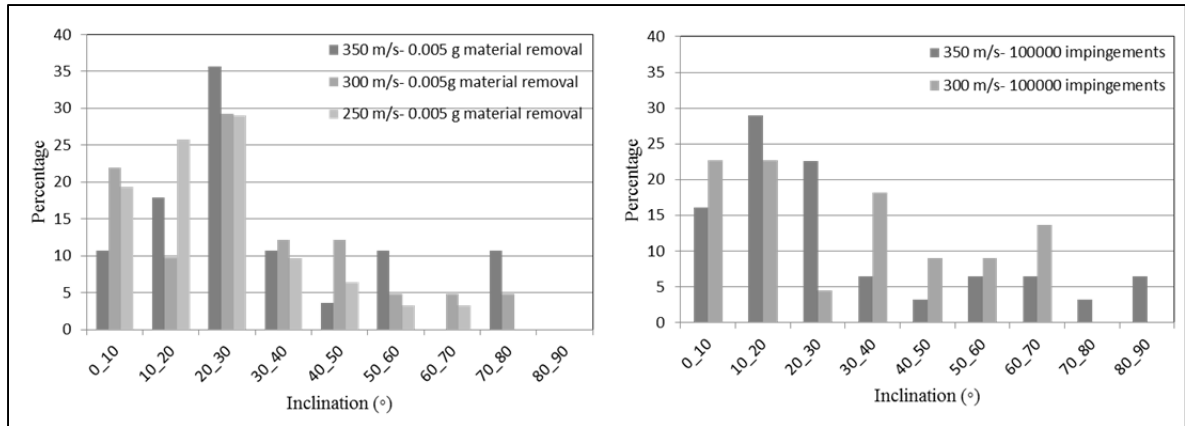
Figure 4-10 Distribution of cracks inclination relative to water droplets impact direction:
a) same amount of material loss (0.005g) and b) same impingements number (100000)

The distributions of the cracks inclination, the angle between impingement direction ID and the main crack propagation direction observed on cross section, clearly show that the cracks inclined around 20-30 degrees relative to the rolling direction when the amount of removed material is the same (Fig. 4-10(a)).

In case of same number of impingements the distribution varied from 350 m/s to 300 m/s. For the coupons impacted with 300 m/s, although the distribution is pronounced around 0-20 degree to the extent to which showing the preferential crack orientations, the cracks inclination is more divers relative to the coupon impacted with 350 m/s where the higher percentage of cracks inclined by 10-20 degree toward the impinging direction (Fig. 4-10(b)). This difference may be due to the smaller size of the cracks in coupon impacted with 300 m/s. In fact in this relatively early stage of erosion the cracks did not propagate enough to be oriented in the direction relative to the microstructure. Such non-random distribution in crack inclination shows that cracks tend to propagate in a preferential orientation, which in this case is the rolling direction. The microscopic observations were also showing that type of behavior (Fig. 4-8(e)).

Study of the cracks inclination shows a significant influence of the microstructural characteristics (Fig. 4-10), i.e. the preferential orientation of the cracks along the rolling

direction. This is particularly more pronounced for impact velocity of 350 m/s. This, in combination with the observation of larger cracks in the higher velocity impacted coupon than lower velocity ones, explains evidently the influence of grains morphology and microstructural effect in cracks behavior (Fig. 4-11(a) and (b)). Cracks under higher impact velocity propagate faster at each cycle of impingements and preferably orient along the rolling direction. Longer cracks resulted from higher impact velocity lead to greater material removal and sub-tunnel formation similarly along the rolling direction (Fig. 4-11(c)). Therefore illustration of microstructural influence is more noticeable with the higher velocity impacts.
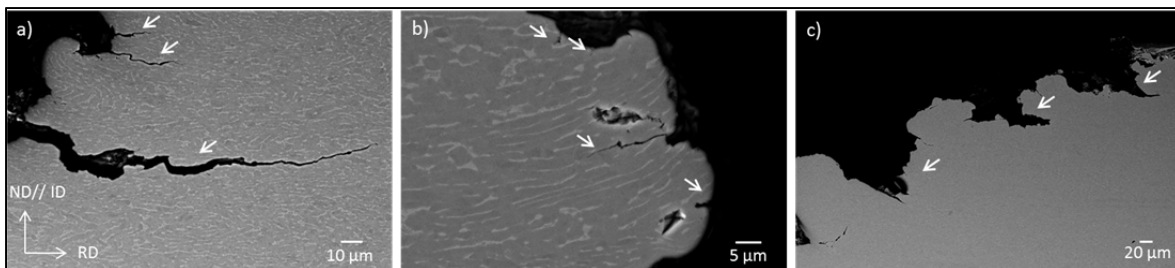
Figure 4-11 a) 350 m/s impacted coupon showing larger cracks with preferential orientation, b) 300 m/s impacted coupon showing smaller cracks which are not yet oriented in a preferential direction (RD), and c) Sub-tunnels formation in preferential orientation (RD)

4.4 Discussion

4.4.1 Incubation period and erosion rate

According to the erosion curves plotted in Fig. 4-4 it is clear that the incubation period is shorter for higher impact velocity. The values obtained for the incubation times indicate that increasing the impact velocity shortens the incubation period. Therefore, the significant influence of impact velocity on incubation time shows that higher impact velocity promotes the erosion phenomenon while lower impact velocity delays the material removal initiation. The number of impingement at the incubation time is plotted in Fig. 4-12(a) relative to the

impact velocity showing an exponentially trend. Fig. 4-12(b) gives the same data with inversed axes and a logarithmic scale.
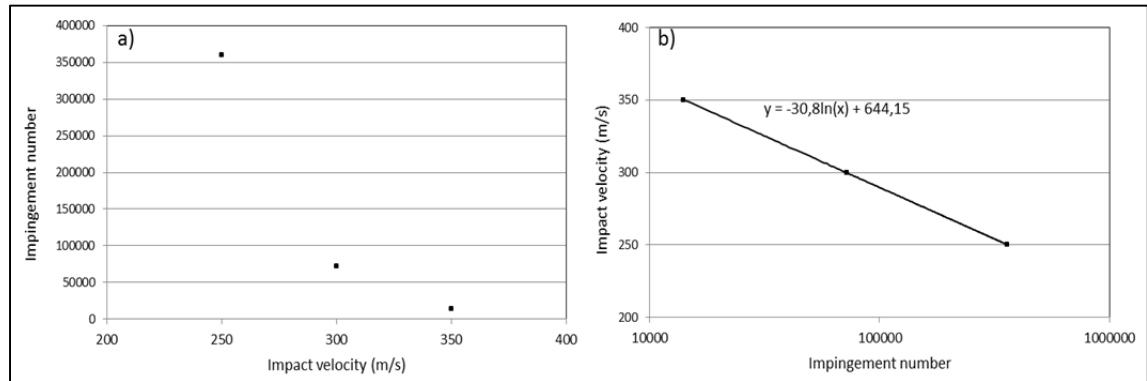
Figure 4-12 Relation between impingement number showing the incubation time and impact velocity

In order to investigate the erosion behavior after the incubation period, the erosion rate was calculated for each condition and the curves are plotted in Fig. 4-13. The curves present the erosion rate (gs^{-1}) relative to the impingement number after the incubation periods. Erosion rate is defined as cumulative mass loss per cumulative exposure time). The different slops clearly indicate that the maximum erosion rate (E_R) is higher with the higher impact velocity from the onset of material removal to the advanced stages of erosion. As an example, the erosion rate versus impact velocity for 0.005 g material removal is plotted in Fig. 4-14 in which the erosion rate is related to the impact velocity in power law function with the velocity exponent of 9 for a particular investigated condition (0.005 g removed material). Therefore in contrary to the incubation time, which decreases with an increased droplet velocity, the erosion damage rate increases rapidly with an increased droplet velocity.
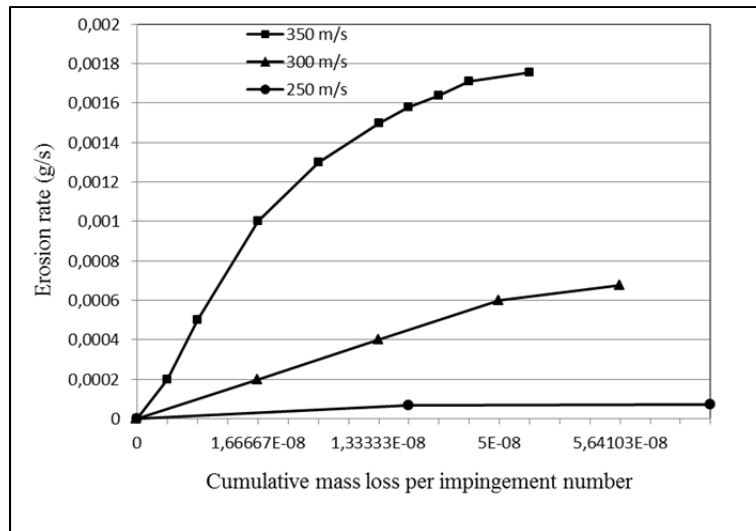
Figure 4-13 Erosion rate (Cumulative mass
loss/cumulative time) vs. (cumulative mass loss per
impingement number) after the incubation period
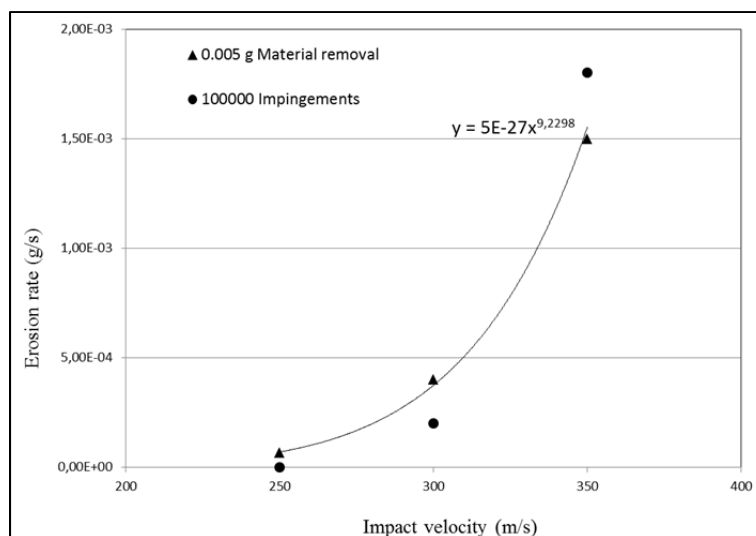
Figure 4-14 Erosion rate vs. impact velocity (after
incubation period)

4.4.2   Width and depth of damage

The two sets of experiments were evaluated in terms of erosion width and depth of
penetration in order to investigate the influence of impact velocity on damaged zone

development. Fig. 4-5 and 4-7 illustrate the width and depth of the damage. The influence of impact velocity on the amount of erosion damage caused by water droplet impingement is plotted in Fig. 4-15 based on Mean Depth of Erosion (MDE) [17]. MDE is found through progressive polishing (minimum of 8 cross section measurements) and SEM measurements on coupons where maximum damage occurs.

Fig. 4-5 showed that when the same amount of material is removed (0.005 g) (although the exposure time to erosion and impingement numbers are significantly different); the average erosion widths are roughly the same for the three investigated speeds. The induced pressure (P) by a single droplet impingement can be obtained by equation $P=\rho CV$ where ρ is the density of water (1000 Kgm^{-1}), C is the speed of sound in water (1500 m/s), and V is the impact velocity (m/s) [18]. Therefore the pressure values of 375 MPa, 450 MPa, and 525 MPa were calculated for 250 m/s, 300 m/s, and 350 m/s respectively. Given these pressure values, it should be noted that, although the crater width induced by few droplets is greater for higher speed impacts (Fig. 4-6) mostly due to the greater impact pressure [18]; the erosion line width is almost the same for the given amount of removed material. Similarly the variation of average erosion depth is not as considerable in this condition. This can be related to the damage spreading with increased testing time [18].

For the same numbers of impingements (100000 revolutions), the aspect of erosion line with impact velocity is however quite significant (see the series of images on Fig. 4-5). Indeed, it is found that with 100000 impingements, the three coupons stand in three different stages of erosion according to Heymann's classification [1]: i.e., Incubation, acceleration, and first steady state stages of erosion for the coupons impinged for 250 m/s, 300 m/s, and 350 m/s, respectively (Fig. 4-4). As illustrated in Fig. 4-15, mean depth of penetration is greater when the impact velocity is higher for the same number of impingements. The damage depth rate might be calculated using the equation proposed by Oka et al. for an aluminum alloy [18]:

$$R_d = E_d / (t - I_p) \tag{4.1}$$

where E_d is the erosion damage depth (μm), R_d is the damage depth rate (μm/s), t is the testing time (s), and I_p is the incubation period (s). From the present results and following the equation given by Oka et al. with the extension for Titanium alloy under investigation, it could be possible to relate the damage depth rate to the impact velocity. A damage depth rate of 7 μm/s, 32 μm/s, and 69 μm/s were obtained for 250 m/s, 300 m/s, and 350 m/s, respectively, for 0.005g material loss . For the same number of impingement, the damage depth rate were found to be 0 μm/s, 62.3 μm/s, and 240 μm/s for 250 m/s, 300 m/s, and 350 m/s, respectively. The damage depth profiles for the investigated speeds were obtained accordingly (Fig. 4-16). The data present the linear dependence of damage depth rate on impact velocity for 0.005g material loss. Therefore the increase in the impact frequency of water droplets directly induces an increase in damage depth rate and a decrease in incubation period which explains how the coupons under the same conditions (for example 100000 impingement) present different stages of erosion.
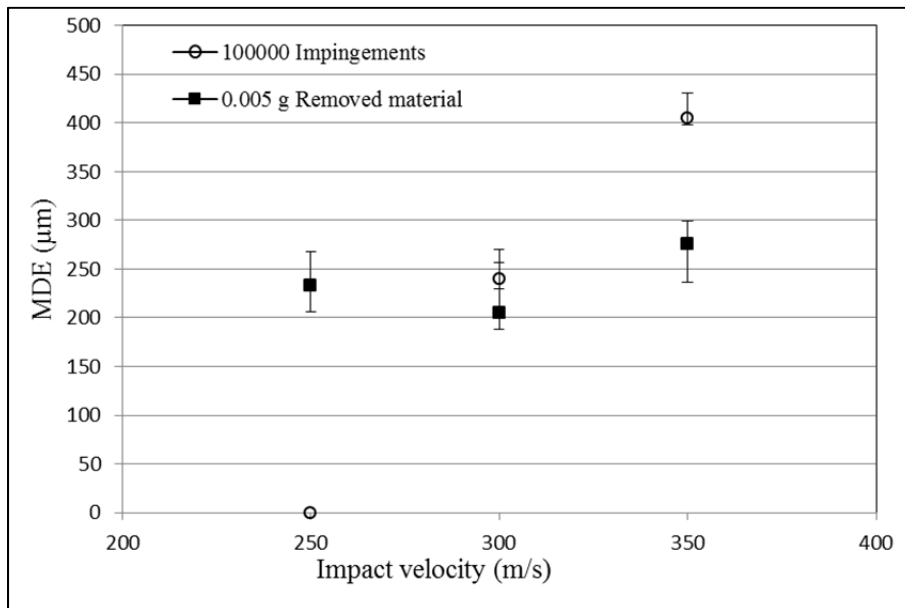
Figure 4-15 Relation between impact velocity and MDE
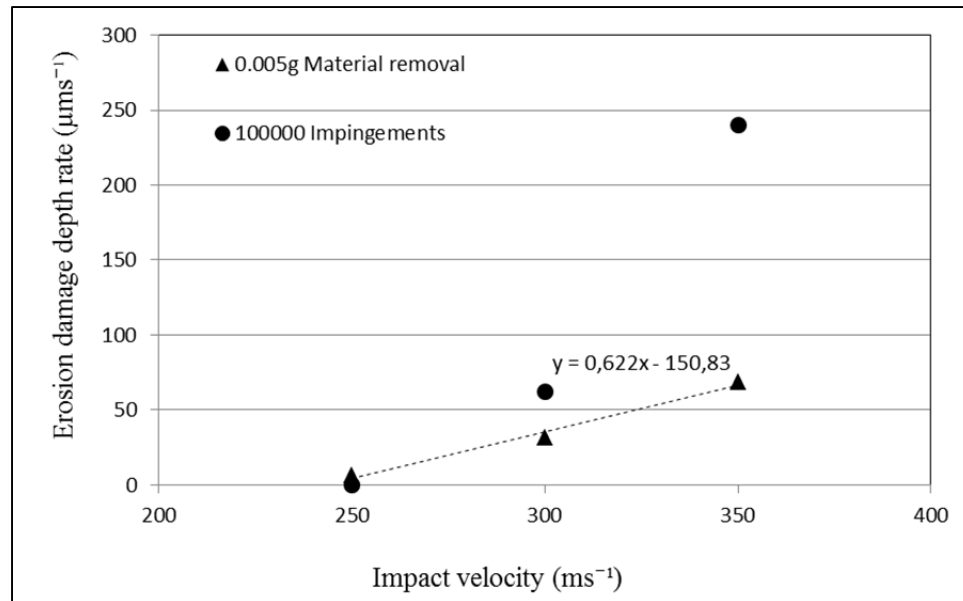
Figure 4-16 Influence of the impact velocity on erosion damage depth rate

4.4.3   Erosion mechanisms

Erosion features such as cracks nucleation and propagation mode resulting in material removal were similar for all impact velocities as presented in Fig. 4-10, however, various volume of material were chipped off depending on the impingement conditions. The observed mechanisms related to crack formations and propagation modes is also reported for a rolled Ti-6Al-4V under 350 m/s in the previous work [10]: surface and sub-surface transgranular crack propagation, striation marks, linking and merging resulting in large material removal and sub-tunnel formation. Thus the mechanisms of material removal are similar, for the covered impact velocities. However, the influence of impact velocity exists and is mainly on erosion rate.

The influence of impact velocity on damage characteristics can be discussed through amount of erosion damage caused by water droplet impingement relative to the impact velocity. The amount of erosion damage caused by solid particle is generally related to the square of the particle impact velocity [19]. Thus it might be applied also for liquid impact erosion, which gives the plot in Fig. 4-17. The trend line between the square of impact velocity and the

amount of material loss for acceleration stage seems to give a linear fit to the data. This linear relation illustrates the velocity dependence of the material loss. Therefore the amount of erosion damage can be basically proportional to the impact energy through equation by Oka et al. [18]:

$$E_k \; \alpha \; mV^2 \tag{4.2}$$
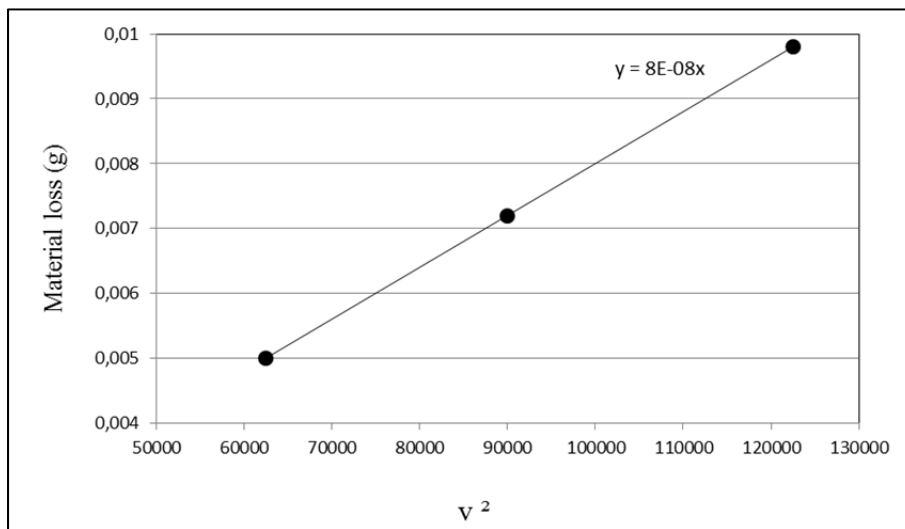
Figure 4-17 Amount of material loss at acceleration stage vs. V^2

To summarize, erosion damage is dependent on both water pressure and impact energy. Increasing the impact velocity exponentially shortens the incubation time and speeds up the onset of material removal. Craters size and erosion damage are directly proportional to the impact velocity indicating that the impact pressure may control this type of damage parameters. On the other hand, the amount of erosion damage might be proportional to the square of the impact velocity. Time of exposure and number of impingements can result in wider eroded area since liquid impingement repeatedly acts on the formed craters, the area gradually expands and form bigger craters. Erosion features are not dependent on impact velocity, while erosion rate and cracks size are significantly influenced by the impact velocity. Since the impact energy is greater with higher velocity and the process is cyclic fatigue, cracks grow faster during each contact with the water jet comparing to lower velocity

impacts. Larger cracks then meet each other leading to chipping off large fragments of material. Increasing the impact velocity induces greater pressure as well as impact energy and thus speeding up the erosion process and decreasing the incubation period. Thus the erosion process and material removal action occurs faster with the greater impact velocity.

4.5   Conclusions

Water erosion tests were conducted on Ti-6Al-4V alloy under the conditions of different impact velocity (Related to the in-service conditions). The influence of three speeds (250 m/s, 300 m/s, and 350 m/s) on erosion behavior was examined for two sets of experiments: coupons with the same amount of material loss (0.005 g) and coupons with the same number of impingements (100000 impingements). The conclusions are:

- Erosion mechanisms were found to be in a good agreement with mechanisms reported earlier for the rolled Ti-6Al-4V. Material removal occurs due to the surface and sub-surface cracks formation, transgranular crack propagation and linking together leading to chipping off the material. These erosion features as well as sub-tunnel formation and striation marks are not influenced by the impact velocity and the erosion by water droplet impingement in Ti-6Al-4V alloy proceeds due to fatigue mechanism.

- The two sets of test results, although varied in extent, proved the microstructural influence exists in erosion behavior of rolled Ti-6Al-4V. It was found that the cracks tend to orient along the rolling direction in their propagation process. This phenomenon appears to be more noticeable for the damage induced by higher speed droplets which results in longer crack sizes.

- The relation between incubation period and droplet velocity was obtained. The incubation period is found to be exponentially influenced by the impact velocity. The impingement velocity versus the incubation period curve on logarithmic scale was similar to an S-N curve for fatigue and thus can be useful for predicting the life span of component materials.

- Craters' size increases with the increased pressure induced by higher speed impacts. Increasing the time of exposure spreads the induced damage and increases the craters' width. Mean depth of penetration is greater with the higher impact velocity and the damage depth rate found to be increased linearly with increasing the impact velocity for the same material removal.

- The amount of material loss at acceleration stage is linearly proportional to the square of the impact velocity and so the impact energy. Erosion rate increases with increasing the impact velocity. The droplet velocity dependence of the erosion rate for the same material removal condition was in power function of impact velocity on logarithmic scale and the velocity exponent was 9.

Acknowledgements

References

[1] F.J. Heyman, Liquid impingement erosion, Wear, ASM Handbook-18, (1992) 221-232.

[2] R.K. Bhargava, C.B. Meher-Homji, M.A. Chaker, B. Bianchi, F. Melino, A. Peretto, S. Ingistov, Gas turbine fogging technology: a state-of-the-art review- Part1: Inlet evaporative fogging-Analytical and experimental aspects, Journal of engineering for gas turbines and power 129 (2007) 443-453.

[3] J.R. Khan, T. Wang, Simulation of inlet fogging and wet-compression in a single stage compressor, Proceedings of the ASME Turbo Expo (2008) GT2008-50874.

[4] S. Hattori, Effects of impact velocity and droplet size on liquid impingement erosion, International Symposium on the Ageing Management and Maintenance of Nuclear Power Plants (2010) 58-71.

[5] B. Lee, K. Riu, S. Shin, S. Kwon, Development of a water droplet erosion model for large steam turbine blades, KSME International Journal 17-1 (2003) 114-121.

[6] M. Ahmad, M. Casey, N. Surken, Experimental assessment of droplet impact erosion resistance of steam turbine blade materials, Wear 267 (2009) 1605-1618.

[7] S. Yerramareddy, S. Bahadur, Effect of operational variables, microstructure and mechanical properties on the erosion of Ti-6Al-4V, Wear 142 (1991) 253-263.

[8] N.L. Hancox, J.H. Brunton, The erosion of solids by the repeated impact of liquid drops, Philosophical Transactions, Royal Society of London Series A260-1110 (1966) 121-140.

[9] P.A. Coulon, Erosion-corrosion in steam turbines II: a problem largely resolved, Lubrication Engineering 42 (1986) 357-362.

[10] N. Kamkar, F. Bridier, P. Bocher, P. Jedrzejowski, Water droplet erosion mechanisms in rolled Ti-6Al-4V, wear 301 (2013) 442-448.

[11] Y.N. Wong, J.C. Huang, Texture analysis in hexagonal materials, Materials Chemistry and Physics 81 (2003) 11-2.

[12] M.R. Bache, W.J. Evans, Impact of texture on mechanical properties in an advanced Titanium alloy, Materials Science and Engineering A319-321 (2001) 409-414.

[13] F. Bridier, P. Villechaise, I. Mendez, Analysis of the different slip systems activated by tension in a α/β Titanium alloy in relation with local crystallographic orientation, Acta Materialia 53 (2005) 555-567.

[14] G.L. Sheldon, Effects of surface hardness and other material properties on erosive wear of metals by solid particles, Journal of Engineering and Materials Technology Transaction ASME 99 (1977) 133–137.

[15] I. Finnie, Some observations on the erosion of ductile metals, Wear 19 (1972) 81-90.

[16] ASTM Standard G73, 2004 (2010), standard test method for liquid impingement erosion using rotating apparatus, ASTM International, West Conshohocken, PA, (2010) DOI: 10. 1520/C0033-03R06, www.astm.org.

[17] R.H. Richman, W.P. McNaughton, Correlation of cavitation erosion behaviour with mechanical properties of metals, Wear 140 (1990) 63–82.

[18] Y.I. Oka, S. Mihara, H. Miyata, Effective parameters for erosion caused by water droplet impingement and application to surface treatment technology, Wear 263 (2007) 386-394.

[19] Y.I. Oka, K. Okamura, T. Yoshida, Practical estimation of erosion damage caused by solid particle impact, Part 1: Effect of impact parameters on a predictive equation of erosion damage, Wear 259 (2005) 95-101.

CHAPTER 5

DISCUSSION

This chapter aims to discuss the results as a whole and thus link the different items together in order to draw overall conclusions based on all work done in this thesis.

5.1 Erosion mechanisms

To understand the liquid droplet erosion mechanisms in a specific alloy, it is clear that the material removal behavior should be investigated through the entire process, meaning from the damage initiation to the advanced stages of material removal. In this regard, as discussed earlier in Chapters 2 and 3, the investigation of the erosion mechanism is divided into two parts; damage initiation and advanced stages of erosion.

Initial erosion damage was studied on a forged Ti-6Al-4V focusing on incubation period and onset of material removal. These are earlier stages of erosion where the erosion is either not observable or the material removal is just initiated (Figs. 3-7 and 3-8). The erosion progression from induced shallow damages at early incubation to the material removal initiation damage was then thoroughly captured and certain mechanisms were identified. The erosion initiates from a slight local damage and appearance of surface protrusions due to the sub-surface crack or local sub-surface plasticity. Larger scale material removal takes place leading to the formation of craters. Induced local impact pressure results in high stress field and severe plasticity underneath the surface. Sub-surface transgranular cracks formation implies that the maximum pressure and plasticity occur under the surface which is in accordance with the Hertz theory of impact (Stronge 2004). This transgranular cracks just at very earlier stages is originally reported in this work and is as opposed to the intergranular damages reported by researchers for the initial damage mechanisms (Huang et al. 2012). It should also be pointed out that, the grain boundary damage on the surface was also observed (Fig. 3-15(a)) as a result of impacts repetition followed by yet again transgranular cracks and striation marks. These secondary transgranular cracks are responsible for the damage

progression to the severer stages and together with the observed striation marks indicate cyclic nature of material removal process. Largely distribution of transgranular mode of crack propagation and striation marks were observed at the damaged zones for advanced stages of erosion in both rolled and forged microstructures, as discussed in Chapter 2 and Appendix I. It therefore points to the fatigue based mechanism of water droplet erosion process from initiation to the advanced stages of material removal. The advanced stages of erosion, discussed comprehensively in Chapter 2 and Appendix I for rolled and forged base material and their differences, leads to propose a typical mechanism. It is found that in both cases, cracks nucleate from the craters' edges (surface cracks) and/or under the stress concentration beneath the surface (sub-surface cracks) and propagate to the main eroded crater. Cracks propagate in transgranular manner which is more noticeable for forged microstructure as the grains are well equiaxed.

Transgranular cracks initially form usually at about 45° of the impact direction underneath the surface which points to the stage I fatigue cracks that once nucleated, particularly adopt an angle of about 45° relative to the loading direction along high shear stress planes (45°). In LCF, high plastic deformation takes place along with inhomogeneous plastic strain field formation. It is then, expected to develop localized regions of preferential slip leading to localized regions of crack initiation. Strong localized plasticity region in this work occurs below the surface at about 100 μm resulted from high speed droplet impacts (sub-surface plasticity) providing the crack initiation site. Given the crack nucleation and propagation mode resulted from accumulation of high localized plasticity, together with the knowledge of impingement number (consider as the number of cycles), it is possible to relate the process with the suggested fatigue-like mechanism and particularly low cycle fatigue nature of water droplet impact erosion.

Stating the crack propagation modes, no evidence of intergranular propagation was observed in advanced stage neither for forged microstructure nor for rolled one. Given the observation of transgranular cracks just at the beginning of the process as well as the advanced stages of erosion, it can be concluded that the transgranular damage is the dominant responsible for the erosion damage. It is while the intergranular damage takes the lead only at the onset of

material removal (i.e. after the incubation) and is a typical of the initiation stage due to the local plasticity and grain tilting.

As the process advances, it involves merging of both surface and sub-surface cracks and leading to material removal, forming the craters, and occasionally forming the lateral sub-tunnels. Crack coalescence, introduced in this work, is typical of rolled microstructure wherein multiple cracks, nucleated in a similar orientation, link together forming a longer crack and consequently larger removal of material fragment. This is an example of microstructural influence which is discussed hereafter along with comparison between the two microstructures.

Removal of material fragments usually leaves a rough fracture surface. Water smoothing phenomenon, introduced firstly in this work, was observed in both cases, during which water impacts act on the fractured surface and wash out the freshly fractured fragments until the surface becomes very smooth. This explains the observation of both smooth and rough fracture surfaces at a damaged part. The process then returns to start from nucleation of surface and sub-surface cracks up to the material removal.

To summarize, the erosion mechanism of Ti-6Al-4V under water droplet impact erosion through the whole process is proposed as:

(i)   High local stress field formation underneath the surface resulted from droplet impact pressure

(ii)   Plastic deformation and generation of a local compressive residual stress field close to the elastic limit

(iii)   Generation of high local deformation cycles and sub-surface cracks formation similar to LCF condition

(iv)   Surface upheaval appearance more likely attributed to the sub-surface plasticity

(v)   Grain tilting and intergranular damage at surface due to the local plastic deformation

(vi)   Secondary transgranular crack formation

(vii)   Linking and/or merging of trangranular cracks

(viii)   Detachment of the material fragments and occasional formation of sub-tunnels resulting the rough surfaces

(ix)   Water smoothing of the rough surface

(x)   New cycle of sub-surface plasticity and cracks nucleation (step I), propagation, material chipping off, and sub-tunnel formations.

5.2   Influence of microstructural characteristics

The erosion mechanisms of both rolled and forged microstructures were compared at advanced stages of erosion and published in the proceeding of the international solid/liquid impact erosion conference in Milan, Italy 2012 (Appendix I). The material loss curves obtained for both base materials under the same experimental conditions are presented in Fig. 5-1. It clearly shows a significant difference in amount of material loss and erosion rate especially at advanced stages of erosion which was the focus of erosion evaluation. Under the same experimental conditions, the forged microstructure shows better erosion resistance after the damage initiation. In other words when the erosion starts, it goes faster in rolled base material than in forged one. This gives rise to observation of longer cracks in rolled material which is related to the microstructural features such as elongated grains.
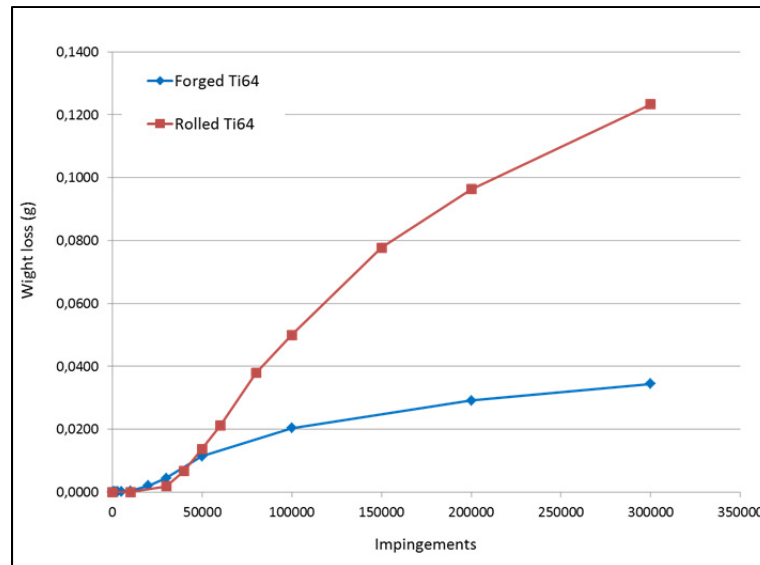
Figure 5-1 Water droplet erosion curves for forged and rolled Ti-6Al-4V

Hundreds of cracks analyses through SEM imaging and quantification methods (Appendix II) illustrate the microstructural influence in cracks behavior. As explained earlier in section 5.1, crack coalescence is introduced as a mechanism of crack propagation in rolled microstructure. This trend was observed entirely in rolled microstructure while less observed in the forged one. This can, therefore, be typical crack behavior in rolled base material due to the elongated grains as well as presence of macrobands with the similar crystallographic orientation, that is, cracks tend to nucleate and propagate with similar orientation along the rolling direction. The appearance of such coalescence in forged base material can be due to the existence of the macrozones bearing the similar crystallographic orientations. The macrozones are more vulnerable to slips (basal or prismatic), provide the suitable environment for microcracks nucleation and their coalescence, considering that slip is a main mechanism leading to fatigue crack nucleation. Therefore, crack coalescence can also occur in forged microstructure at the scale of macrozones which needs further investigations.

Crack coalescence appear to be another key process leading to crack growth, and thus, additional illustration for longer crack size observed mostly in rolled microstructure, along with the faster crack propagation due to the morphological reasons (elongated grains) as

explained in Chapter 2. The single cracks also tend to propagate along the rolling direction while in the forged microstructure cracks tend to propagate in any directions (Appendix I). The equiaxed grains in forged microstructure makes the cracks growth harder, given the grain boundaries acting as the barrier for crack propagation. The quantification of the cracks also showed the preferential inclination toward the rolling direction (around 20°) in the rolled base material and a random distribution of inclinations in forged one (around 45° relative to the impingement direction). Therefore, the orientation of the cracks and their inclination relative to the impingement direction are directly linked with the morphology and crystallographic texture of the alloy, which is more noticeable in rolled microstructure given the strongly textured base material.

Water droplet erosion phenomenon is therefore quite a microstructure dependent process. Given the significant influence of the manufacturing processes (e.g. rolling and forging) on microstructure of the Titanium alloy which determine the size and shape of the grains, this parameter should stand on the primary considerations in material selection for the most industrial components. On the other hand, the microstructure and mechanical properties, typically fatigue behavior, are closely related (Le Biavant et al. 2001) and water droplet impact erosion phenomenon is considered as a fatigue-based process that also emphasize on the necessity of the microstructural consideration. For example, here in the present work, a bimodal forged Ti-6Al-4V showed higher resistance to crack propagation and thus presents less erosion damage than a rolled microstructure which is more vulnerable to crack growth and damage propagation. Therefore a fine grain duplex Ti-6Al-4V with the equiaxed grains, together with the texture considerations is expected to provide a good resistance to water droplet erosion relative to the rolled microstructure. The influence of texture and loading/impingement direction (for example loading parallel to C-axis), also need to be taken into account. Implementation of these considerations in material selection, design, and manufacturing of the parts will therefore lead to improve the mechanical behavior of the material, increase the water droplet erosion resistance, and consequently the lifetime of the components under potential erosion damage which is the primary objective of this study.

5.3   **Representativeness of the in-service conditions**

Although erosion evaluation of the blade was studied by many investigators through numerical modeling with the attempt to identify mainly the erosion pattern and material loss on the blade (summarized and developed by Krzyzanowski et al. (1994)), the erosion representativeness through the experimental assessment was not investigated in the previous works as discussed earlier. Given the complexity of the subject, it is not thoroughly discussed in the present study either. However, two parameters were considered here: base material characteristics and droplet velocity. As discussed earlier in Chapter 4, a specific material was selected which presents similar texture characteristics as the in-service blade since it is proved that microstructural features have influence on erosion behavior. Therefore, to study the influence of the impact velocity corresponding to the in-service conditions, evaluation needs to be conducted on a similar base material firstly to make the evaluation more representative and secondly to avoid microstructural variation influence. The erosion behavior along the leading edge showed that the damage is severer at the tip of the blade and decreases along the leading edge down to the bottom of the blade. This trend in erosion damage occurs due to the different conditions along the leading edge including the rotational speed of the blade, and so the variation of droplet impact velocity which is the focus of the present work. The erosion damage evaluation on the coupons impacted with the impact velocities of 250 m/s, 300 m/s, and 350 m/s, resulted in realizing the influence of impact velocity on damage severity, cracks behavior, and material removal rate. The detailed discussion on erosion dependence on impact velocity, water pressure, and impact energy is presented in Chapter 4. It is found that impact velocity influences the incubation time with an exponential function and increases the erosion rate in the acceleration stage in a power law function. Damage distribution, crater size and amount of erosion damage are related to the impact pressure and energy (Chapter 4). Therefore, it can be generally concluded that the impact velocity influences the erosion process from initiation to the advanced stages of erosion relative to the conditions. However, for the purpose of full representation of the in-service condition, other parameter such as droplet parameters and geometry of the coupons should also be taken into account in the future works.

5.4 Erosion resistance and application of surface treatment

Since the phenomenon can be recognized as the fatigue process, the surface enhancement to increase the fatigue life of the component can be considered for erosion resistance improvement as well. Surface roughness and the deformation induced by droplet impacts on the surface can cause stress concentration that lower the fatigue strength of the material. Compressive residual stresses can be introduced on the surface by various processes to increase fatigue life of the component. Low plasticity burnishing (LPB) and laser shock (LSP) peening can produce this surface compressive stress and consequently increase the fatigue life.

Such treatments are known to significantly improve resistance to wear, and in particular to increase the fatigue strength of metallic parts. The results of the previous works clearly indicate the beneficial effect of surface treatments, specifically by laser shock peening, in enhancing both the HCF and LCF resistance of Ti-6Al-4V. The results showed that these surface treatment techniques increase the lifetime and lower initial crack propagation rates which are reported to be due to the compressive residual stress formation close to the surface, together with the work hardening effect in the near-surface layer (Prevey et al. 2001, Montrose et al. 2002, Nalla et al. 2003).

This improvement in fatigue properties of Ti-6Al-4V, resulting from surface treatments, is expected, as well, for droplet impact erosion behavior of this alloy given the cyclic nature and fatigue based mechanism of the process. While such improvements is still questioned for water droplet erosion, it is possible that the benefits of surface treatments, such as residual stress and work hardening, which might result in finer grain size and high dislocation density, help improving the erosion resistance, particularly by controlling the crack nucleation and initial growth. This is likely expected due to the decreasing of the plastic strain amplitude as a result of introducing the surface treatments, since fatigue damage mostly occurs due to the strong plastic strain field. However needs further investigations.

The surface treatments influence was partly investigated in this work and the results are presented hereafter (Annex II).

CONCLUSIONS

Water droplet impact erosion damage is studied in Ti-6Al-4V alloy used as the compressor blade material in gas turbine engine. This study allowed characterizing the erosion behavior of Ti-6Al-4V thoroughly from damage initiation to the advanced stages of erosion relative to the microstructure of the base material. Moreover the induced damage at various speeds corresponded to the in-service conditions were analyzed and the influence of the impact velocity was obtained for the investigated conditions.

From the analysis and discussion of the results, the main contributions of this thesis are:

- The water droplet impact erosion damage in Ti-6Al-4V alloy starts with the severe local plastic deformation underneath the surface due to the impact pressure resulting in sub-surface transgranular cracks. High local deformation cycles similar to LCF conditions are generated, resulting in network of sub-surface cracks. Surface protrusions are formed as a consequence of sub-surface plasticity. With the appearance of plasticity, grain tilting, and consequently grain boundary damage develop at the surface, and secondary transgranular cracks form afterwards which are responsible for the advanced stages of material removal.

- Advanced erosion mechanisms are proposed to cyclically involve the formation of surface and sub-surface network of cracks which propagate in a transgranular manner. Cracks merge together leading to the detachment of the material fragments. Sub-tunnels appear to form occasionally as a result of large material removal due to cracks linking and merging together leaving a rough fracture surface followed by water smoothing phenomenon. Water smoothing is introduced in this study presenting the action of surface polishing due to the water droplet impacts on a rough surface developing a smooth surface. Therefore the resulted rough surface of the sub-tunnels formation smoothens due to the water polishing/smoothing effect. New cycle of crack

nucleation till the material removal and water smoothing occurs afterward as a result of droplet impacts repetition; i.e. the mechanism is a cyclic phenomenon.

- This work showed that a new approach in methodologies for erosion characterization should be used in order to involve detailed evaluation of the surface and the cross section of the eroded coupons, quantification of the erosion by measurement of cracks size and inclination systematically relative to the impingement direction.

- Representation of the in-service conditions, made in this study in terms of base material characteristics as well as velocity of the impact correlating to the blade's speeds along the leading edge, corresponds to the different stages of erosion. It is found that impact velocity exponentially influences the incubation period. Higher impact velocity induces greater impact pressure and energy resulting in greater damage and faster material removal. Damage depth rate increases linearly with increased impact velocity when the amount of removal is the same. The amount of material loss is linearly proportional to the impact energy at acceleration stage and the erosion rate increases with the 9th power of impact velocity for a certain amount of damage.

- Microstructure features are found to influence the erosion mechanisms. The features such as crystals orientation and morphology of the grains are of the parameters which control the crack behaviors. Grain boundaries and morphology of the grains are the microstructural barrier for crack propagation. For instance, crack growth is slower in forged microstructure with equiaxed grain than rolled with elongated grains that actually promote crack growth in the rolling direction which is not desirable. Therefore base material characteristics, typically microstructure and texture, should be considered in material selection for in-service components.

- Microstructural influence is documented through quantification method as well. It is reported that the cracks propagation and inclination are directly linked with the

morphological and crystallographic aspects of the microstructure. Cracks tend to orient in a preferential direction relative to the microstructure and grain morphology. This phenomenon appears to be more noticeable for the damage induced by higher speed droplets which results in longer crack sizes.

- It is realized that cracks nucleate and propagate in a transgranular manner at the initiation (inclined by 45° from impingement direction) and advanced stages of erosion which indicate LCF condition for near-α and α/β Titanium. Transgranular mode of crack propagation and striation marks together with the cyclic nature of water droplet impact erosion strengthen the conclusion on the fatigue-based mechanism of the water droplet impingement of Ti-6Al-4V.

RECOMMENDATIONS

This section presents some other aspects of the subject for future investigation to help covering the issues and responding the problems.

Identifying the erosion mechanisms and microstructure related issues

The erosion mechanism was thoroughly investigated in the present study but only for specific microstructure and texture base materials. It is clearly stated that there is microstructure effect; however, the influence of the texture on erosion behavior were not primarily addressed. The subject of texture influence is very interesting topic to pursue for complete understanding of the base material properties influence on erosion mechanisms as it might have significant influence on material removal behavior. This is typically more pronounced for Titanium alloy which presents elastic/plastic anisotropic behavior.

Texture influence for the purpose of water droplet impact erosion characterization can be investigated through different impingement directions. As explained in chapter one the impingement direction can be selected along ND, RD and at 45° based on the anisotropic behavior of Ti-alloy, where the greatest variation in elastic/plastic anisotropy of this alloy is expected. The angles might be a little varied due to the specific texture under investigation. A rolled Ti-6Al-4V is suggested for this study as it presents strongly textured base material. The coupons can be extracted at different angles relative to the material texture. Fig. 5.1 illustrates the way of sample extraction from a rolled Ti-6Al-4V plate and the impingement directions. The impingement directions are along ND, RD, and at 45∘ which are selected based on the anisotropic behavior of the alloy and thus the influence of microstructure and texture can be obtained.

The samples were extracted from a rolled Ti-6Al-4V on two directions: RD and ND. However, the width of the coupons are not enough to fit the holder for the erosion test at Concordia university unless the two coupons get to be used next to each other which was indeed the idea of the work at the beginning. The coupons on 45° could not be extracted due

114

to the thickness limitation of the rolled plate. For this, finding a thicker plate seems to be an option, however, it should be considered that a thicker plate normally does not present as strongly textured microstructure as a thinner one does. That is clearly due to the rolling process.
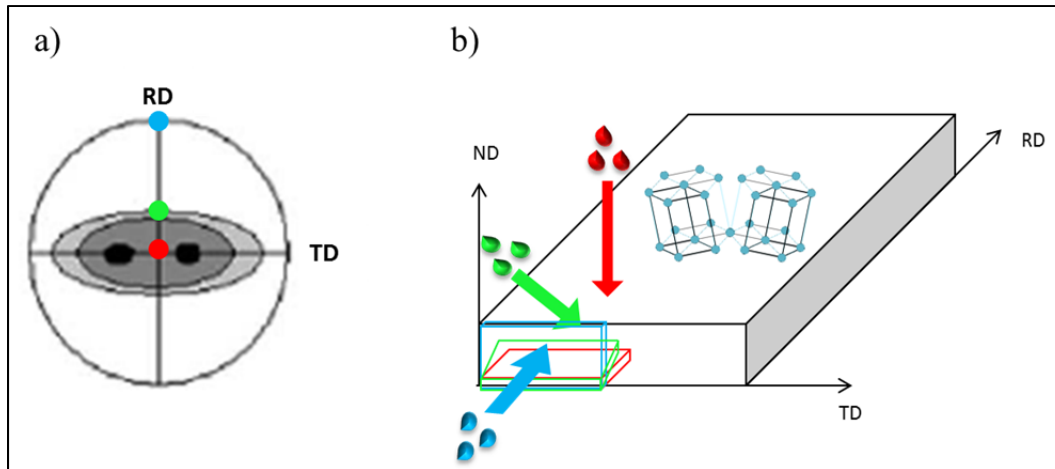

Figure 5-2 a) pole figure presenting the typical texture of cold rolled Ti-6Al-4V, and b) sample extraction and impingement directions relative to the texture

Another interesting subject to better understand the erosion mechanism, especially at the initial stage, is the stress state analyses during the impacts. This can make it easier to relate the formation of the surface upheaval to the generated stress underneath the surface at earlier stages of erosion.

Influencing parameters and rig test representation
Droplet size which has significant influence on erosion behavior of the blade along the leading edge should also be considered in future works to represent the in-service conditions. The experimental part of this asset was done during the course of this Ph.D work and presented in Annex I. It is noteworthy that one of the issues concerning the use of inlet fogging system in gas turbine engine, the droplet sizing, is important because of the wide range of statically distributed droplet size created by the fog nozzles, droplet coalescence,

etc. (Chaker et al. 2004). As droplet size influences the erosion of compressor blades to the good extent, it is worth to be investigated relative to the in-service conditions.

To investigate the droplet size influence, three droplet sizes relative to the defined terminologies (Chaker et al. 2002) should be selected for the in-service conditions. The erosion tests then should be carried out on different coupons with varied nozzles corresponds to the selected droplet sizes. The tests on this were performed on 200μm, 400μm, and 600μm nozzle sizes as presented in Annex I. Following characterization and comparisons result in understanding the influence of droplet size. Other parameters can also be considered to make the comprehensive representation.

One of the very important factors that should be taken into account is the influence of the geometry of the component. Although in the present work, the efforts were made to find a similar microstructure and texture to the in-service blade and to realize the main impingement direction relative to the texture of the in-service blade, the impingement direction is neither a certain direction, nor it remains the same along the leading edge. Therefore, using the airfoil coupons in a laboratory scale is an option to better represent the in-service condition with the similar geometry. Erosion test then can be performed on the similar geometry to investigate the influence of other parameters on erosion behavior.

Influence of the surface treatments

Surface treatment is one of the common methods to improve the erosion resistance of materials by increasing the hardness and inducing compressive residual stress on the component. Residual stress is a parameter which plays a major role in increasing the water droplet erosion resistance (Baker 2010). Indeed application of surface treatments or coatings extends the incubation periods and delay the material removal process (Robinson and Reed 1995, Shipway and Gupta 2011). Compressive residual stress can be introduced in the surface by, for example, shot peening to increase the fatigue life. LSP and LPB are known as the two relatively novel methods to induce compressive residual stresses and improve the resistance to crack nucleation and propagation and increase the fatigue life. Recently, few

researchers have studied some aspects of LSP and LPB processing on various materials (Prevey et al. 2001, Montrose et al. 2002). It is generally reported that LSP and LPB increase the surface hardness and fatigue strength depending on the processing conditions, alloy type, and microstructure of the alloy. The influence of LSP and LPB and particularly residual stress effect were not investigated for the Titanium alloy especially in water droplet impact erosion. It is then worth to study the topic of residual stress on Ti-6Al-4V alloy especially on airfoil coupons to understand whether or not it can improve the erosion resistance of the blades. This topic is partially investigated in this work and the results are presented in Annex II. Together with the stress state analysis it sounds very interesting to continue this work toward understanding the hardness and residual stress effect on water droplet impact erosion damage resistance.

ANNEX I

Influence of droplet size on water droplet erosion mechanisms of Ti-6Al-4V

In order to identify the influence of the droplet size on material removal action, rig tests were performed on the rolled Ti-6Al-4V coupons at Concordia University. The impact velocity of 350 m/s was selected corresponding to the blade tip were the maximum erosion occurs. Various nozzle sizes were selected: 200, 400, and 600 μm given the average droplet sizes of 250, 450, and 650 μm respectively which are corresponded to the droplet size distribution of the in-service compressor blade, obtained by Rolls-Royce, Canada. The results of this work are presented as follow.

Material removal behavior and erosion curves

The erosion curves were obtained for each coupon illustrated in Fig-A I-1 and Fig-A I-2 presenting the cumulative mass loss versus volume injected water and impingement number respectively.
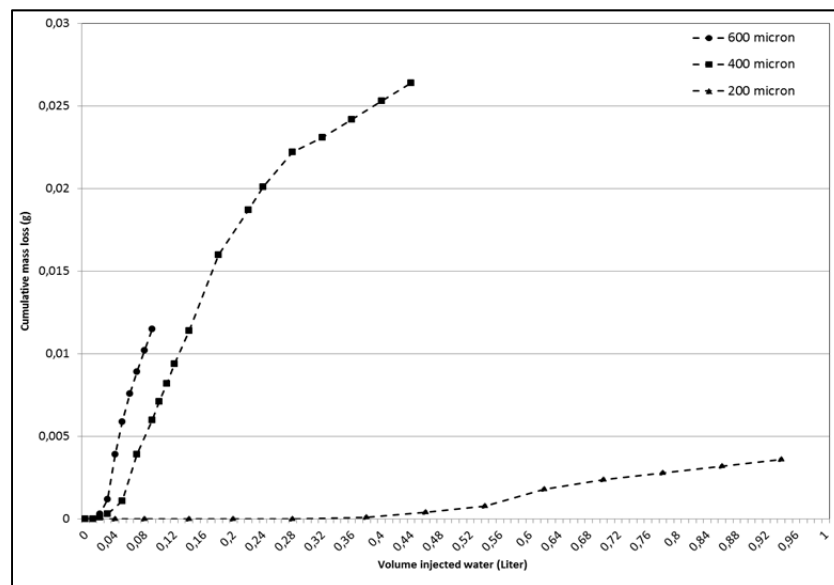
Figure-A I- 1 Cumulative mass loss vs. volume injected water
for different droplet sizes
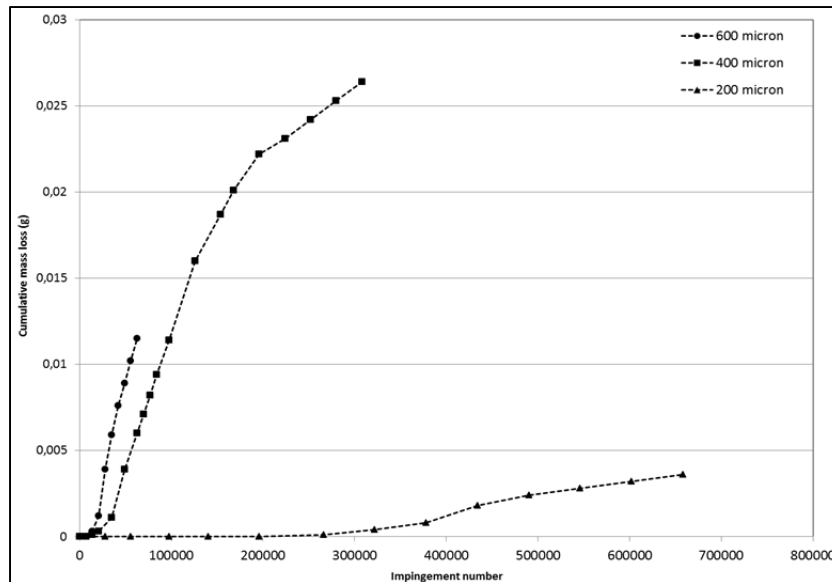
Figure-A I- 2 Cumulative mass loss vs. impingement number

The coupons were eroded up to the advanced or steady state stages of erosion in order to obtain the curves; however, other coupons were extracted at different stages of erosion in order to thoroughly study the erosion evolution from the early stages of erosion to the advanced stage material removal. Fig-A I- 3 shows the SEM images of the extracted eroded coupons at final stages of erosion.
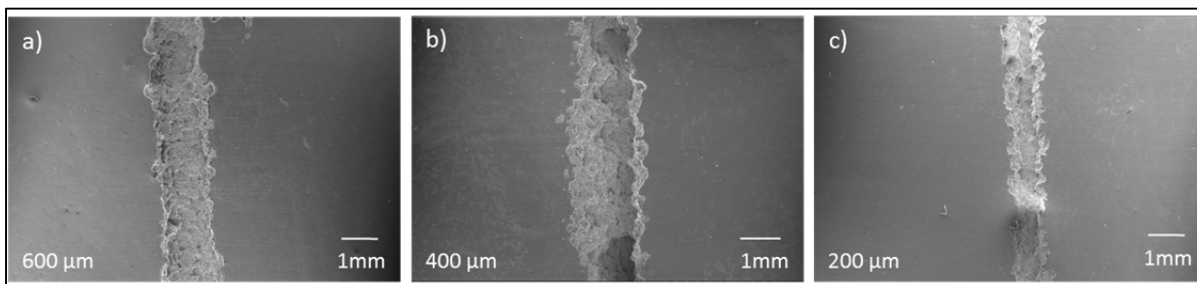
Figure-A I- 3 SEM micrograph of the coupons at advanced stages of erosion impacted through a) 600 μm, b) 400 μm, and c) 200 μm nozzle sizes

Damage characterization and erosion mechanisms

Material removal behavior can be characterized at different stages of erosion via SEM and AFM as stated in Chapters 2, 3, and 4 in terms of craters width and depth, cracks

nucleation/propagation mode, sub-tunnel formation, and material removal behavior. Quantification should be done in terms of crack size and inclination as well as erosion rate and roughness calculation in order to compare the coupons in different conditions so that the influence of droplet size on erosion rate and mechanisms can be obtained.

ANNEX II

Surface treatment influence on water droplet erosion resistance on Ti-6Al-4V

As explained in section 10.5, surface treatments selected for this study are LSP and LPB. Coupons were made of forged Ti-6Al-4V alloy, LSP and LPB treated to compare with untreated coupon. LSP was performed on the coupons with two different conditions: two layers of peening (standard LSP) and three layers of peening (heavy LSP). Two different conditions of LPB treatment were also applied on the coupons: High Load Parameters (HLP) and Low Load Parameters (LLP). The coupons were then water eroded under the conditions of 350 m/s impact velocity and 600μm droplet size at Alstom, Switzerland.

Base material studies

Characterization of the base material microstructure was done on the coupons illustrated in Fig-A II-1 for LPB coupons. It should be noted that base material characterization as well as erosion behavior of the untreated forged Ti-6Al-4V were thoroughly investigated in this work as presented before. LSP coupons present the same microstructure and texture as the forged untreated Ti-6Al-4V discussed in article2, chapter 3, taken from the same part. The LPB coupons, however, present globular microstructure with some area of elongated grains as well. Texture evaluation is also needed.
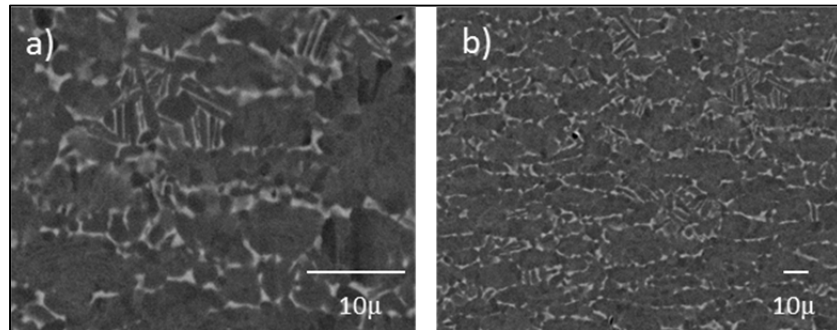
Figure-A II- 1 SEM micrograph of forged LPB microstructure a) lower and b) higher magnification

Hardness measurements

Hardness and residual stress measurements provide the information of the surface modification depth so that the relative information to the erosion damage on the treated zone can be achieved.

Microhardness profiles were performed on both LSP and LPB coupons on cross sections (Figs-A II-2 and 3) in order to relate the erosion behavior to the depth of treated zone in term of hardness. The hardness value should also be obtained on erosion direction so that the cumulative hardness that might influence the erosion behavior can be obtained. Each of the hardness values is the average of five indentations and the measurements were conducted at ETS using the Clemex CMT microhardness indenter with 500N load.

It is realized from the microhardness profiles that there is a general increase in hardness values under the surface treatments; however, the amount of increase is not as significant in LPB coupons as in LSP coupons.
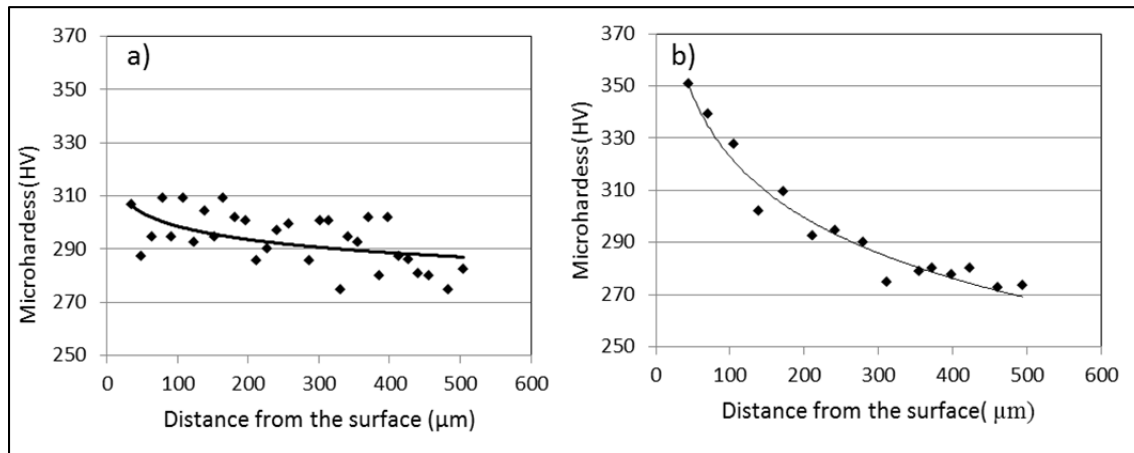
Figure-A II- 2 Microhardness profiles of the LSP coupons, a) standard LSP, and b) heavy LSP
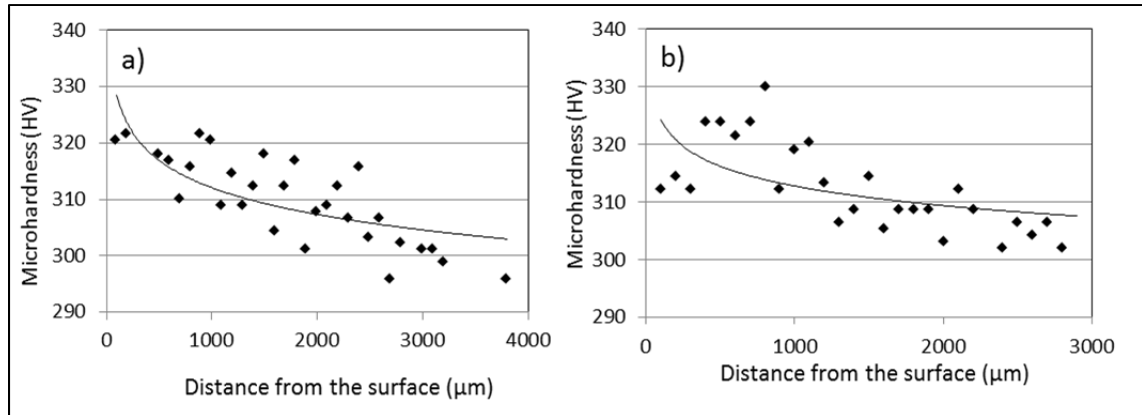
Figure-A II- 3 Microhardness profiles of the LPB coupons, a) LLP, and b) HLP

Residual stress measurements

Residual stress measurements are carried out on the surface treated samples at ETS through X-ray diffraction and progressive electro-polishing. Measurements were done on two directions; longitude direction (LD) and transvers direction (TD) and the values were corrected using ANSYS (Savaria et al. 2012). The measurements reveal the depths and magnitudes of residual stresses induced by surface treatments so that they can be related to the erosion rate and material removal mechanisms. The residual stress values are illustrated in Figs-A II-4 and 5 for LSP and LPB coupons.
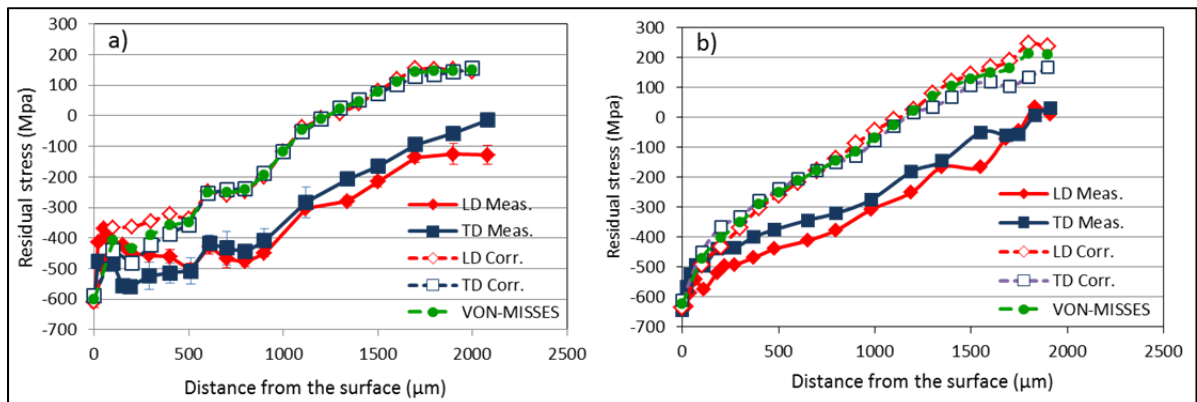
Figure-A II- 4 Residual stress measurements for LSP coupons, a) standard LSP, and b) heavy LSP
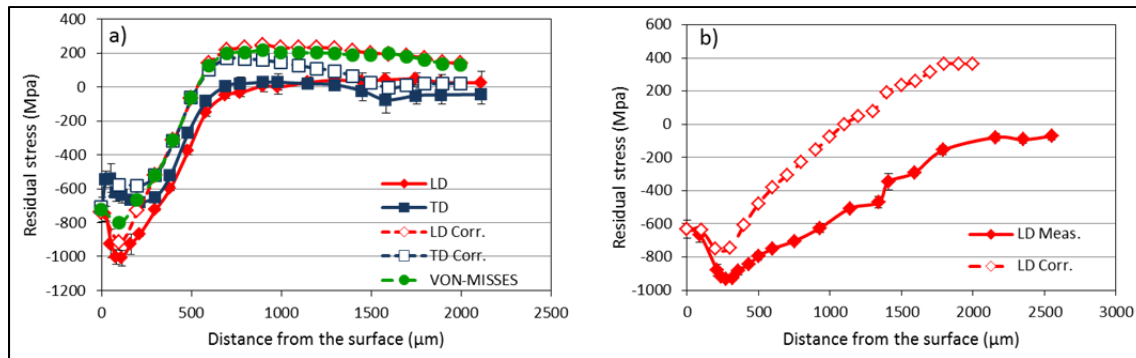
Figure-A II- 5 Residual stress measurements for LPB coupons, a) LLP, and b) HLP

Material removal behavior and erosion curve

Interrupted erosion rig tests were carried out on the coupons up to the advanced stages of erosion as plotted in Fig-A II-6. The erosion rate can be obtained using the provided data for each stages of erosion to analyze the erosion behavior and the effect of surface modification on erosion mechanism and kinetic of the material removal. The erosion behavior should be investigated through the whole process meaning from initiation of the damage to the advanced material removal; however, with the focus on earlier stages where more likely there is an influence of surface treatments.
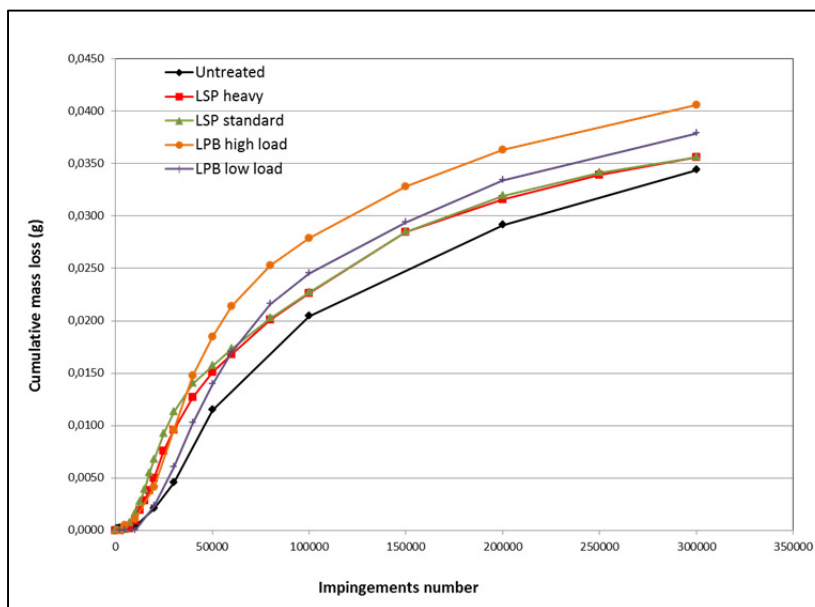
Figure-A II- 6 Cumulative mass loss vs. impingement number

Macroscopic characterization

Macroscopic analyses should be conducted through observation from above the coupons to realize the erosion lines widths as well as from cross sectional view to investigated the depth of erosion damage and sub-tunnels formation through progressive polishing.

Widths of the erosion damage were measured for LSP and LPB coupons as illustrated in Table-A II-1. It shows that LPB coupons present smaller erosion damage width (almost half of the LSP coupons). Also no significant decrease were observed in damage width from low parameter to high parameter LPB coupons, neither for LSP coupons from standard to heavy treatments. Depth of the damage also needs to be investigated and compared to the untreated coupons.

Table-A II- 1 Width of the erosion line

Standard LSP	Heavy LSP	LLP LPB	HLP LPB
1.12± 0.07 mm	1.13±0.05 mm	545 μm	577μm

Microscopic characterization and cracks quantification

Micro-analyses of the erosion features such as crack nucleation, propagation mode and material removal behavior needs to be done on the coupons to identify the erosion mechanisms and the influence of surface treatments on erosion behavior.

Cracks studies as discussed in the articles, chapter 2, 3, and 4, give a quantified insight on the damage dependence on the material characteristics and surface treatments influence. Cracks' size and inclination were measured for LPB coupons presented in Fig-A II-7. The similar studies should be done on LSP coupons and then compared to the untreated one to investigate the influence of surface treatments on cracks behavior and material removal mechanisms.
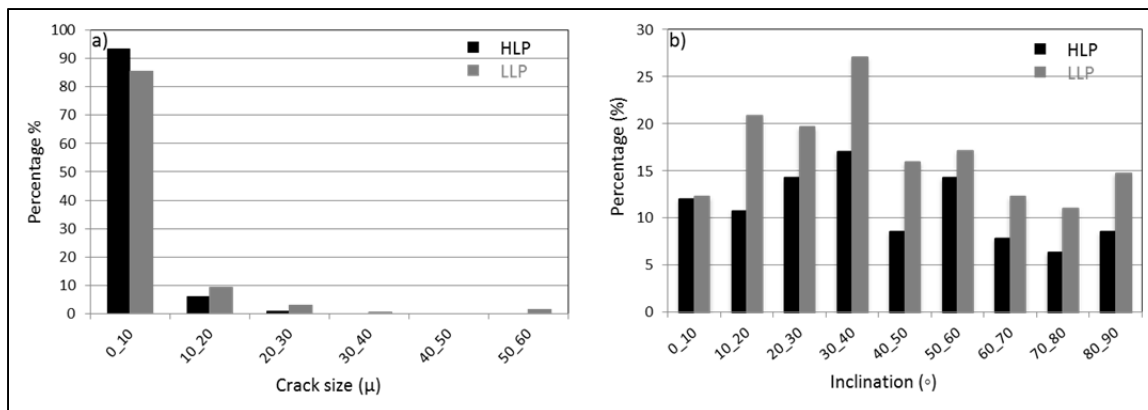
Figure-A II- 7 a) cracks size and b) cracks inclination for LLP and HLP coupons

APPENDIX I

Erosion mechanisms of rolled and forged Ti-6Al-4V presented at EPRI/RSE erosion

conference, June 2012

128

Content

1. Introduction

2. Experimental procedure
   - Water droplets erosion tests
   - Different investigated microstructures of Ti64

3. Water erosion damage on coupons at final stage
   - Eroded craters description: depth and width
   - Crack nucleation, crack propagation, and subtuneling
   - Quantitative analyses
   - Erosion mechanisms and material removal

4. Conclusions

2

Introduction

○ Water droplet erosion is becoming a significant challenge for gas turbine engines.

○ When the ambient temperature increases (especially in hot days), the air density become lower and consequently decreases the turbine performance.

Solution

○ Inlet fogging (the most common method in order to power efficiency)

Consequence

○ Water droplet erosion on compressor blade induced by the droplet impingements.

http://www.siratec.com/content.php?action=show&id=301&&a=1

Fog Nozzle Array
Fog Evaporates
Cooling Inlet Air
High Pressure Fog Line
MeeFog™ Skid

http://www.netl.doe.gov/newsroom/features02-2011.html

3
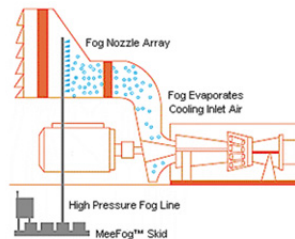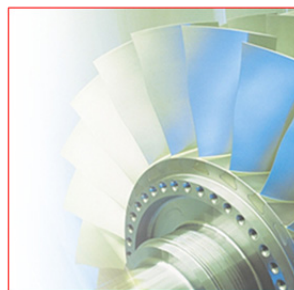
Part 1 - Experimental procedure

<u>Water droplet erosion test were done under ASTM G73 standard</u>

- Normal impact angle
- Impact velocity of 350m/s
- Two droplet sizes of 0.2mm and 0.6mm (Droplets were controlled by calibrated nozzles)
- 20 minutes exposure time to erosion

<u>Samples</u>

✓ rolled Ti-6Al-4V

✓ forged Ti-6Al-4V

Ti64 Hardness
- rolled RD hardness 10% higher than forged
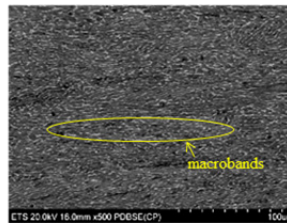- rolled TD hardness 20 % higher than forged

Part 1 - Experimental procedure

<u>Characterization of the 2 investigated Ti64 materials</u>

SEM images **x500**

↳ mostly elongated primary alpha grains α_p

↳ α_p grains appear organized into elongated macrobands of a few hundreds of microns
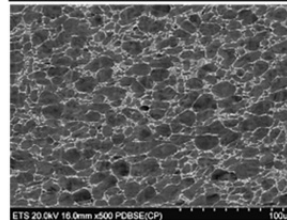
↳ globular microstructure with a large proportion of primary alpha grains α_p

↳ no morphological macrobands are noticeable
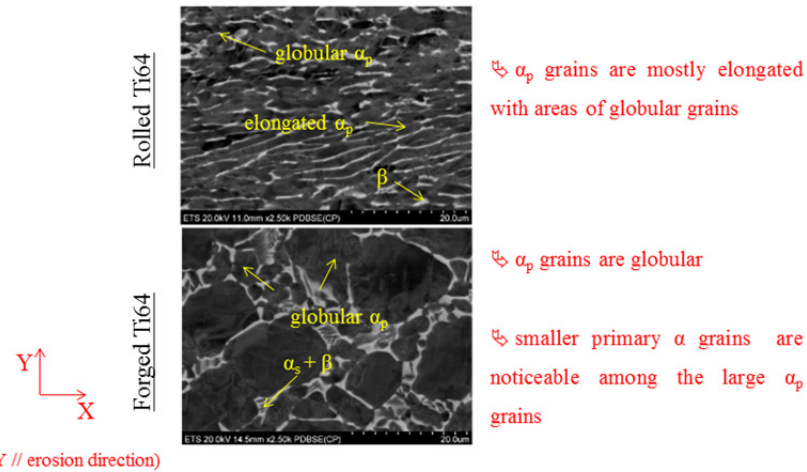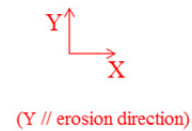
(Y // erosion direction)

130

Part 1 - Experimental procedure

Characterization of the 2 investigated Ti64 materials

SEM images **x2500**
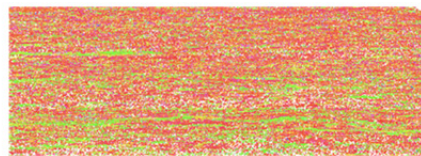
Rolled Ti64

↳ α_p grains are mostly elongated with areas of globular grains

Forged Ti64

↳ α_p grains are globular

↳ smaller primary α grains are noticeable among the large α_p grains

Y
X

(Y // erosion direction)

ÉTS

Rolls-Royce

6

Part 1 - Experimental procedure

Characterization of the 2 investigated Ti64 materials

EBSD mapping
Rolled Ti64

1mm

Forged Ti64

1mm

Y
X

(Y // erosion direction)

ref. axis : Y

0001   11-20

1-100

ÉTS
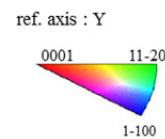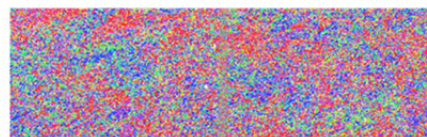
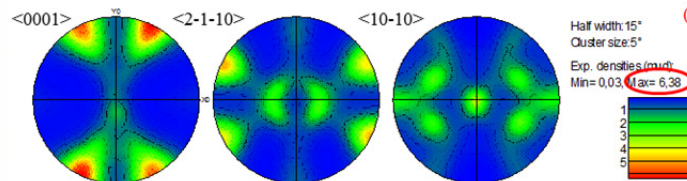Very large EBSD maps (1 week SEM scanning for each sample)

7

Part 1 - Experimental procedure

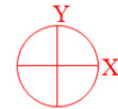Characterization of the 2 investigated Ti64 materials

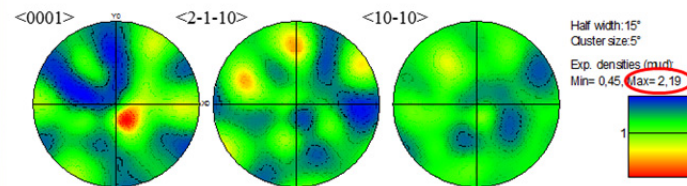   Crystallographic texture : pole figures

Pole figures reference:

Rolled Ti64

(Y // erosion direction)

Forged Ti64

8

Part 1 - Experimental procedure

Summary of materials characterization :

    ↳ investigation of rolled and forged microstructures

    ↳ strong differences in morphology and crystallographic textures between the two microstructures relative to water erosion direction

   ↳ variation of hardness observed relative to crystallographic texture for rolled microstructure

9

132

Part 2 - Water erosion damage on coupons at final stage

Characterization of eroded featuress at the **macro**scopic scale :

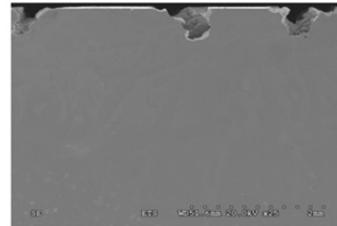• Description of craters depth and width:

- Observation from above

 ⇒ localized damage (not homogeneously distributed)

 ⇒ observation from above shows smooth eroded surface
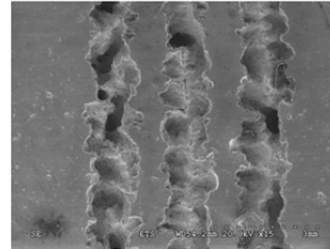
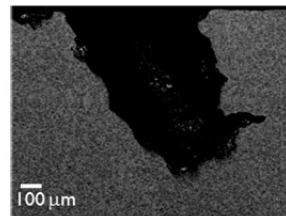- Observation from the cross section

 => very original approach

o Observation in terms of:

   o Differences on eroded surfaces

   o Crack nucleation

   o Crack propagation

   o Sub tunnel formation

100 μm

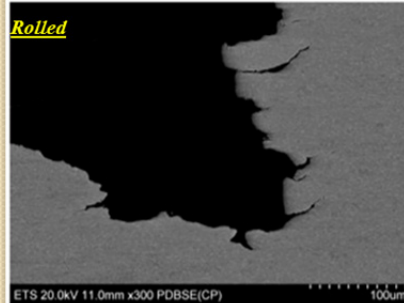↳from cross sectional view craters are not just smooth. There are area of rough and smooth surfaces.
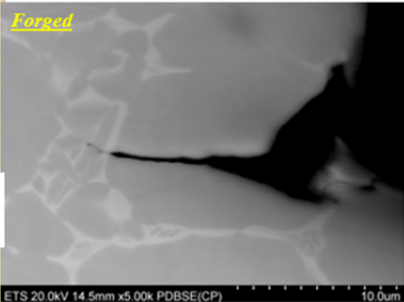
Typical sketch of a crater

Part 2 - Water erosion damage on coupons at final stage

Crack nucleation; surface cracks

Rolled

* Red circles show where the features have been observed in both rolled and forged.
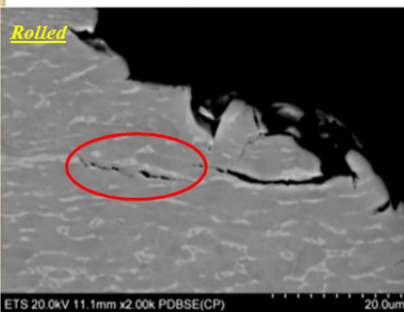
Forged

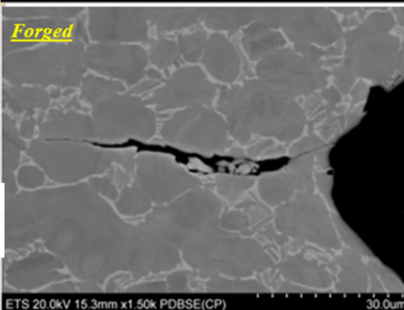==> nucleation of crack from

the crater surface.

12

Part 2 - Water erosion damage on coupons at final stage

Crack nucleation; sub-surface cracks

Rolled

Network of sub-cracks nucleation

==> Cracks may nucleate under stress concentration and then propagate to the main eroded crater.

Forged

13

134

Part 2 - Water erosion damage on coupons at final stage

Propagation; striation

Rolled

Forged

ETS 20.0kV 27.6mm x1.00k SE(M)   50.0um

ETS 20.0kV 30.7mm x1.00k SE(M)   50.0um
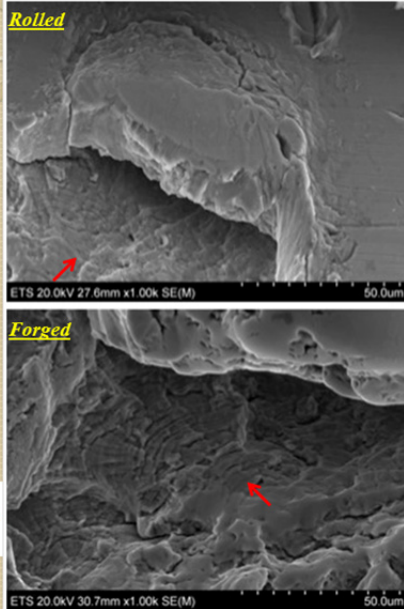
↪Presence of striations indicating a cyclic ductile crack propagation mode

14

Part 2 - Water erosion damage on coupons at final stage

Propagation; transgranular

Rolled

Forged

ETS 20.0kV 16.8mm x2.00k PDBSE(CP)   20.0um

ETS 20.0kV 15.3mm x1.30k PDBSE(CP)   40.0um

↪transgranular crack propagation and within α_p grains (No intergranular propagation)

15

Part 2 - Water erosion damage on coupons at final stage

Propagation; linking

Rolled

Forged
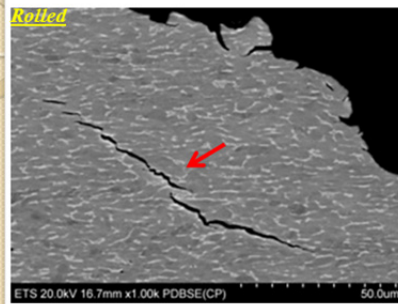
✎crack coalescence as a propagation mechanism

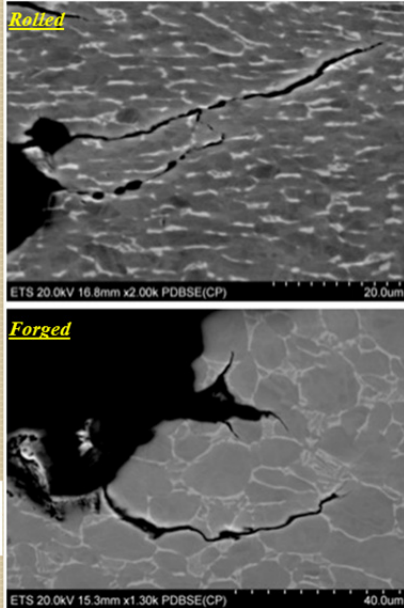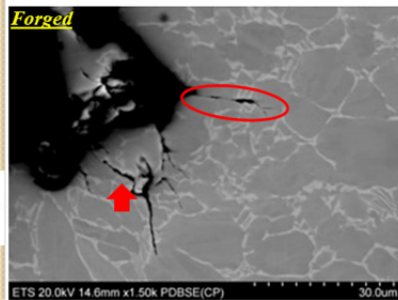✎ multiple crack nucleation and linkage in the case of strongly texture alloy (rolled Ti64); due to the nucleation of multiple cracks with similar orientation : elongated and textured grains

16

Part 2 - Water erosion damage on coupons at final stage

Propagation; material chipping off

Rolled

Forged
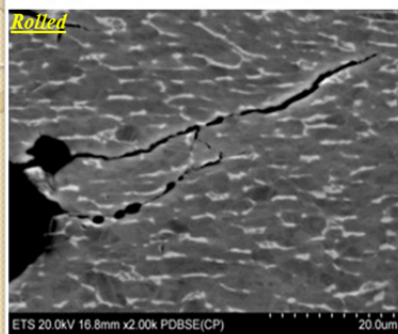
✎Propagation of cracks from the surface and linking of two cracks results in material chipping off.
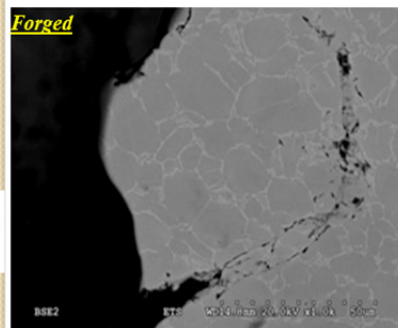
17

Part 2 - Water erosion damage on coupons at final stage

Propagation; periodic propagation of cracks and formation of sub-tunnel

Rolled

ETS 20.0kV 11.0mm x1.30k PDBSE(CP)   40.0um

Forged

ETS 20.0kV 14.5mm x1.50k PDBSE(CP)   30.0um
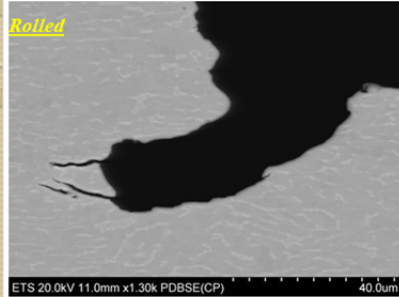
↬propagation and linking of the crack and sub-tunneling formation.

↬start of a new cycle: multiple crack nucleation, crack propagation, crack coalescence and material chipping off.
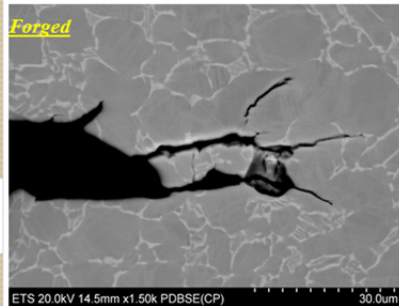
18

Part 2 - Water erosion damage on coupons at final stage

Propagation; crack direction

Rolled

ETS 20.0kV 10.9mm x2.00k PDBSE(CP)   20.0um

Forged

ETS 20.0kV 15.3mm x500 PDBSE(CP)   100um
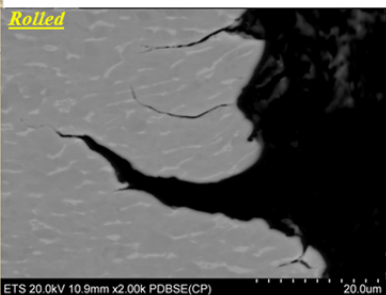
↬oriented propagation of cracks in rolling direction for rolled Ti64
↬propagation of cracks in any direction in forged Ti64
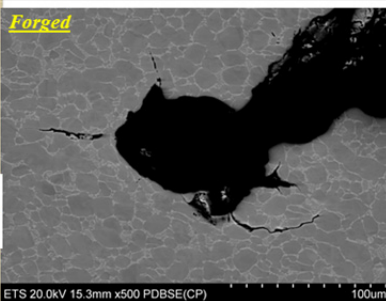
19

Part 2 - Water erosion damage on coupons at final stage

• measurement of hundreds of cracks in terms of inclination and length

Y↑
→X

(Y // impingement direction)

↳ a procedure has been developped to measure cracks in length and inclination relative to water impingement direction

ETS 20.0kV 11.1mm x1.00k PDBSE(CP)   50.0um
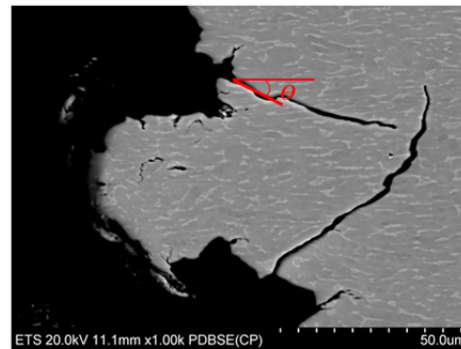
20

Part 2 - Water erosion damage on coupons at final stage

- Inclination
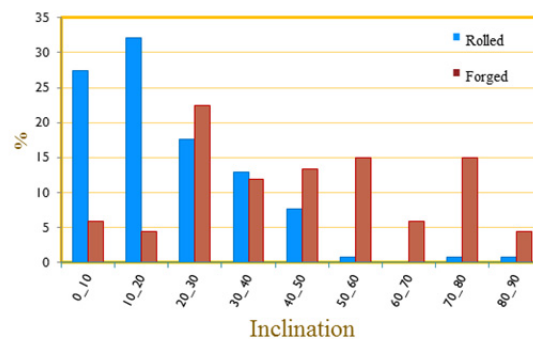
Rolled
Angle average: 20°
Max: 86° & Min:0°
Number of cracks: 131

Forged
Angle average: 45°
Max: 88° & Min: 0°
Number of cracks: 67

↳ cracks in forged sample are randomly distributed in inclination

↳ cracks in rolled sample have a preferential inclination, i.e, perpendicular to impingement direction and along the rolling direction

ETS 20.0kV 16.8mm x1.00k PDBSE(CP)   50.0um

138

Part 2 - Water erosion damage on coupons at final stage

- Size

Rolled
Size average: 27μ
Max: 230μ & Min: 1.45μ
Number of cracks: 131

Forged
Size average: 14μ
Max:272.26μ &Min: 1.58μ
Number of cracks: 67

↪ cracks in forged sample are relatively small (a few metallurgic grains size)

↪ cracks in rolled sample are long : due to merging of multiple nucleated cracks and/or due to faster crack propagation kinetic in this microstructure

22

Part 2 - Water erosion damage on coupons at final stage

Differences on eroded surfaces

↪Crack propagation/material chipping off makes rough surfaces, while they look to be smooth observing from above as water polishing phenomena takes place.

23

Part 2 - Water erosion damage on coupons at final stage

- Proposed mechanism of water droplet erosion in Ti64:

(eventually) water "smoothing"

nucleation of cracks

chipping out of material particles

propagation/ merging of cracks
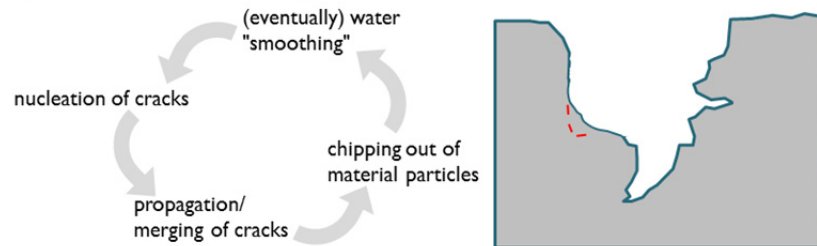
- Cyclic nature relative to cyclic droplet impingements:
  ↳ measurement/prediction of stress fields : presentation 12:50PM "Water Impingement Modeling and Testing", M.Medraj , Concordia University - Montreal, Canada.

- Same mechanism observed on the different coupons (different Ti64 microstructures/surface treatment):
  ↳ differences in the incubation time and erosion rate dependant on the kinetic of these mechanisms ?
  ↳ material parameters which control erosion rate : HV, E, σ_f, etc. ?

24

Conclusions

✓ **We have compared the water erosion behaviour of two different base material and have found that:**

    -Erosion mechanisms are found in both materials

      -at *Macro-scale*

        ↳very localized damage (not homogeneously distributed)

        ↳ sub tunnel formation

      -at *Micro-scale*

        ↳progressive mechanism of network of crack nucleation, merging, material removal, followed by water polishing is proposed.

- Kinetics of the above described mechanisms are dependent on the microstructure characteristics, and different water erosion resistance is expected for both materials.
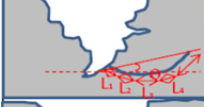
25

APPENDIX II

Crack quantification methods

The quantification method in this work is introduced for the first time, presented in the chapter two. It is noteworthy to explain it in detail here since it is not mainly addressed previously. The idea lies on identifying the dependence of the induced damage to the base material characteristics typically microstructure through measurements of cracks size and inclination. Therefore, images of each observed crack along the erosion craters is taken at high magnification via SEM. Rules in the measurement of both crack features were defined in order to normalize the evaluation (Table- Ap II-1). Indeed, many different types of crack were observed. The size of the crack (L) is sum of the segments plotted on each crack and Θ illustrates the way of inclinations measurement. As shown in table Ap II-1, if the crack changes its direction, depending on the length of the segments, the longest segment is considered for the measurement of the inclination.

Table- Ap II- 1 Measurement of crack size and inclination for various crack types

Crack type	Size	Inclination	Comments
	$L=L_1$	$\Theta = \Theta_1$	crack nucleation and propagation from the main crater surface.
	$L=L_1$	$\Theta = \Theta_1$	Crack nucleation and propagation at the bottom of the sub-tunnel.
	$L=L_1 +L_2+ L_3+ L_4+L_5$	$\Theta = \Theta_1$	Crack changes its direction and contains some segments.
	$L=L_1 +L_2$	$\Theta = \Theta_1$	Crack changes its direction at very begining.
	$L=L_1 +L_2$	$\Theta = \Theta_1$	Crack changes its diretion at the end.

LIST OF BIBLIOGRAPHICAL REFERENCES

Adler, W.F., Analysis of particulate erosion, Wear 37 (1976) 345-352

Adler, W.F., Particulate impact damage predictions, Wear 286-187 (1995) 35-44

Adler, W.F., Morris, J.W., Wahl, N.E., Supersonic rain and sand erosion research: Characterization and development of erosion resistant materials, AFML-TR-72-85 (1972)

Adler, W.F., Vyhnal, R.F., Rain erosion of Ti-6A1-4V, 4th International Conference on rain erosion and associated phenomena, Meersburg, Germany, May (1974)

Ahmad, M., Casey, M., Surken, N., Experimental assessment of droplet impact erosion resistance of steam turbine blade materials, Wear 267 (2009) 1605-1618

ASTM Standard G73, 2004 (2010), standard test method for liquid impingement erosion using rotating apparatus, ASTM International, West Conshohocken, PA, (2010) DOI: 10. 1520/C0033-03R06, www.astm.org

Bache, M.R., Evans, W.J., Impact of texture on mechanical properties in an advanced Titanium alloy, Materials Science and Engineering A319-321 (2001) 409-414

Baker, T.N., Laser surface modification of Ti alloys. In: Surface Engineering of Light Alloys Aluminium, Magnesium and Titanium Alloys, Woodhead Publications (2010)

Balasubramanian, S., Anand, L., Plasticity of initially textured hexagonal polycrystals at high homologous temperatures: application to Titanium, Acta Materiala 50 (2002) 133-148

Beckwith, D.J., Marriott, J.B., Factors affecting Erosion in a 12% Chromium steel, Second Meersburg Conference on Rain erosion, Royal Aircraft Establishment (1967) 761

Bhargava, R.K., Meher-Homji, C.B., Chaker, M.A., Bianchi, B., Melino, F., Peretto, A., Ingistov, S., Gas turbine fogging technology: a state-of-the-art review-Part 1: Inlet evaporative fogging-Analytical and experimental aspects, Journal of engineering for gas turbines and power 129 (2007) 443-453

Bhargava, R.K., Meher-Homji, C.B., Chaker, M.A., Bianchi, B., Melino, F., Peretto, A., Ingistov, S., Gas turbine fogging technology: a state-of-the-art review-Part 3: Practical considerations and operational experience, Journal of engineering for gas turbines and power 129 (2007) 461-472

144

Bridier, F., Villechaise, P., Mendez, J., Analysis of the different slip systems activated by tension in a α/β Titanium alloy in relation with local crystallographic orientation, Acta Materialia 53 (2005) 555-567

Bridier, F., Villechaise, P., Mendez, J., Slip and fatigue crack formation processes in an α/β Titanium alloy in relation to crystallographic texture on different scales, Acta Materialia 56 (2008) 3951–3962

Chaker, M., Meher-Homji, C.B., Mee III, T., Inlet fogging of gas turbine engines-Part B: Fog droplet sizing, analysis, nozzle types, measurement and testing, Proceeding of ASME Turbo Expo (2002) June

Chaker, M., Meher-Homji, C.B., Mee III, T., Inlet fogging of gas turbine engines-Part1: Fog droplet thermodynamics, heat transfer, and practical considerations, Journal of Engineering for Gas Turbines and Power 126 (2004) 545-558

Chillman, A., Ramulu, M., Hashish, M., Waterjet peening and surface preparation at 600 MPa: A preliminary experimental Study, Journal of Fluids Engineering 129 (2007) 485-490

Coulon, P.A., Erosion-Corrosion in steam turbines part II: A problem largely resolved, Journal of the American Society of Lubrication Engineers 42-6 (1985) 357-362

Date, H., Futakawa, M., effect of tensile waves on impact erosion at solid/liquid interface, International Journal of Impact Engineering 32 (2005) 118-129

Feller, H.G., Kharrazi, Y., Cavitation erosion of metals and alloys, Wear 93 (1984) 249-260
Finnie, I., Some observations on the erosion of ductile metals, Wear 19 (1972) 81-90

Field, J.E., Liquid impact: theory, experiment, applications: ELSI conference: invited lecture, Wear 233-235 (1999) 1-12

Frees, N., Cavitation erosion of Titanium carbide coatings on cemented carbides and other substrates, Wear 88 (1983) 57–66

Futakawa, M., Kogawa, H., Hino, R., Date, H., Takeishi, H., Erosion damage on solid boundaries in contact with liquid metals by impulsive pressure injection, International Journal of Impact engineering 28 (2003) 123-135

Garcia, R., Hammitt, F.G., Cavitation damage and correlations with material and fluid properties, Journal of Basic Engineering by ASM (1967) 753-763

Gariépy, A., Bridier, F., Hoseini, M., Bocher, P., Perron, C., Lévesque, M., Experimental and numerical investigation of material heterogeneity in shot peened aluminum alloy AA2024-T35, Surface & Coatings Technology 219 (2013) 15-30

Germain, L., Gey, N., Humbert, M., Vo, P., Jahazi, M., Bocher, P., Texture heterogeneities induced by subtransus processing of near α Titanium alloys, Acta Materialia 56 (2008) 4298-4308

Giampaolo, A., The Gas Turbine Handbook: Principles and Practice, 3rd Edition, Fairmont Press Inc (2006)

Hammond, D.W., Meguid, S.A., Crack propagation in the presence of shot-peening residual stress, Engineering Fracture Mechanics 37-2 (1990) 373-387

Hancox, N.L., Brunton, J.H., The erosion of solids by the repeated impact of liquid drops, Philosophical Transactions, Royal Society of London Series A260 1110 (1966) 121-140

Hattori, S., Effects of impact velocity and droplet size on liquid impingement erosion, International Symposium on the Ageing Management and Maintenance of Nuclear Power Plants (2010) 58-71

Haugen, K., Kvernvold, O., Ronold, A., Sandberg, R., Sand erosion of wear-resistant materials-erosion in choke valves, Wear 186-1 (1995) 179-188

Hayes, M., Connexions between the moduli for anisotropic elastic materials, Journal of Elasticity 2 (1972) 135-141

Heymann, F.J., Liquid impingement erosion, Wear, ASM Handbook 18 (1992) 221-232

Huang, L., Folkes, J., Kinnell, P., Shipway, P.H., Mechanisms of damage initiation in a Titanium alloy subjected to water droplet impact during ultra-high pressure plain waterjet erosion, Materials Processing Technology 212 (2012) 1906-1915

Kamkar, N., Bridier, F., Bocher, P., Jedrzejowski, P., Water droplet erosion mechanisms in rolled Ti-6Al-4V, Wear 301 (2013) 442-448

Khan, J.R., Wang, T., Simulation of inlet fogging and wet-compression in a single stage compressor, Proceedings of the ASME Turbo Expo (2008) GT2008-50874

Kim, J., Cheong, S.K., Effect of laser peening process on the mechanical behavior of Ti-6Al-4V, Report for Seoul National University of Technology (2010) 1

Kong, M.C., Axinte, D., Voice, W., Aspects of material removal mechanism in plain waterjet milling on gamma Titanium aluminide, Materials Processing Technology 210 (2010) 573-584

Krzyzanowki, J.A., Kowaiski, A.E., Shubenko, A.L., Some aspects of erosion prediction of steam turbine blading, Journal of Engineering for Gas Turbine and Power, Transaction of the ASME 116 (1994) 442-451

Le Biavant, K., Pommier, S., Prioul, C., Local texture and fatigue crack initiation in a Ti-6Al-4V Titanium alloy, Fatigue Fracture of Engineering Materials Structures 25 (2002) 527-545

Lee, B., Riu, K., Shin, S., Kwon, S., Development of a water droplet erosion model for large steam turbine blades, KSME International Journal 17-1 (2003) 114-121

Mann, B.S., Arya, V., An experimental study to correlate water jet impingement erosion resistance and properties of metallic materials and coatings, Wear 253 (2002) 650-661

Manson, S.S., Hirschberg, M.H., Fatigue behavior in strain cycling in the low and intermediate Cycle Range, Proceeding of the 10th Sagamore Army Materials Research Conference, Syracuse University Press (1963) Syracuse, NY, Aug 13-16 (1963) 133-178

Marriott, J.B., Rowden, G., The erosion of a cobalt-chromium alloy by liquid impact, Philosophical Transaction A 260 (1966) 144-149

Meher-Homji, C.B., Mee, T.R., Gas turbine power augmentation by fogging of inlet air, Proceedings of the 28th Turbomachinery Symposium, Houston, TX, Sept (1999)

Montross, C.S., Wei, T., Ye, L., Clark, G., Mai, Y., Laser shock processing and its effects on microstructure and properties of metal alloys: a review, International Journal of Fatigue 24 (2002) 1021-1036

Nalla, R.K., Altenberger, I., Noster, U., Liu, G.Y., Scholtes, B., Ritchie, R.O., On the influence of mechanical surface treatments-deep rolling and laser shock peening-on the fatigue behavior of Ti-6Al-4V at ambient and elevated temperatures, Materials Science and Engineering A355 (2003) 216-230

Obara, T., Bourne, N.K., Field, J.E., Liquid-jet impact on liquid and solid surfaces, Wear 186-187 (1995) 388-394

Oka, Y.I., Mihara, S., Miyata, H., Effective parameters for erosion caused by water droplet impingement and application to surface treatment technology, Wear 263 (2007) 386-394

Oka, Y.I., Okamura, K., Yoshida, T., Practical estimation of erosion damage caused by solid particle impact, Part 1: Effect of impact parameters on a predictive equation of erosion damage, Wear 259 (2005) 95-101

Prevey, P.S., Shepard, M.J., Smith, P.R., The effect of low plasticity burnishing (LPB) on the HCF performance and FOD resistance of Ti-6Al-4V, Proceeding of 6th National Turbine Engine High Cycle Fatigue (HCF) Conference (2001) Jacksonville, Fl, March 5-8

Richman, R.H., McNaughton, W.P., A metallurgical approach to improve cavitation erosion resistance, Materials Engineering and Performance 6-5 (1977) 633–641

Richman, R.H., McNaughton, W.P., Correlation of cavitation erosion behaviour with mechanical properties of metals, Wear 140 (1990) 63–82

Robinson, J.M., Reed, R.C., Water droplet erosion of laser surface treated Ti-6Al-4V, Wear 186-187 (1995) 360-367

Savaria, V., Bridier, F., Bocher, P., Computational quantification and correction of the errors induced by layer removal for subsurface residual stress measurements, International Journal of Mechanical Science 64 (2012) 184-195

Schmitt, G.F., Liquid and solid particle impact erosion, Technical report AFML-TR-79-4122 (1979)

Sheldon, G.L., Effects of surface hardness and other material properties on erosive wear of metals by solid particles, Engineering Materials Technology Transaction ASME 99 (1977) 133–137

Shipway, P.H., Gupta, K., The potential of WC-Co hard metals and HVOF sprayed coatings to combat water-droplet erosion, Wear 271 (2011) 1418-1425

Stanisa, B., Ivusic, V., Erosion behavior and mechanisms for steam turbine rotor blades, Wear 186-187 (1995) 395-400

Stronge, W.J., Impact mechanics, Cambridge University Press, March 25 (2004)

Szczepanski, C.J., The role of microstructural variability on the very high cycle fatigue lifetime variability of the α+β Titanium alloy, Ti-6Al-2Sn-4Zr-6Mo, university of Michigan (2008)

Thomas, G.P., Brunton, J.H., Drop impingement erosion of metals, Proceeding of Royal Society of London A 314 (1970) 549-565

Uihlein, A., Maggi, C.M., Keisker, I., Water droplet erosion at steam turbines: testing method and validation, Proceeding of Milan international conference on solid particle and liquid droplet erosion: Part 2 (2012) 81-93

Wong, Y.N., Huang, J.C., Texture analysis in hexagonal materials, Materials chemistry and physics 81 (2003) 11-2

Www.materials-laboratory.power.alstom.com

Yasugahira, N., Namura, K., Kaneko, R., Satoh, T., Erosion resistance of Titanium alloys for steam turbines blades as measured by water droplet impingement, Titanium Steam Turbine Blading, Palo Alto, 2988, Pergamon, New York (1990) 385-401

Yerramareddy, S., Bahadur, S., Effect of operational variables, microstructure and mechanical properties on the erosion of Ti-6Al-4V, Wear 142 (1991) 253-263

Zhou, Q., Li, N., Chen, X., Yonezu, A., Xu, T., Hui, S., Zhang, D., Water dropl erosion on turbine blades: Numerical framework and applications, Materials Transaction 49-7 (2008) 1606-1615

Zhou, Q., Li, N., Chen, X., Xu, T., Hui, S., Zhang, D., Analysis of water drop erosion on turbine blades based on a nonlinear liquid-solid impact model, International Journal of Impact Engineering 36 (2009) 1156-1171